20 APPLICATIONS OF THIN FILM COATINGS

20.1 INTRODUCTION

20.1.1 General uses of thin films. Quite frequently optical components are coated with thin layers of various solid materials for the purpose of altering either their physical or optical properties. As an example of the former purpose, aluminum mirrors are often coated with a thin layer of silicon monoxide in order to increase their resistance to abrasion and chemical attack. The addition of this layer alters the spectral reflectivity of the mirror, although this is not the primary purpose of such a coating. More frequently, however, thin film coatings are used for the primary purpose of altering the spectral reflection and transmission of optical components. Sometimes a thin film coating consists of only one layer deposited upon a suitable substrate. In other cases, many layers, often as many as forty or fifty, are used to produce a given optical filter. Hence this type of filter is called a multilayer filter, or simply a multilayer. In Section 20, the term multilayer is used as a generic term for such thin film coatings, even though the "multilayer" coating may consist of a single-layer antireflection coating on a glass surface.

20.1.2 Typical applications.

20.1.2.1 Antireflection coatings. Whenever light traverses an interface between two media of different refractive index, such as an air-glass interface of a lens, some of the light is reflected. Often the spacing of optical elements is such that these reflections are manifested in the image plane as "flare images". Before the advent of antireflection coatings, many otherwise acceptable lens configurations were rejected because they produced these flare images. The coating of optical surfaces with antireflection coatings has practically eliminated this problem. It is important that antireflection coatings be applied to infrared optical components, such as lenses or domes, which contain germanium, silicon, or other materials with a high refractive index. The loss of light at uncoated surfaces would be prohibitive otherwise. Antireflection coatings are discussed in more detail in Section 20.3.

20.1.2.2 Achromatic beam splitters. Many optical devices, such as interferometers, range finders, optical gunsights, utilize beam splitters which divide a light beam and divert it into two directions. Thin metal films have been used as beam splitters for many years, but they are inefficient because the metal absorbs part of the light. More recently, multilayer beam splitters have been developed which are much more efficient, because they contain only non-absorbing materials. Less than one percent of the light is absorbed in a typical multilayer beam splitter; the remaining 99% of the light is either reflected or transmitted. The properties of multilayer beam splitters are expounded in Section 20.7.

20.1.2.3 Color filters and band-pass filters. Multilayer filters are used to transmit (or "pass") a broad band of wavelengths in one spectral region, but attenuate in other regions. For example, a multilayer filter is available which transmits more than 90% in the blue but has a transmission of less than 0.5% in the green and red. This multilayer filter is superior to the conventional glass or dyed-gelatin absorption filters, which have a much lower transmission in the blue. Similar types of band-pass filters have been developed for the ultraviolet and infrared spectral regions. The spectral transmission of some typical multilayer filters is shown in Figures 20.86, 20.91 and 20.92; a general discussion is given in Sections 20.5.2 and 20.6.2.

20.1.2.4 Color-selective beam splitters. Figure 20.1 shows a multilayer which is used as a color-selective beam splitter. In this example, the beam splitter transmits blue light, but reflects the green and red. Such beam splitters are useful as color separation devices in color photography and color television. This type of beam splitter is often called a dichroic mirror; its properties are explained in Section 20.7.2.

20.1.2.5 Narrow pass-band (interference) filters. Multilayer filters are used to transmit a narrow band of wavelengths. For reasons which are described in 20.10.2.2, these narrow-band filters are called interference filters, although in a technical sense all multilayer filters are interference filters, because they depend upon the interference of light reflected from the various films. One type of interference filter which is manufactured commercially in large quantities has a pass band which is from ten to twenty millimicrons wide in the visible spectral region. Custom-made filters have been produced which have a pass band as narrow as 0.1 mμ. A filter of this type has been used to isolate one of the sodium D lines at 589.0 mμ from its neighbor at 589.6 mμ. Such filters have many potential uses in the field of spectro-chemical analysis and are discussed in more detail in Section 20.10.

20.1.2.6 Semi-transparent mirrors. Multilayer mirrors have been produced which not only have a high reflectivity, but also transmit almost all of the light which is not reflected with a small absorption loss. A typical multilayer mirror might reflect 95% of the incident light and transmit 4.5%, the remaining 0.5% being absorbed or scattered. These multilayer mirrors have a much lower (absorption) loss than the conventional semi-transparent films of silver or aluminum and are useful for coating the plates of a Fabry-Perot interferometer or the ends of an optical maser. The spectral reflectivity of a semi-transparent metal mirror

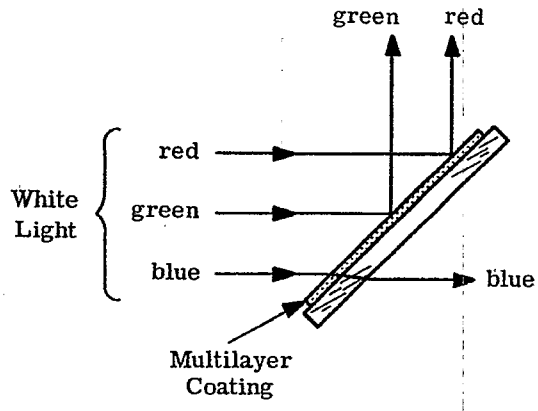

Figure 20.1-A color selective beam splitter which reflects the red and green, but transmits the blue.

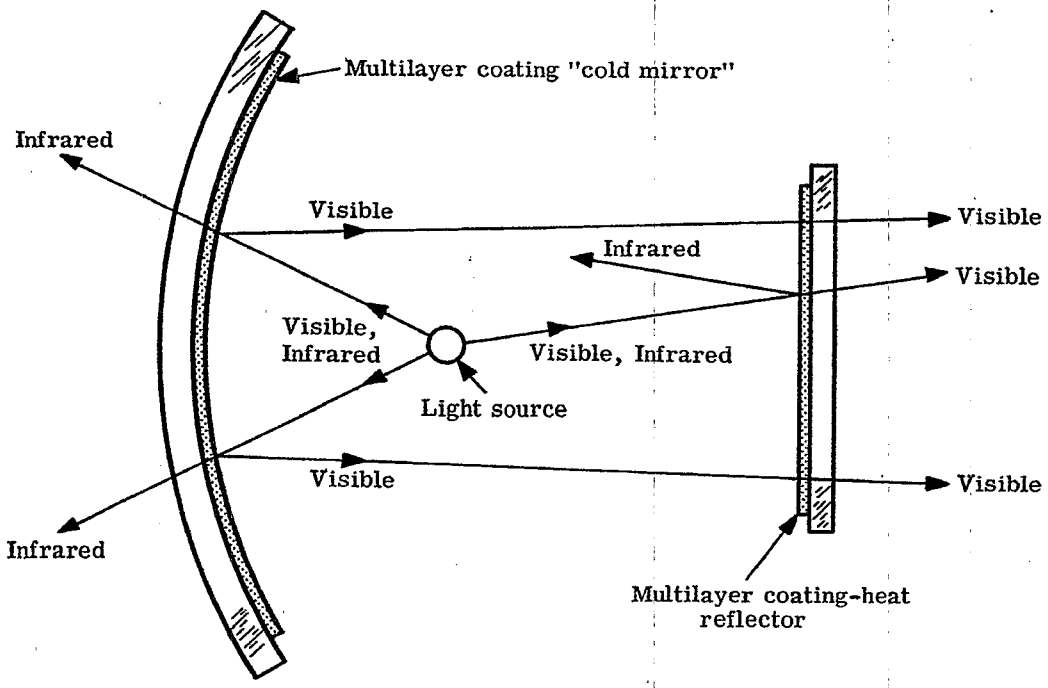

Figure 20.2-A cold mirror and heat reflector reduce the heat directed towards the film in a projection system.

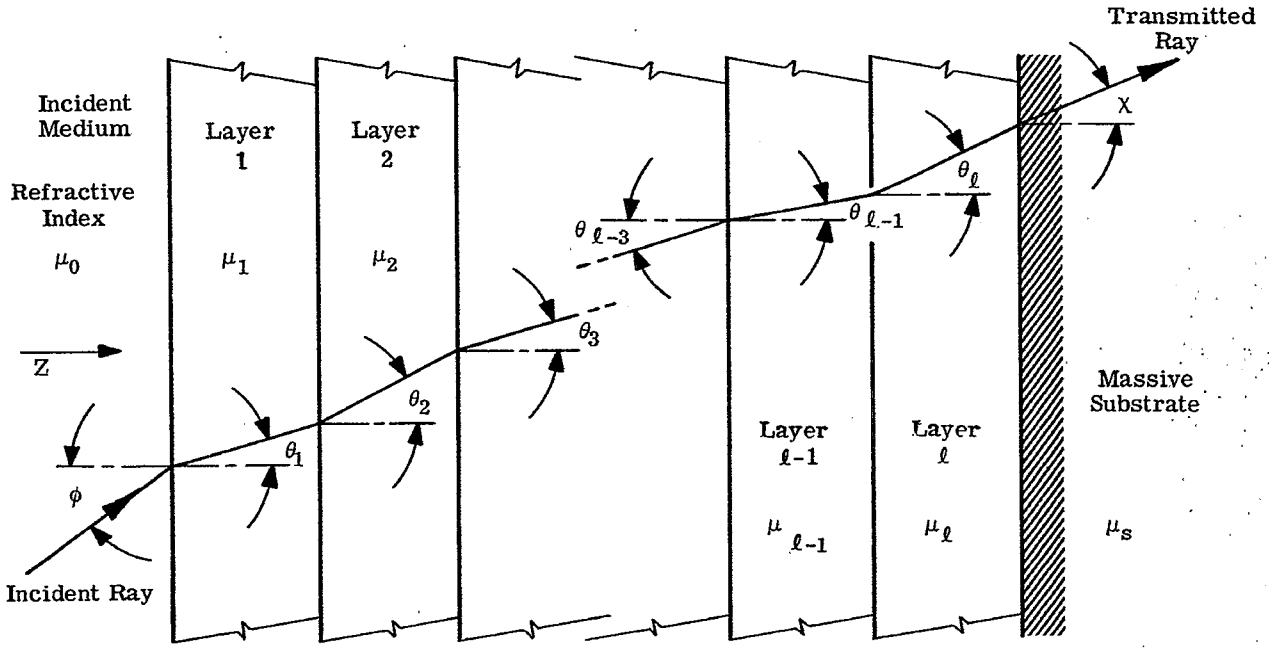

Figure 20.3 - Nomenclature used in designating the thickness, refractive index, and angle of refraction θ in each of the layers. For sake of clarity, the reflections which take place at each interface are not shown.

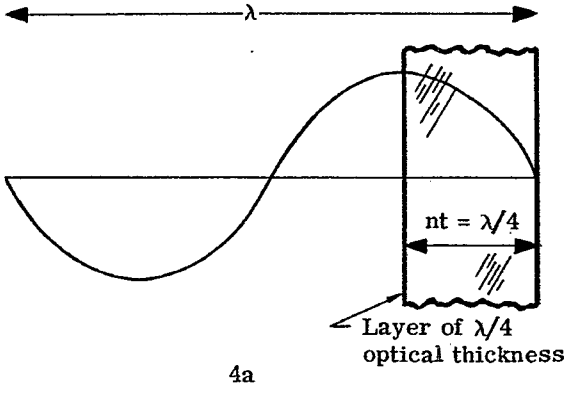

4a

Figure 20.4 (a) - A comparison of the wavelength of light (in vacuo) with the optical thickness of a quarter-wave layer.

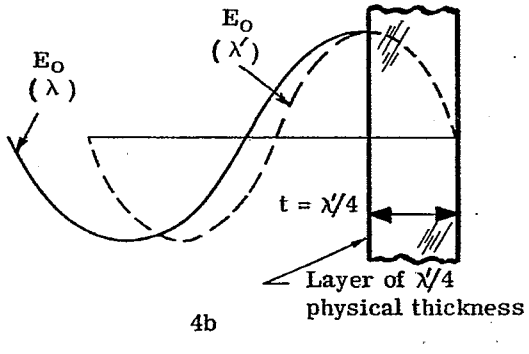

4b

Figure 20.4 (b) - An instantaneous picture of the electric vector of a wave entering a denser medium. (see text 20.1.3.4)

is usually quite "flat," whereas the reflectivity of a typical multilayer mirror changes quite rapidly with wavelength. Further information is presented in Section 20.8.

20.1.2.7 Heat control filters. One type of a multilayer mirror, called a cold mirror, is used to reflect the visible light and transmit the infrared. Figure 20.2 shows a typical use of a cold mirror as a reflector behind a light source in a film projector. The cold mirror reflects the visible light towards the film, but permits the heat in the infrared to pass out the back. This system is even more efficient if a heat reflector is inserted between the arc and the film. This reflector, which has a high transmission in the visible spectral region but a high reflectivity in the infrared, reflects the heat away from the film but permits the visible light to pass through to the film with little attenuation. Another type of heat control filter is the cover glass which is placed over solar cells which are used to power a space vehicle. These cover glasses are designed to reflect the radiant energy at wavelengths longer than 1.2 μ. The radiant energy from the sun in the wavelength range from 1.2 μ to 2.5 μ does not generate power, but only increases the temperature of the solar cell, thereby decreasing its efficiency. Heat control filters are discussed briefly in Sections 20.5.3 and 20.6.2.

20.1.2.8 High-reflectivity mirrors. By overcoating aluminum and other metals with dielectric films, it is possible to obtain a reflectivity as high as 99.5%. The spectral reflectivity of a typical overcoated mirror is shown in Section 20.8.

20.1.2.9 Polarizers. Multilayers can be used to produce linearly polarized light. They are particularly useful in the infrared, where conventional polarizers which utilize birefringence cannot be used because most optical materials are optically isotropic. This application of multilayers is not discussed in Section 20; the reader can refer to Heavens[1] for further details.

20.1.2.10 Reflection filters. A multilayer has been developed which has a high reflectivity in certain spectral regions, but absorbs strongly in other regions. Such a mirror has been used to absorb the visible light and reflect the infrared. It should be noted that the type of reflection filter we are discussing here is different from the heat reflector described in 20.1.2.7. Both types of multilayer filter reflect the infrared, but the former absorbs the visible light, whereas the latter transmits the visible. This type of filter is not discussed in Section 20; further information is given in Heavens[2].

20.1.3 Nomenclature

20.1.3.1 General considerations. In Section 20, we consider only the case where the thin films are optically homogeneous; that is, the optical constants of a given layer do not vary along the direction of the propagation of the light, which is shown as the Z-direction in Figure 20.3. At the present time, almost all commercially manufactured multilayer filters are composed of films which are homogeneous. However, multilayer coatings which contain optically inhomogeneous films have some very interesting properties and it is possible that they will come into more extensive use in the future. A simple antireflection coating which contains an optically inhomogeneous film, sometimes called a "graded film", is described by Strong[3].

20.1.3.2 The multilayer stack. An idealized multilayer stack is shown in Figure 20.3. It consists of a total of ℓ layers deposited upon a substrate which has an optical constant $\mu_s = n_s - j k_s$. Each of the layers has a physical thickness t_i and optical constant $\mu_i = n_i - j k_i$, where n_i is the refractive index and k_i is the absorption coefficient. It should be noted that the absorption coefficient (represented by a lower case "k") is related to the parameter "K" in Section 21.2 by the relationship $k_i = -n_\nu K_\nu$. The light is incident at an angle ϕ from a non-absorbing incident medium of refractive index n_o. Since the layer boundaries are parallel, the angle of refraction in the i^{th} layer, θ_i, is determined simply from Snell's law, if the layers are non-absorbing. Thus each layer in the stack is specified by three parameters, namely t_i, n_i, and k_i. These quantities, along with n_o, n_s, and k_s, completely specify the optical properties of the multilayer. Given these quantities and ϕ it is a straightforward, although tedious, task to calculate the reflectivity R and transmission T of a multilayer as a function of the wavelength λ of the incident light. Methods of computing R and T are presented in Sections 20.1.5, 21.2.8, and 21.2.12.

20.1.3.3 The wave number. The retardation of phase of the i^{th} layer is defined* as

$$\delta_i = 2\pi \sigma n_i t_i \qquad (1)$$

where σ is the wave number of the incident light, $\sigma = 1/\lambda$. The wave number is proportional to the

* S_i is related to the parameter B_ν defined in Equation 21 - (47) by the relationship $2\delta_i = \beta_\nu$.

(1) All references are listed separately at the end of this section.

frequency of the light. In computing the spectral transmission of a multilayer filter, there are many advantages to using some parameter, such as σ, which is proportional to frequency rather than wavelength. One advantage is that many spectral transmission curves have even symmetry about some point, when plotted on a frequency scale, whereas the curves are quite asymmetrical when plotted versus wavelength. This is illustrated by Figures 20.32 and 20.34, which show the reflectivity of the same coatings. It is evident that the curves plotted versus frequency, as in Figure 20.34, have even symmetry about the center, whereas the wavelength plot of Figure 20.32 is quite asymmetrical. Another advantage of using frequency as a variable is that very often maxima and minima in the reflectivity curve are spaced at equal intervals on a frequency scale, whereas on a wavelength scale they are spread out in the long wavelength region and compressed together in the short wavelength region. This is illustrated in reflectivity curve shown in Figure 20.59. The maxima and minima near 500 mμ are so close together that they cannot be plotted accurately, whereas they would be spaced at equal intervals if plotted versus σ. In many cases in Section 20 we use as a variable a dimensionless quantity, $g = \lambda_o/\lambda$, which is proportional to frequency. The disadvantage of using σ as a variable rather than λ lies in our educational system; most persons are unfamiliar with wave number. Most of us have been educated to think in terms of wavelength and thus we associate "green light" with a wavelength of 540 mμ rather than with a wave number of 18519 cm^{-1}. A useful factor to remember in converting wavelength into wave number is that

$$1\mu = 1000\ m\mu = 10{,}000\ A \quad \text{is equivalent to } 10{,}000\ cm^{-1}.$$

Thus using the fact that "ten thousand angstroms 'equals' ten thousand wave numbers", and the fact that the wave number is inversely proportional to wavelength, we see that

5000A is equivalent to $20{,}000\ cm^{-1}$

2500A is equivalent to $40{,}000\ cm^{-1}$

and so on.

20.1.3.4 The QWOT. Not infrequently multilayers are composed entirely of dielectric (non-absorbing) materials. In this case it is convenient to refer to the thickness of the layers in terms of their optical thickness, which is defined as the product of the geometrical thickness, t_i, and the refractive index, n_i. Reference is frequently made to the quarter-wave optical thickness, QWOT, which is defined as

$$QWOT = 4\, n_i\, t_i \quad . \tag{2}$$

Since n_i is a dimensionless quantity and t_i has the dimensions of length, the QWOT also has the dimensions of length and is usually expressed in units of microns or millimicrons. Thus, if a layer has a QWOT of 550 mμ, this means that one-quarter wavelength of light at 550 mμ has the same length as the optical thickness of the layer, as illustrated in Figure 20.4(a). Sometimes one refers to a film of quarter-wave optical thickness simply as a "quarter wave". A note is interpolated to delineate clearly exactly what is drawn in diagrams such as in Figures 20.4, 20.55, 20.107, and others. This represents a comparison of the optical thickness of the film with the wavelength in vacuo of the incident light. To elucidate this point, at a given instant of time, the electric vector E of a light wave propagating in a homogeneous film of refractive index n can be represented by

$$E = E_o \cos\left(\frac{2\pi}{\lambda'} z\right)$$

where z is the coordinate shown in Figure 20.3. The wavelength λ' in the foregoing equation has a "primed" superscript as a reminder that λ' is the wavelength in that medium, of index n. λ' is related to the wavelength λ in vacuum by

$$\lambda' = \frac{\lambda}{n}$$

and consequently λ' changes when the wave enters a medium of different refractive index, as is shown in Figure 20.4b. Thus Figure 20.4b represents the actual E field in the film and vacuum at a given instant of time and the thickness of the film is represented by its actual physical thickness. Another approach, which is extensively used in Section 20, is to compare the optical thickness of the film with the wavelength in vacuo. This is accomplished by writing equation as

$$E = E_o \cos\left(\frac{2\pi}{\lambda} n z\right).$$

The quantity n z is the optical thickness. The film shown in Figure 20.4a is drawn thicker in proportional to its optical thickness, but this is compensated for by the fact that the wavelength which is shown is not the wavelength in the film, but the vacuum wavelength.

20.1.3.5 "H" and "L" layers. Quite often multilayers are composed of films which are all of quarter-wave optical thickness, or some multiple thereof. In this case it is convenient to use a shorthand notation to specify the design. The letters "H" and "L" are used to specify films of high and low refractive index, respectively, which have the same QWOT. For example, the design of the double-layer coating shown in Figure 20.5 is designated as

glass HH L air,

where $n_H = 1.70$ and $n_L = 1.38$. The optical thickness of the film next to the glass is two quarter waves, or a single half wave. Similarly, the design of the double-layer coating shown in Figure 20.37 is

silicon H L air,

where $n_H = 2.40$ and $n_L = 1.38$.

20.1.3.6 The reflectivity and transmission. In Section 20 reference is made to computed values of the reflectivity, R, and the transmission, T. R and T are synonymous with the "reflection coefficient", and the "transmission coefficient" which are defined in terms of a time average of the Poynting vector, as is specified in Equations 45 and 45a in Section 21.2.6. In Section 20 the terms "reflectance" and "transmittance" are reserved for measured, rather than computed, values.

20.1.3.7 Non-normal incidence. When light is incident upon a multilayer at oblique incidence, both R and T must be computed separately in each plane of polarization. Thus one refers to R_p and T_p in the "p" plane of polarization when the electric vector is parallel to the plane of incidence and to R_s and T_s in the "s" plane of polarization when the electric vector is perpendicular to the plane of incidence. In general, if unpolarized light is incident upon a multilayer at non-normal incidence, both the reflected and transmitted light is partially plane-polarized. If the incident light is elliptically polarized, then the degree of elliptical polarization of both the reflected and transmitted light is altered. This is because not only the reflection and transmission are different in the two planes of polarization, but also because the phase shift upon reflection is different for the two planes of polarization. If the light which is obliquely incident upon a multilayer is initially unpolarized and if the light detector, such as the human eye or a photographic plate, is not sensitive to the polarization of the light, then the polarizing effect of the multilayer can be neglected. In this case we simply refer to the average reflectivity, R_{av}, and the average transmission, T_{av}.

$$R_{av} = \frac{1}{2}(R_p + R_s), \qquad T_{av} = \frac{1}{2}(T_p + T_s). \tag{3}$$

20.1.4 Analogies.

20.1.4.1 Electrical transmission lines. It is useful to note the interesting analogy between the propagation of light through a thin film and the propagation of radio waves in an electrical transmission line. The propagation equation for the thin film is identical with the transmission line equation if one identifies the electric vector and magnetic vector in the thin film with the electrical voltage and current in the transmission line. The optical thickness* of the thin film is analogous to the "electrical length" of the transmission line, while the refractive index of the thin film is analogous to the "characteristic admittance" of a section of transmission line. A dielectric thin film corresponds to a "lossless" transmission line. The refractive index of the substrate and incident medium are analogous to the load admittance and the "characteristic admittance of the generator". The equations for the "optical admittance" of a thin film are identical to the equations for admittance of a transmission line. Graphical devices which have been invented for computing the voltage standing ratio of an electrical transmission line, such as the Smith Chart and the Admittance Chart, are used for computing the reflectivity of a stack of thin films[4,5,6]. This analogy cannot be extended too far, however. Shunt transmissions lines and lumped constant elements such as resistors, capacitors, and inductors can be added to an electrical transmission line. No exact analogous devices exist in thin film optics, although at certain wavelengths a thin gold or silver film can be represented as an inductance and an inconel film as a pure resistance.

20.1.4.2 Similarities with geometrical optics. There are some similarities between problems in multilayer filters and lens design. In both cases, it is a straightforward task to compute the performance of a given system, once the design has been specified. The design of a multilayer filters is given by specifying the thickness and optical constants of each layer, and the substrate and incident medium. The design of a lens is specified by the physical dimensions of each optical component and its refractive index. In both cases, it is quite difficult to synthesize a design. In order to synthesize a multilayer filter design, it is

* Note that the electrical length of a transmission line does not change with admittance as the optical thickness of a film changes with index.

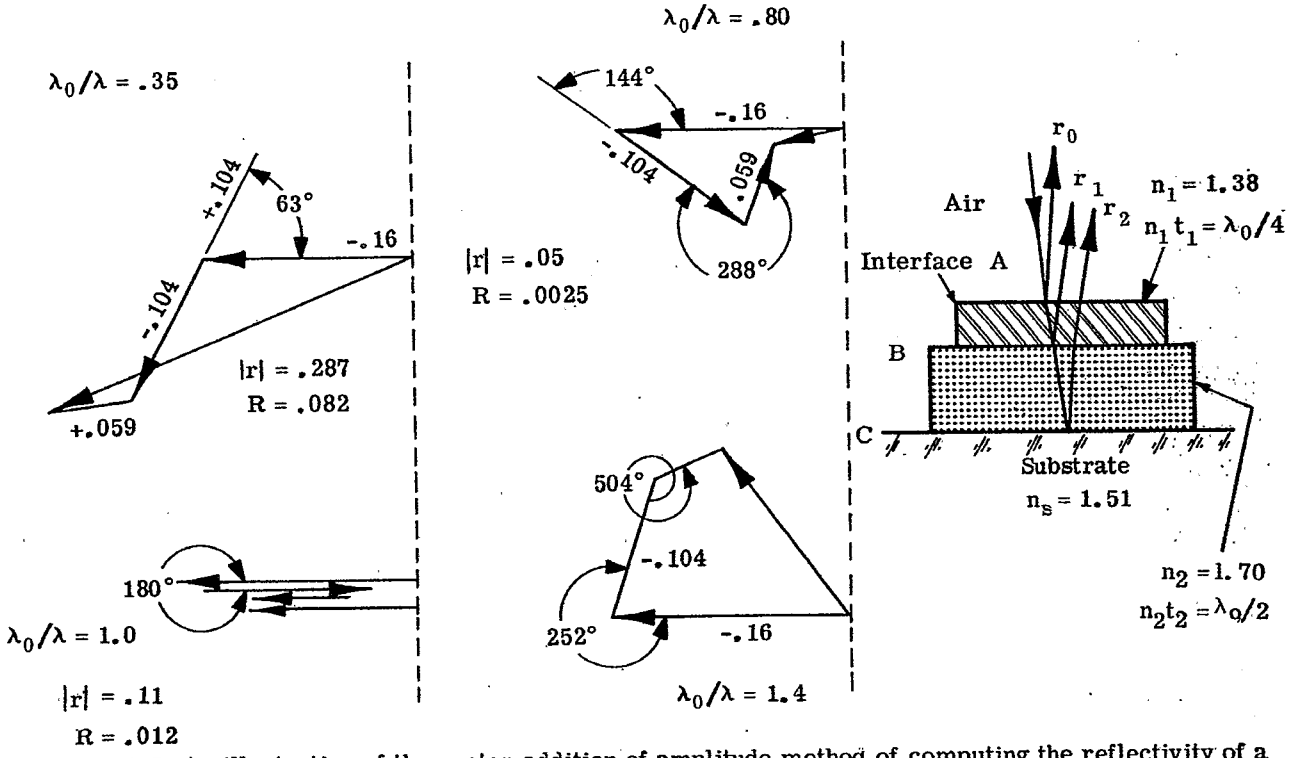

Figure 20.5 - An illustration of the vector addition of amplitude method of computing the reflectivity of a antireflection coating. (Vectors are not drawn exactly to scale.)

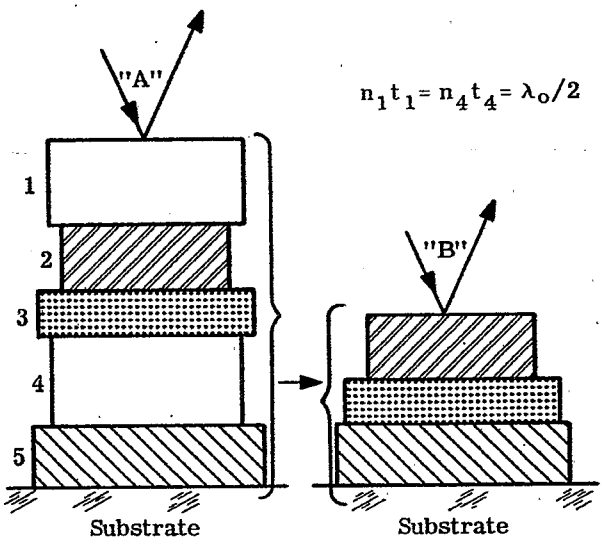

Figure 20.6 - Stack "B" is equivalent to stack "A" when layers 1 and 4 in stack "A" are absentee.

necessary to choose the thickness and optical constants of each layer so that the filter has a prescribed spectral transmission or reflectivity. In synthesizing a lens, one must choose the curvature of the surfaces, spacing and refractive index of the optical elements so that the lens has a prescribed amount of aberration at various points in the image plane. In both lens design and multilayer filters, only approximate methods have been developed to accomplish this synthesis.

20.1.4.2.2 There are several differences between multilayer filters and lenses. The first difference is that the parameters which specify the design of a lens are given to a high degree of precision. The physical dimensions and the refractive indices of the optical components are usually specified to an accuracy of a few thousandths of a percent. In thin film optics, however, it is usually difficult to control the thickness of individual layers to a precision of better than one percent. The refractive index of thin films can vary widely, because the optical constants of thin film materials depend not only upon the thickness of the layer, but also quite markedly upon the conditions in the vacuum when the film is evaporated. For example, the refractive index of the material "silicon monoxide" can vary from 1.40 to 1.90 depending upon the partial pressure of oxygen during the evaporation.[7,8]

20.1.4.2.3 Another difference is that the design of a lens is usually patent, whereas the design of a multilayer can be kept secret quite easily. Even if the design of a lens were not specified, one could disassemble a lens and measure the refractive index and dimensions of its components. In order to ascertain the design of a multilayer filter, however, it would be necessary to "peel off" each of the layers, which might be as thin as a few hundred angstroms. This is practically impossible to accomplish. The amount of material in a layer which has a QWOT of 500 mμ is about thirty micrograms per square centimeter. Hence, it is quite difficult to perform a chemical analysis to determine the composition of the layers. Because of these facts, one finds quite frequently that the designs of multilayer filters and the materials which are used in their manufacture are kept secret for proprietary reasons. This secrecy has been a detriment to the progress in this field.

20.1.5 Methods of computing R and T*

20.1.5.1 Vector addition of amplitudes. This is an approximate method which is most useful for stacks which contain a small number of layers. It essentially neglects the multiple reflections which take place between various interfaces and hence is most accurate when the difference between the refractive indices of adjacent layers is small. As an example of the application of this method, consider the problem of computing reflectivity of the double-layer antireflection coating shown in Figure 20.5 . The incident light reflects from each of the three interfaces. The amplitude of the wave which is reflected at each interface is proportional to the Fresnel amplitude coefficient

$$r_i = (n_i - n_{i+1})(n_i + n_{i+1})^{-1} \qquad (4)$$

where n_{i+1} and n_i refer to the refractive index on each side of the interface. However, these waves are not in phase and hence their amplitudes must be added vectorially. The difference in phase between the wave reflected from interfaces A and B is $2\delta_1$, and similarly for the other interface. In the example in Figure 20.5 , the r_i are -0.16, -0.104, and 0.059, respectively for interfaces A, B, and C. From Equation 20-(1) we readily determine that 2_1 is 63° and 2_2 is 126° when λ_o/λ = 0.35. Extending this procedure to other values of λ_o/λ, we can construct the vector diagrams which are shown in Figure 20.5 . When λ_o/λ = 1.0, the vectors are colinear and hence the r_i can be added algebretically. In Figure 21.8 the reflectivity computed by the vector method is compared with the results of the more exact matrix method described in the next section.

20.1.5.2 The characteristic matrix.[11,12]

20.1.5.2.1 The electric field E and the magnetic field H at one boundary of a film are related to the fields E' and H' at the other boundary by two linear simultaneous algebretic equations. These equations can be written in matrix form:

$$\begin{bmatrix} E \\ H \end{bmatrix} = M_i \begin{bmatrix} E' \\ H' \end{bmatrix} \qquad (5)$$

where the matrix M for a non-absorbing film at normal incidence is

$$M_i = \begin{bmatrix} \cos\delta_i & j\, n^{-1}_i \sin\delta_i \\ j\, n_i \sin\delta_i & \cos\delta_i \end{bmatrix} \qquad (6)$$

* The derivations of the equations which are cited in this section for computing R and T are given in section 21.4 or in references 9 and 10.

and where $j = \sqrt{-1}$ and $\begin{bmatrix} E \\ H \end{bmatrix}$ and $\begin{bmatrix} E' \\ H' \end{bmatrix}$ represent column vectors. As is shown in Section 21.4, Equation 20-(5) can readily be extended to more than one layer and thus this can be regarded as a recursion relationship. The reflectivity of a multilayer is computed by first writing down the matrix M_i for each layer according to Equation 20-(6). Then the matrix product is computed, as for example in Equation 21-(129) in Section 21.4. For example, if a stack consists of three layers, the matrix product M is

$$M = M_1 * M_2 * M_3 \tag{7}$$

where the symbol * denotes a matrix multiplication. The matrix product M has in general four elements:

$$M = \begin{bmatrix} A & j\,B \\ j\,C & D \end{bmatrix} . \tag{8}$$

The four variables, A, B, C, and D, are all real variables if all the films are non-absorbing. However, only three of the variables are independent, since the determinate of the matrix M is unity and hence $A \cdot D + B \cdot C = 1$. The reflectivity R is computed from

$$R = \frac{(X - U)^2 + (Y - V)^2}{(X + U)^2 + (Y + V)^2} \tag{9}$$

where

$$X = n_o A + n_o k_s B \qquad U = n_s D$$
$$Y = n_o n_s B \qquad V = C - k_s D \tag{10}$$

If the substrate is non-absorbing, i.e. $k_s = 0$, conservation of energy requires that $R + T = 1$ and in this case T can be written:

$$T = \frac{4}{2 + A^2 \frac{n_o}{n_s} + D^2 \frac{n_s}{n_o} + \frac{C^2}{n_o n_s} + B^2 n_o n_s} . \tag{11}$$

20.1.5.2.2 Whenever the optical thickness of any layer is $\lambda/2$, λ, $3\lambda/2$, 2λ, etc. the δ of that layer is 180°, 360°, 540°, etc. and the characteristic matrix for that layer reduces to the unit matrix:

$$M = \begin{bmatrix} 1 & 0 \\ 0 & 1 \end{bmatrix} . \tag{12}$$

However, the unit matrix has no effect upon the matrix product and hence this "half-wave" film does not contribute to the reflectivity of the multilayer stack at that wavelength. In other words, any "half-wave" layer acts as though it is absent from stack - that is, it is an absentee layer (see Section 21.2.14). As an example, consider the five-layer stack which is shown in Figure 20.6 . It is specified that at some wavelength, λ_o, optical thickness of layers #1 and #4 is $\lambda_o/2$. Then at λ_o layers #1 and #4 are absentee, and the reflectivity of the five layer stack is equivalent to the reflectivity of the three-layer stack shown in Figure 20.6 , which is the five-layer stack with layers #1 and #4 removed.

20.1.6 The computation of R and T at non-normal incidence.

20.1.6.1 Extension of the normal-incidence equations. Equations 20-(4), 20-(6), 20-(10) and 20-(11) strictly apply to normal incidence. However, they can be extended to include a non-absorbing multilayer stack at non-normal incidence. This is accomplished as follows: [13]

Step 1. Given the angle ϕ in the incident medium, the angle of refraction, θ_i, is computed from Snell's law.

Step 2. The "s" plane of polarization is considered first. The refractive index of the layer, n_i, as it appears explicitly in Equations 20-(4) and 20-(6) is replaced by an effective index,

$$n_{eff} = n_i \cos \theta_i . \tag{13}$$

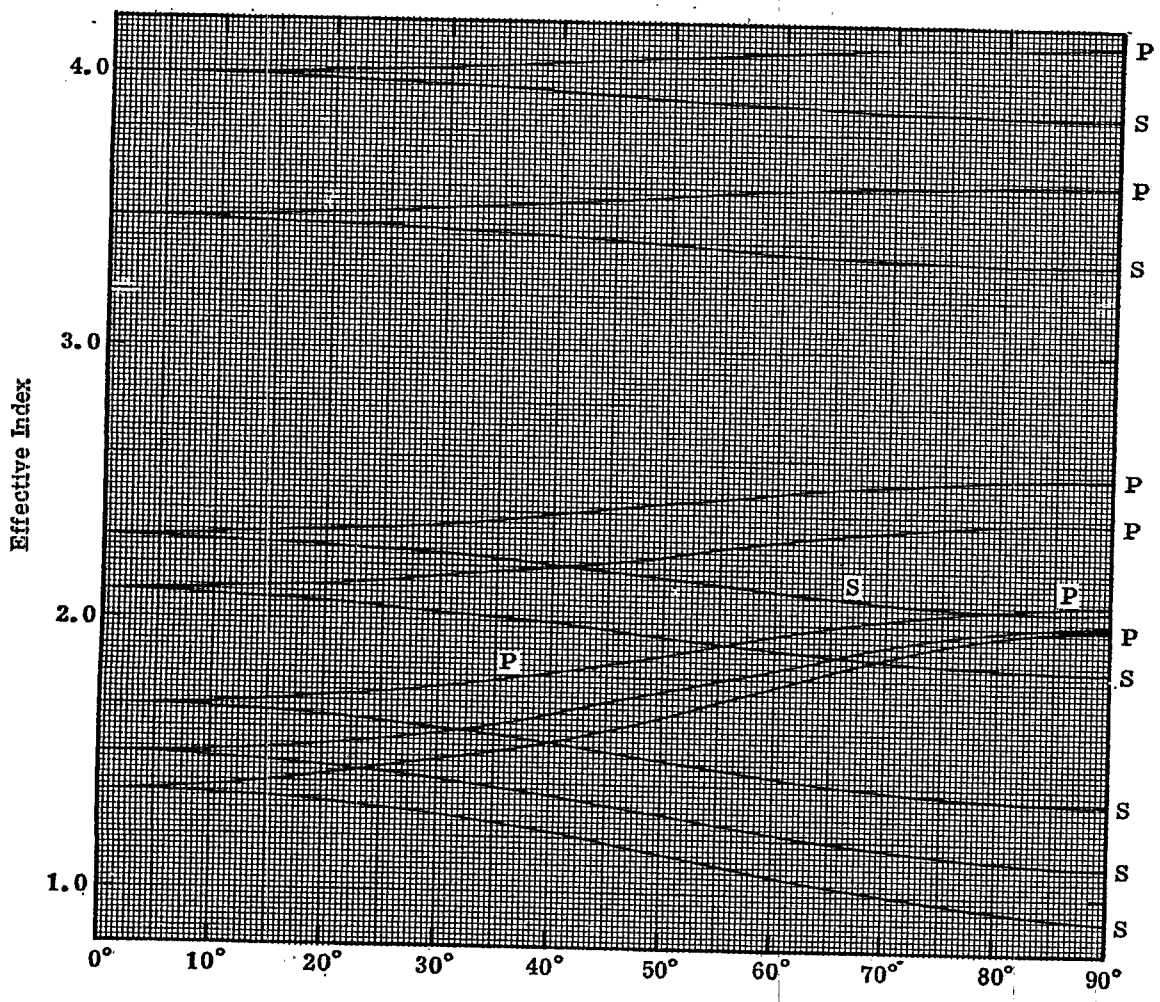

Figure 20.7 - The effective index (given by Eqs. 20.13 or 20.15) for the " p "and "s" planes of polarization, as a function of the angle of incidence in air.

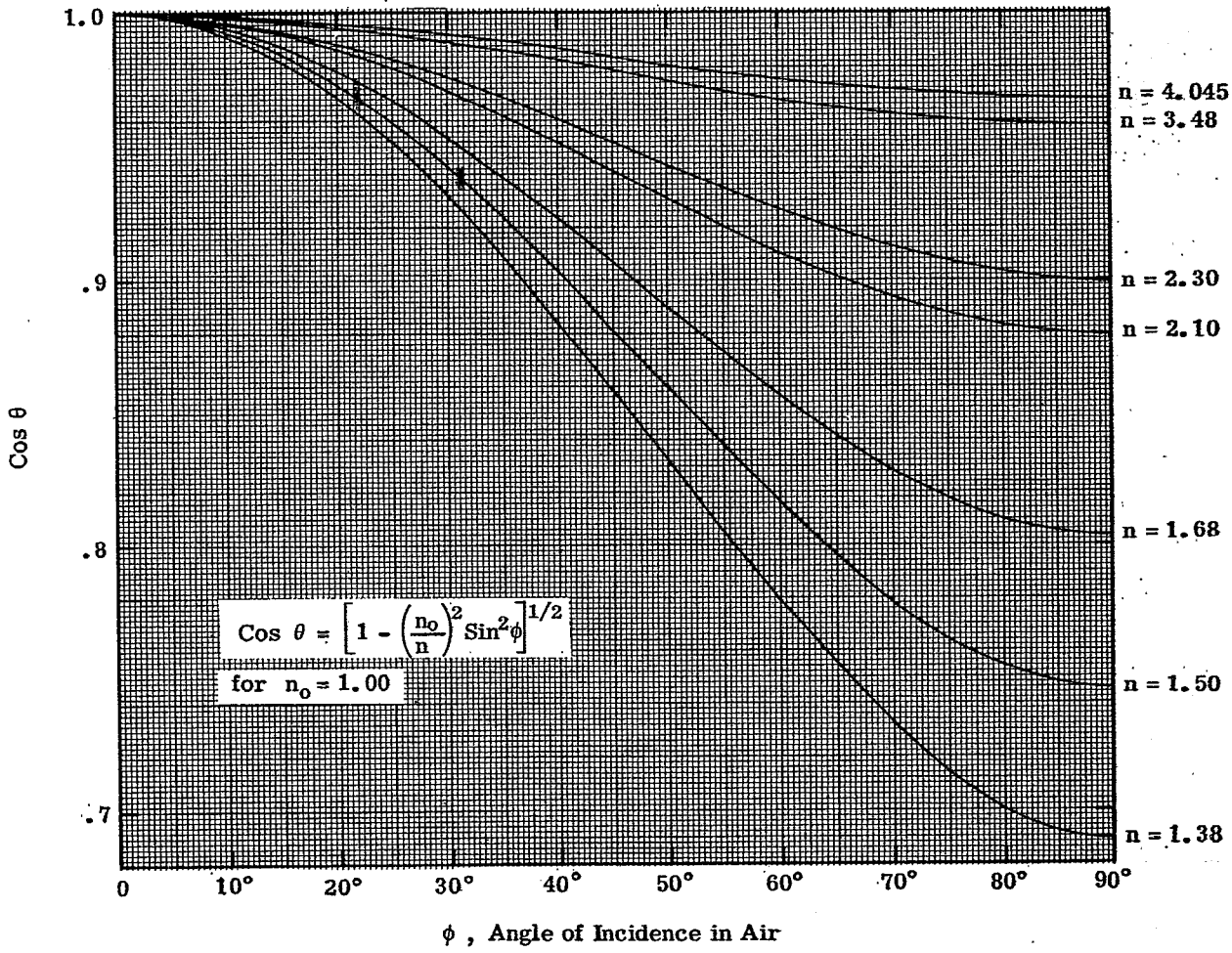

Figure 20.8 The effective thickness (normalized to 1.00 at normal incidence) as a function of the angle of incidence in air.

This substitution does not apply to the n_i which appears in Equation 20-(1). The indices n_o and n_s are replaced by the effective indices $n_o \cos \phi$ and $n_s \cos \chi$, respectively.

Step 3. The optical thickness of each layer is replaced by an effective thickness,

$$(n_i \; t_i)_{eff} = n_i \; t_i \; \cos \theta_i \; . \qquad (14)$$

Step 4. Having executed steps 1, 2, and 3, R_s and T_s are computed, using either the vector addition of amplitude method or the matrix method.

Step 5. The "p" plane of polarization is considered next. Rather than Equation 20-(13), we use for the effective index:

$$n_{eff} = n_i / \cos \theta_i \; . \qquad (15)$$

Again, Equation 20-(15) does not apply to the n_i in Equation 20-(1). The indices n_o and n_s are replaced by the effective indices $n_o / \cos \phi$ and $n_s / \cos \chi$, respectively.

Step 6. Having made the substitutions indicated in steps 3 and 5, R_p and T_p are computed, using either the vector method or the matrix method.

20.1.6.2 Use of the effective index.

20.1.6.2.1 Figure 20.7 shows the plot of the effective index as a function of ϕ for an incident medium of refractive index $n_o = 1.00$. As ϕ approaches 90°, the effective index approaches the limiting value of

$$n_{eff} = \sqrt{n_i^2 - n_o^2} \qquad (16)$$

and

$$n_{eff} = n_i^2 / \sqrt{n_i^2 - n_o^2} \qquad (17)$$

for the "s" and "p" planes of polarization, respectively. From Figure 20.7 we see that the effective index of a material with a large refractive index, such as germanium, changes by less than three percent between $\phi = 0$ and $\phi = 90°$. The materials with a lower index show a much larger change.

20.1.6.2.2 Figure 20.8 shows the fractional change in the effective thickness, $\cos \theta_i$, as a function of ϕ for various values of the index n_i. As one might expect, the change in the effective thickness between $\phi = 0$ and 90° is much greater for low-index materials than for high-index materials.

20.1.6.2.3 Since the effective thickness at oblique incidence is always less than at normal incidence, this means that the reflectivity and transmission peaks of multilayer filters shift to shorter wavelengths as ϕ increases. Although the author does not know of a rigorous proof of the statement made in the foregoing sentence. he has never found any exception to it in his work with multilayer filters.

20.1.6.3 Matched layers.

20.1.6.3.1 By definition, two or more layers in a multilayer stack are matched when there is a prescribed ratio between the optical thickness, $n_i \; t_i$, and hence between the δ_i of those layers.

20.1.6.3.2 As an example, consider the three-layer stack which is shown in Figure 20.9. For the purpose of this illustration, we shall arbitrarily define a matched condition to be:

$$n_1 \; t_1 \; : \; n_2 \; t_2 \; : \; n_3 \; t_3 \; = \; 1 \; : \; 2 \; : \; 2.5 \; . \qquad (18)$$

Equation 20-(18) states that when the optical thickness of the second layer is twice that of the first layer and the $n_3 \; t_3$ of layer three is 2.5 times $n_1 \; t_1$. If this film combination is tipped at an angle of 60°, then the optical thickness of each layer must be replaced by its effective thickness. Since the refractive index for each layer is different, the percentage change in the effective thickness is different. Referring to Figure 20.8 we see that the optical thickness of layer one is multiplied 0.98, layer two by 0.78, and layer three by 0.86.

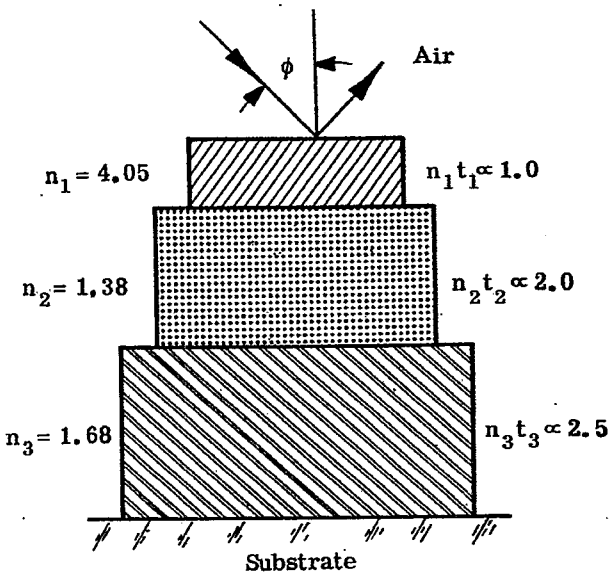

Figure 20.9 - Diagram of a three-layer stack. The layers are drawn proportional to their optical thickness.

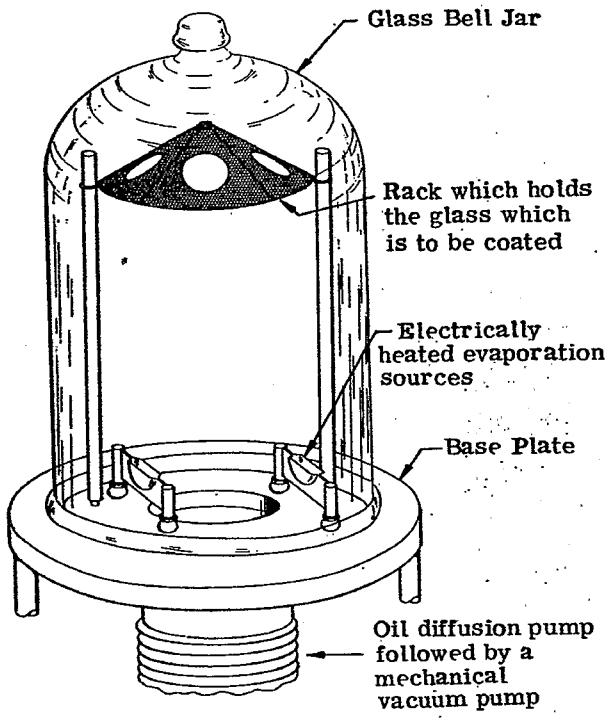

Figure 20.10 - The essential parts of an evaporator which is used to deposit thin films.

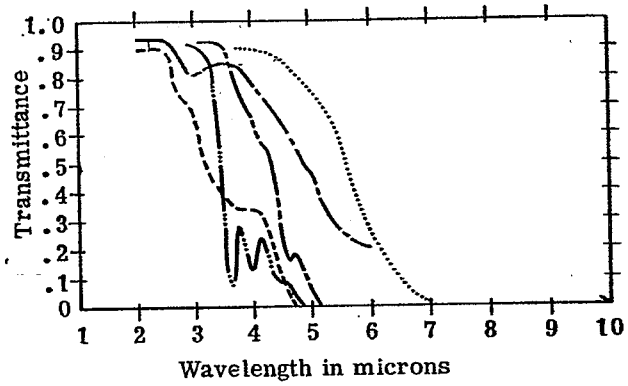

..... Sapphire, 2.6 mm

- - - - - Microglass, .005"

——— Quartz, 2 mm

- - - - - - - Corning No 0160, 2 mm

——— Vycor, 2 mm

Figure 20.11 - The optical transmission in the infrared of some substrate materials.

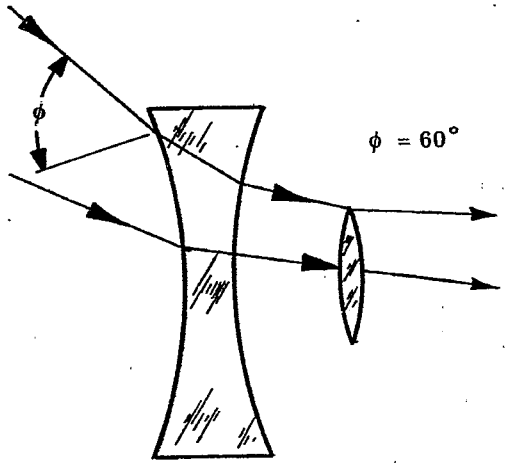

Figure 20.12 - The light is incident at a large angle upon the front surface of a wide-angle lens.

This means that at 60° incidence, the ratio of the thickness of the layers is no longer 1 : 2 : 2.5, but is

$$\left[n_1 \; t_1 \right] : \left[n_2 \; t_2 \right] : \left[n_3 \; t_3 \right] = 0.977 : 1.56 : 2.14 = 1 : 1.60 : 2.19 \qquad (19)$$

where the brackets $\left[\; \right]$ indicate "effective thickness". This means that the layers are no longer matched at 60° incidence, or for any other non-zero angle, for that matter. If all of the layers were composed of high refractive index materials, the deviation of the optical thickness ratios from the matched condition prescribed in Equation 20-(18) would be much smaller.

20.1.6.4 Layers matched at oblique incidence.

20.1.6.4.1 From the discussion in the foregoing subsection, we see that if the layers were deliberately made thicker in proportion to $\sec \theta_i$ then the layers are matched at non-normal incidence for a particular value of ϕ. In the foregoing example, if the $n_i \; t_i$ of the layers were in the ratio of

$$n_1 \; t_1 : n_2 \; t_2 : n_3 \; t_3 = 1.024 : 2.57 : 2.92 \qquad (20)$$

then at an incidence angle of 60° the layers will be matched with the prescribed ratio stated in Equation 20-(18).

20.1.6.4.2 It only makes sense to speak of matched layers provided there is more than one layer. In the case of a single layer if the $\delta_1 = 2\pi/\lambda \; (n_1 \; t_1)$ of that layer has some value at normal incidence, say, for example, 1.25 radians at some wavelength, λ_1. Then as ϕ increases, the effective thickness decreases. It is always possible to find some new wavelength λ_2, at which δ_1, is still 1.25 radians. If $n_o < n_1$, then λ_2 is less than λ_1. This shift to shorter wavelengths is clearly illustrated in reflectivity curves of single-layer reflecting coatings which are shown in Figure 20.20.

20.2 THE MANUFACTURE OF MULTILAYER FILTERS

20.2.1 Practical considerations. Using the computational methods which were described in 20.1.5, the spectral transmission and reflectivity of a given multilayer filter can be computed. However, if this filter is not to be a mere theoretical abstraction, but is to be actually manufactured, then we must keep in mind that there are certain practical problems which are encountered. Just as the lens designer is limited by the fact that the optical glasses which are presently manufactured have refractive indices within in a certain range, the films of a multilayer filter must be composed of materials which have certain specific values of refractive index.

20.2.2 Methods of deposition.

20.2.2.1 Progress in optical filming. Multilayer filters are manufactured by depositing solid films of various materials on an appropriate substrate. Although there are many methods which are used to deposit these films, such as chemical reaction in a vapor or liquid, sputtering, or anodization, the most important and widely-used methods is evaporation in a vacuum.* Consequently, progress in the production and manufacture of multilayer filters has for many years been related to advances in vacuum technology. Although the theory of multilayer filters has been known for more than a century, the production of such useful devices as antireflection coatings for lenses and silver-dielectric-silver interference filters did not start until the decade of the 1930's, when high-capacity oil diffusion pumps were developed which could evacuate a large volume to a pressure of less than 10^{-7} of atmospheric pressure. Antireflection coatings for lenses were used extensively during the Second World War. After the war, all-dielectric interference filters and multilayer beam splitters for use in the visible spectral region became commercially available. In the decade from 1950 to 1960, multilayer coatings have been produced for wavelengths as short as 110 mμ in the ultraviolet[15] and for wavelengths as long as 20μ in the infrared.[16]

20.2.2.2 The evaporator. Figure 20.10 shows the essential parts of an evaporator which is used to deposit thin films by evaporation in a vacuum. The circular pieces which are to be coated (i.e. the substrates) are placed in the holes in holder at the top of the chamber. The glass bell jar is sealed to the base plate and the entire chamber is evacuated by means of the oil diffusion pump and the mechanical pump to a pressure of less than 10^{-4} mm of mercury. The boats which contain the material which is to be evaporated are then electrically heated causing the material in the boat to evaporate and deposit in a thin solid film on the substrates. No mention has been made here of how the substrates are cleaned so that the films adhere well, or how the films are evaporated to a predetermined thickness. These topics are covered in detail in references 17 and 18.

* Methods of depositing thin films are summarized in reference 17.

MATERIAL	REFRACTIVE INDEX	TRANSMISSION RANGE	COMMENTS
Hot pressed Mg F_2 (Irtran 1)	1.37	200 mμ to 7.5 μ	
Calcium fluoride	1.42	180 mμ to 6 μ	
Barium fluoride	1.42	150 mμ to 13 μ	
Irtran 3	1.42	1000 mμ to 9 μ	
Fused quartz	1.46	180 mμ to 3.5 μ	1
Vycor (high-silica glass)	1.46	250 mμ to 3.5 μ	
Glass	1.51 to 1.70	320 mμ to 2.5 μ	2
Sapphire	1.70	<20 mμ to 7.5 μ	
Hot pressed ZnS (Irtran 2)	2.26	2000 mμ to 14 μ	
Arsenic trisulfide glass	2.40	800 mμ to 12 μ	
Irtran 4	2.40	1000 mμ to 20 μ	
Silicon	3.50	1100 mμ to 8 μ	
Germanium	4.05	1900 mμ to >22 μ	

NOTES:

1. The wavelength of the absorption edge in the ultraviolet depends upon the purity of the quartz.
2. In general, glasses with a lower refractive index are transparent to shorter wavelengths than glasses with a higher index. However, there are exceptions to this rule. Most glasses have a strong absorption band in the vicinity of 2.6 μ. Very thin glass plates (i.e. "cover slips") are transparent between 2.7 μ and 4.5 μ.

Table 20.1 - Common substrate materials.

MATERIAL	REFRACTIVE INDEX	RANGE OF TRANSPARENCY (See Note 10)		COMMENTS
		From	To	
Cryolite	1.35	<200 mμ	10 μ	1
Chiolite	1.35	<200 mμ	10 μ	1
Magnesium fluoride	1.38	230 mμ	5 μ	2, 3
Thorium fluoride	1.45	<200 mμ	10 μ	
Cerium fluoride	1.62	300 mμ	> 5 μ	4
Silicon monoxide	1.45 to 1.90	350 mμ	8 μ	5
Sodium chloride	1.54	180 mμ	> 15 μ	6
Zirconium dioxide	2.10	300 mμ	> 7 μ	2
Zinc sulfide	2.30	400 mμ	14 μ	7
Titanium dioxide	2.40 to 2.90	400 mμ	> 7 μ	8
Cerium dioxide	2.30	400 mμ	5 μ	2, 3
Silicon	3.50	900 mμ	8 μ	
Germanium	3.80 to 4.20	1400 mμ	> 20 μ	9
Lead telluride	5.10	3900 mμ	> 20 μ	

NOTES:

1. Both materials are sodium-aluminum fluroide compounds, but differ in the ratio of Na to Al and have different crystal structure. Chiolite is preferable in the infrared, because it has less stress than cryolite (see section 20.2.3.2.4).
2. These materials are hard and durable, especially when evaporated onto a hot substrate.
3. The long wavelength is limited by the fact that when the optical thickness of the film is a quarter-wave at 5 μ, the film cracks due to the mechanical stress (see 20.2.3.2.4).
4. There are other fluorides and oxides of rare earths which have refractive indices in this range from 1.60 to 2.0. See reference 22a.
5. The refractive index of SiO_x (called silicon monoxide) can vary from 1.45 to 1.90 depending upon the partial pressure of oxygen during the evaporation. Films with a refractive index of 1.75 and higher absorb at wavelengths below 500 mμ.
6. Sodium chloride is used in interference filters out to a wavelength of 20 μ. It has very little stress.
7. The refractive index of zinc sulfide is dispersive. [23]
8. The refractive index of TiO_2 rises sharply in the blue spectral region. [24]
9. The higher refractive index of 4.2 is given in reference 23. The lower index is quoted by Dr. A. F. Turner of Rochester, N.Y. (private communication).
10. The range of transparency is for a film of quarter-wave optical thickness at this wavelength. These values are approximate and also depend quite markedly upon the conditions in the vacuum during the evaporation of the film.

Table 20.2 - Commonly used thin film materials.

20.2.3 Substrates for multilayer filters.

20.2.3.1 Optical characteristics. If transmission-type filters are used, the substrate must not absorb in the spectral transmission range of the filter. Very often the fact that a substrate material absorbs in certain wavelength regions can be used to advantage. For example, suppose a filter is required for the infrared which has a high transmission at wavelengths longer than 7.0 μ, and a high attenuation at shorter wavelengths. If a germanium substrate were used, then the germanium would absorb at wavelengths shorter than 1.8 μ. Thus the multilayer which is deposited on the germanium would be required to attenuate between 1.8 μ and 7.0 μ. On the other hand, if a substrate of silicon were used, which absorbs at wavelengths below 1 μ, then the multilayer coatings would have to attenuate over a wider range of wavelengths and hence the multilayer coatings would be more complex and expensive to fabricate. The infrared transmission of some optical materials which can be used as multilayer substrates is shown in Figure 20.11. Ballard, McCarthy,and Wolfe [19] have published transmission data on other materials. The refractive index of the substrate is also important. A high-index substrate has high reflection losses at its surfaces if it is not properly coated with antireflection coatings.

20.2.3.2 Chemical and physical properties.

20.2.3.2.1 Certain substrate materials, such as sapphire and fused quartz are hard, durable, and relatively inert to chemical attack. Other materials, notably the rare-earth glasses and some of the alkali halide crystals, are rather soft and delicate. Multilayer coatings are deposited on a substrate and then sometimes rejected because their optical transmission does not meet specifications. If the substrate is expensive, it is desirable to remove the coating from the substrate and recoat it. It is advantageous to use a substrate which is chemically inert, because in this case the coating can be removed with acid or alkali solutions. Otherwise, it is necessary to remove the coating mechanically by the more expensive method of optical polishing.

20.2.3.2.2 The adhesion of the coatings to the substrate is also important. For example, sapphire is a hard and durable substrate, but it has the disadvantage that some thin film materials do not adhere well to its surface.

20.2.3.2.3 The fragility of the substrate is also a consideration. Some thin film materials, such as magnesium fluoride and cerium dioxide, are much harder and more durable when they are evaporated onto a substrate which is heated to a relatively high temperature, often as high as 300° C. It is not an easy task to heat a large piece of optical glass to this temperature without fracturing it, whereas a fused quartz substrate could easily withstand this heating.

20.2.3.2.4 The number of available substrate materials is legion and an exhaustive list would be quite long. Some of the commonly used materials are listed in Table 20.1.

20.2.4 Thin film materials.

20.2.4.1 Optical properties. In most cases, the thickness and refractive index of the films in a multilayer filter are chosen from theoretical considerations. In order to translate this design into a practical filter, it is necessary to select for each layer a thin film material which can be evaporated to the desired thickness and which has a refractive index which is close to the theoretical value. We see from Table 20.2 that in the visible spectral region, non-absorbing films are available with a refractive index in the range from 1.35 to 2.70. In the infrared, materials such as silicon, germanium, and lead telluride are available which have a considerably higher refractive index. In most cases the film does not have the same refractive index as the bulk material. A comprehensive list of thin film coating materials is compiled by Heavens. [22]

20.2.4.2 Physical properties.

20.2.4.2.1 In some applications it is possible to protect a multilayer by cementing on top of it another transparent plate. Thus most silver-dielectric-silver FP type filters (described in 20.10.3.1) are protected in this manner by "sandwiching" the multilayer between two glass plates. If a multilayer is protected, then it is possible to use materials in the stack which are "soft", such as antimony trioxide. In other cases, the multilayer must be "hard" to resist scratching and abrasion because it is exposed and subjected to extreme environmental conditions. Such a coating is called a "hard coating" or simply a "hard coat". A commonly used means of testing the durability of a multilayer is to see if it can withstand rubbing with a soft rubber eraser. Certain coating materials, notably magnesium fluoride, silicon monoxide, cerium dioxide, titanium dioxide, germanium, and silicon, are extremely hard and durable. This does not imply that these materials are the only "hard" coatings. In fact, we must resist the temptation to classify every coating material as either "hard" or "soft" and remember that there is a continuous variation of the durability between the extremely hard materials mentioned in the foregoing sentence and a fragile material such as antimony trioxide. The durability of the coating also depends markedly on the conditions in the vacuum during the evaporation. For

example, techniques have been developed to evaporate zinc sulfide so that it forms a quite durable layer. The durability of a multilayer filter depends not only on the materials, but also on the technical competence of its manufacturer.

20.2.4.2.2 Resistance to moisture. Some coating materials, such as magnesium fluoride and silicon monoxide, can be immersed in water and even in hot saline solutions for some length of time, with no deleterious effects. Other materials, such as cryolite or chiolite, have quite desirable optical properties, but are not widely used as antireflection coatings because they are slightly water soluble. Even though some coating materials are relatively insoluble, moisture can still destroy a multilayer by destroying the bond between the films and the substrate.

20.2.4.2.3 Adhesion to the substrate. It is important that the multilayer coating adhere strongly to the substrate. This is especially true of coatings which have a mechanical stress. Over the years a vast amount of lore has been acquired by the manufacturers of thin film coatings as to what film materials adhere well to various substrates. The adhesion of a film to a substrate depends quite markedly such parameters as the cleanliness of the substrate, its temperature during the evaporation, and the partial pressure of residual gases in the vacuum chamber during the evaporation. There is no substitute for experience in acquiring the "know-how" of producing durable and adherent coatings, although Holland[18] is a source of much useful information.

20.2.4.2.4 Mechanical stress.[20] Early workers found that after a multilayer filter had been evaporated and was moved from the vacuum into the humid air of the laboratory, the entire coating would separate from substrate or craze with many fine cracks. Further investigation showed that this was due to a mechanical stress in the film which is proportional to the thickness of the film.[20] This stress can be demonstrated quite easily by observing that a thin substrate bends as a film is deposited upon it. The substrate bends concave towards the evaporation source if the stress is compressive. It was found that almost all thin film materials have a tensive stress; one exception is zinc sulfide, which has a compressive stress of 0.02 (in arbitrary units). Magnesium fluoride, on the other hand, has a tensive stress of 0.11 units.

20.2.4.2.5 Limit on the thickness[20] It is clear that this stress is one of the principal factors which limits the thickness of films which are deposited by evaporation. When the adhesion of the film to the substrate can no longer balance the stress which builds up as the film grows thicker during an evaporation, the film either parts from the substrate or crazes. Films of either magnesium fluoride or cerium dioxide tend to craze when their physical thickness exceeds one micron. Thus film materials which have a high stress are limited in their application in the infrared, where the films must be quite thick. Another factor which limits the use of some films in the infrared is called the clouding effect. This effect is not observed in a film which is relative thin, say 100 mμ in physical thickness, and hence it is transparent. However, as a much thicker film is evaporated, the film becomes cloudy and scatters light like a ground slab of glass. This is presumably due to the growth of large crystallites in the film which scatter light.

20.2.4.2.6 An effective way of avoiding stress is to use thin film materials which have little or no stress, such as silicon monoxide or sodium chloride. The latter material could only be used in the laboratory, due to its water solubility. Another approach is to deposit a film with compressive stress next to a film with a tensive stress, the thicknesses of each layer being chosen so that the total stress of the pair of films is zero.[20,21]

20.3 ANTIREFLECTION COATINGS

In this section we shall consider the problem of reducing the reflectivity of a dielectric substrate by the addition of one or more non-absorbing thin films. In order to determine how much the transmission of the substrate has been improved by the addition of the multilayer coating, we must first consider the reflectivity of the uncoated substrate.

20.3.1 Reflectivity of an uncoated surface. The reflectivity R for a bare dielectric surface at normal incidence is given by the Fresnel coefficient,

$$R = 1 - T = (n_o - n_s)^2 / (n_o + n_s)^2 \qquad (21)$$

where n_o is the refractive index of the incident medium (which is usually air) and n_s is the refractive index of the substrate. If the light is obliquely incident, then Equation 20-(21) still applies if the appropriate effective index is used in place of n_o and n_s .

20.3.2 Choice of type of coating.

20.3.2.1 Number of layers. In Section 20.3, the spectral reflectivity of antireflection coatings consisting

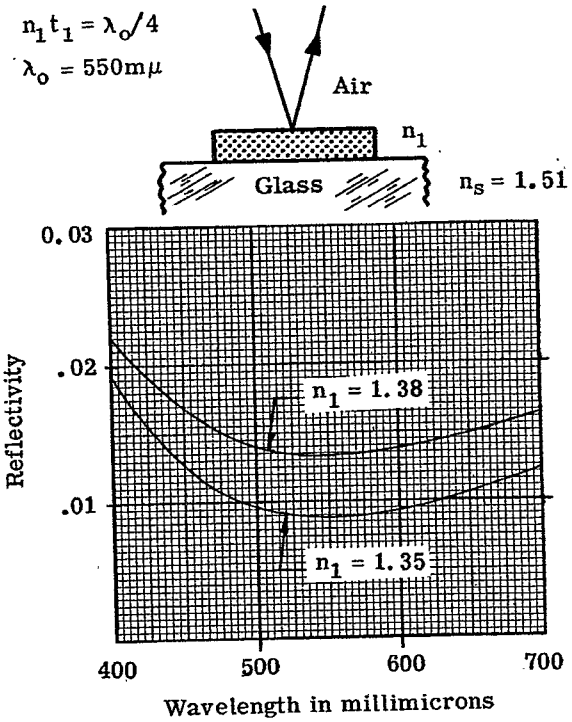

Figure 20.13 - Computed spectral reflectivity of single layers at normal incidence.

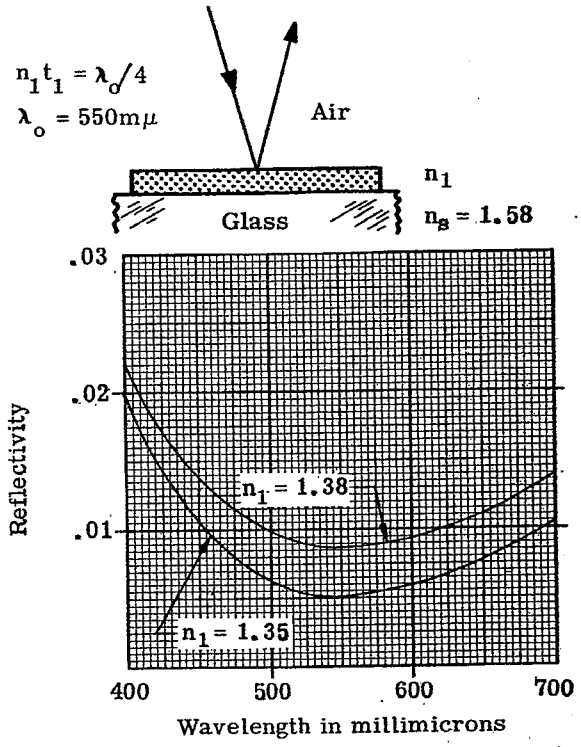

Figure 20.14 - Computed spectral reflectivity of single layers at normal incidence.

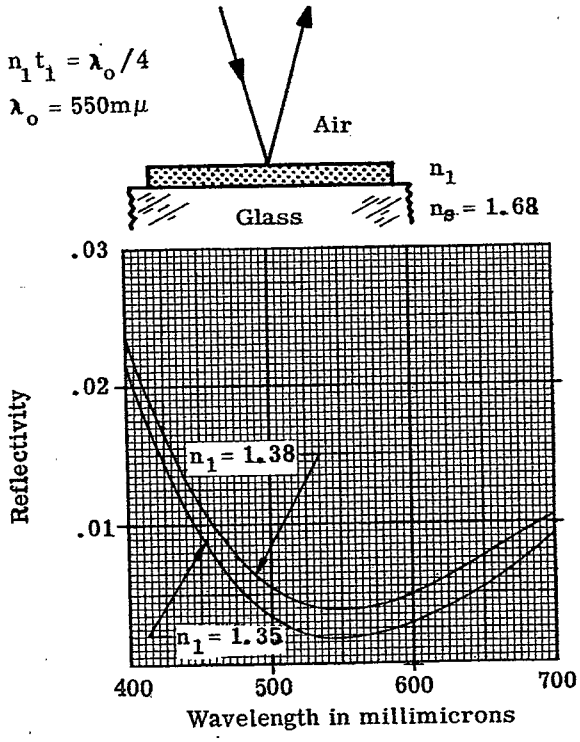

Figure 20.15 - Computed spectral reflectivity of single layers at normal incidence.

of one, two, or three layers is considered. Coatings consisting of more than three layers can be devised, but coatings with less than three layers have proved adequate for most applications; hence coatings with more layers are rarely used. In deciding what type of coating to use, the following points are usually considered:

20.3.2.2 Spectral reflectivity. The type of coating which is selected is often determined by breadth of the spectral region, over which the surface is to have a low reflectivity. For example, suppose that a lens with a large number of elements is used to image a source which emits a considerable amount of radiant energy in the narrow wavelength range from 500 mμ to 550 mμ and a negligible amount of radiant energy at other wavelengths. The best type of antireflection coating for the glass surfaces of this lens would be the two-layer coating which is described in Section 20.3.4.3.2. This coating has a very low reflectivity over a narrow wavelength region and a reflectivity which rises sharply outside of that region. On the other hand, if the source were to emit radiation over a much broader spectral region, say from 400 to 800 mμ, then other types of coatings should be considered, such as a single-layer or three-layer coating, which have a low reflectivity over a much wider wavelength region.

20.3.2.3 Angle of incidence. The reflectivity of all thin film coatings changes with the angle of incidence of the light. The type of antireflection coating which is selected might depend upon the angle of incidence of the light and the amount of convergence in the beam. For example, suppose that a coating is selected for the surfaces of the large negative lens which is the first element in a wide-angle camera lens, as shown in Figure 20.12. The angle of incidence ϕ on the first surface of this lens can easily be as high as sixty or seventy degrees. Thus if excessive vignetting is to be avoided, the antireflection coating on that surface should have a low reflectance at high angles of incidence as well as at normal incidence.

20.3.2.4 Cost. The cost of an antireflection coating is related to complexity of the equipment necessary to evaporate the layers to a prescribed thickness and also to the number of layers in the coating. For example, single-layer coatings of magnesium fluoride are quite easy to produce. The thickness of the magnesium fluoride layer can be easily determined visually during the coating process by examining the color of the reflected light. There are many facilities which have the capability of depositing these coatings because they are quite easy to produce. The production of a three-layer coating requires more elaborate equipment, such as photoelectric monitoring equipment to measure the thickness of the layers and hence the coatings are more expensive.

20.3.3 Single-layer coatings.

20.3.3.1 Basic equations.

20.3.3.1.1 The reflectivity of a dielectric surface coated with a single layer of refractive index n_1 is,

$$R = 1 - T = \frac{a_1 \cos^2 \delta_1 + a_2 \sin^2 \delta_1}{a_3 \cos^2 \delta_1 + a_4 \sin^2 \delta_1} \qquad (23)$$

where

$$a_1 = (n_o - n_s)^2 \qquad a_2 = (n_1 - n_o\, n_s/n_1)^2$$

$$a_3 = (n_o + n_s)^2 \qquad a_4 = (n_1 + n_o\, n_s/n_1)^2$$

where n_o, n_s, and δ_1 have been defined previously in Section 20.1.3.2. The foregoing equation can be derived from Equations (6), (9), and (10) in Section 20.1.5.2. From Equation (23) one can see that when $n_1 t_1 = \lambda/2, 3\lambda/2, 5\lambda/2$, etc., δ_1 is 180°, 360°, 540°, etc. and hence the layer is an absentee layer (defined in 20.1.5.2.2). In this case, the reflectivity is the same as an uncoated surface and Equation (23) reduces to Equation (21).

20.3.3.1.2 When the $n_1 t_1 = \lambda/4, 3\lambda/4, 5\lambda/4$, etc., the reflectivity is either a maximum or a minimum and is given by

$$R_m = \left[\frac{n_1^2 - n_o n_s}{n_1^2 + n_o n_s} \right]^2 . \qquad (24)$$

Some curves of the spectral reflectivity of a single layer on a dielectric substrate are shown in Figures 21.11, 21.12, and 21.13. In Section 20.3, however, we will only consider the case where the reflectivity

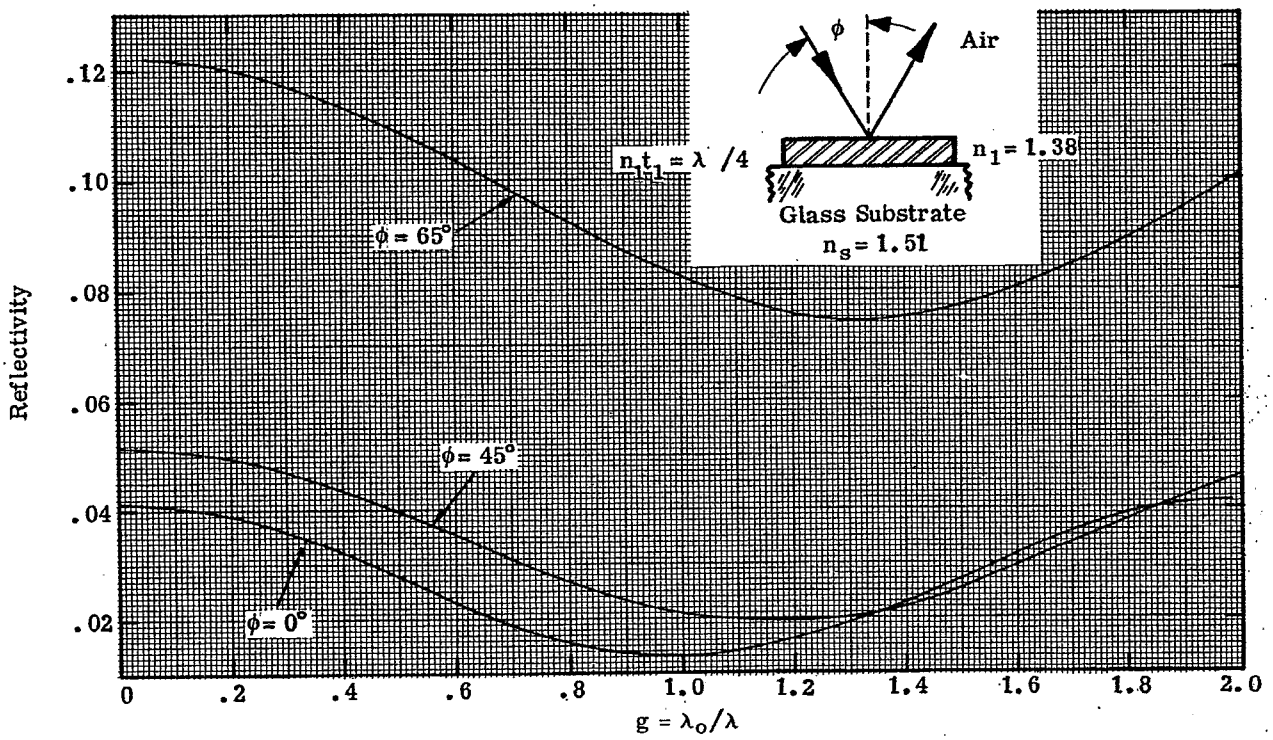

Figure 20.16- Computed spectral reflectivity at various angles of incidence of a single-layer antireflection coating.

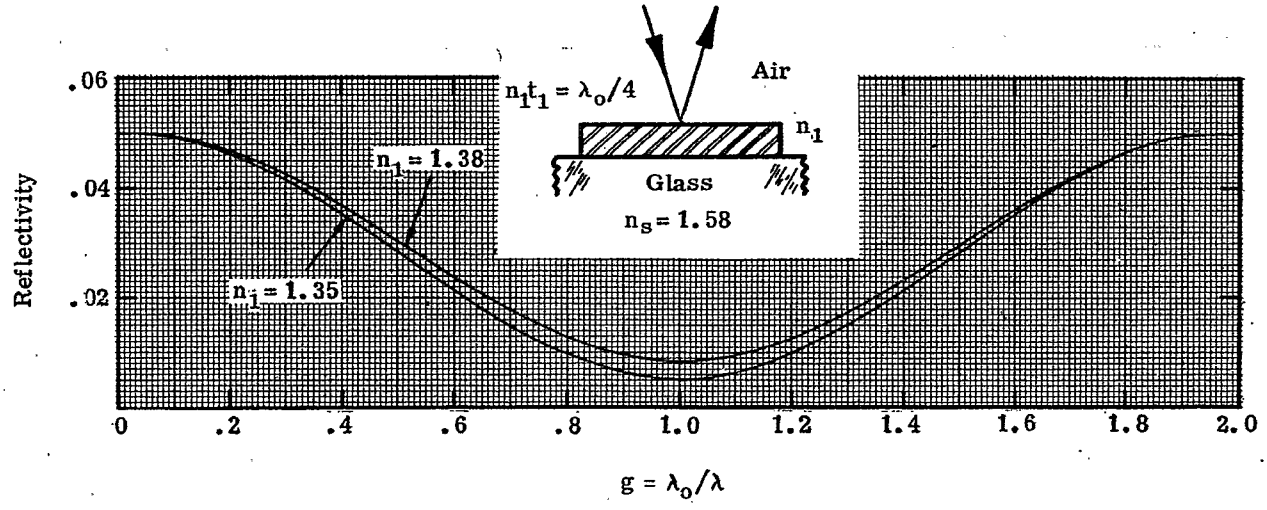

Figure 20.17- Computed spectral reflectivity at normal incidence of a single-layer antireflection coating.

is a minimum, which occurs when

$$n_o > n_1 > n_s \quad \text{or} \quad n_o < n_1 < n_s \ . \tag{25}$$

It is evident from Equation (24) that the reflectivity is zero when

$$n_1 = \sqrt{n_o \, n_s} \ . \tag{26}$$

20.3.3.2 Coatings for substrates with low refractive index.

20.3.3.2.1 We will consider single-layer antireflection coatings for substrates which have a refractive index in the range from 1.5 to 1.7, which includes most of the optical materials which are commonly used in the visible, near-infrared and near-ultraviolet. Crown glass and fused quartz have a refractive index which is close to 1.50, while dense flint glass and sapphire have a refractive index of 1.70.

20.3.3.2.2 In order to obtain a coating which would produce zero reflectivity at a surface between air and glass of refractive index 1.51 at some particular wavelength, say 550 mμ, it is necessary to deposit a film which has an optical thickness of a quarter-wave, three-quarter wave, etc. at 550 mμ and a refractive index given in Equation (26), namely 1.23. No durable coating material has been found which has a refractive index of this low a value. Thus a single-layer coating on such a substrate is a compromise between a coating which is hard and durable and a coating which has an extremely low, if not zero, reflectivity. Two commonly used low-index films are magnesium fluoride (index 1.38) and cryolite (index 1.35). The cryolite film produces a lower reflectivity than the film of magnesium fluoride, because of the lower refractive index of the former. This advantage, however, is offset by the superior physical properties of the magnesium fluoride film. Cryolite films are soft and slightly water soluble, whereas magnesium fluoride films are quite hard and durable, especially when evaporated onto a hot substrate.

20.3.3.2.3 Figures 20.13, 20.14, and 20.15 show the computed spectral reflectivity of some antireflection coatings of both magnesium fluoride and cryolite on substrates of refractive index 1.51, 1.58, and 1.68. The reflectivity of a single uncoated surface at normal incidence in each of these cases is 4.12%, 5.05%, and 6.44%, respectively. The optical thickness of the film is $\lambda_o/4$ at λ_o = 550 mμ so that the minimum reflectivity is in the green region of the spectrum where the eye is most sensitive. Also, 550 mμ is in the center of the visible spectrum (i.e. 400 mμ to 700 mμ) on a wavelength scale. However, 550 mμ is not in the center of the visible spectrum on a wave number (frequency) scale and hence the reflectivity in Figures 20.13, 20.14, and 20.15 is higher at 400 mμ than at 700 mμ. The curves are not symmetrical, about λ_o because they are plotted on a wavelength rather than on a wave number (frequency) scale on the abscissa. The reflectivity of the cryolite coating is lower than the magnesium fluoride throughout the visible spectral region. The minimum reflectivity, R_m, decreases as the index of the substrate progresses from 1.51 to 1.68, because the condition in Equation (26) becomes closer to being satisfied.

20.3.3.2.4 The spectral reflectivity curves shown in Figures 20.13, 20.14, and 20.15 are useful because magnesium fluoride films are used so extensively to coat lenses in the visible spectral region. However, the reflectivity is shown only for a limited spectral region and for a film which has a quarter-wave optical thickness at a particular wavelength, namely 550 mμ. Suppose that a lens is designed to transmit radiant energy not only in the visible, but also in the near infrared to 950 mμ. If a designer wanted to know the reflectivity of a coated surface at 950 mμ, the data in Figures 20.13, 20.14, and 20.15 are of little use to him. Of course, he could compute the reflectivity at this wavelength from Equation (23), but it is much easier to obtain information from a graphical presentation. Suppose that a lens images radiant energy upon a detector which has a maximum response at a wavelength of 700 mμ. This means that the antireflection coatings should have a minimum reflectivity at 700 mμ and hence reflectivity versus wavelength plot depicted in Figures 20.13, 20.14, and 20.15 could not be directly used.

20.3.3.2.5 In order to circumvent the difficulties mentioned in the foregoing paragraph, it is useful to plot the reflectivity as a function of dimensionless parameter, $g = \lambda_o/\lambda$, which is proportional to frequency. Here λ_o is the wavelength at which optical thickness of the film is a quarter-wave. Figures 20.16, 20.17, and 20.18 depict such a plot, for a single layer of magnesium fluoride deposited on substrates of refractive index 1.51, 1.58, and 1.68, respectively. The R_{av} at non-normal incidence is shown for substrates of index 1.51 and 1.68. More extensive data for cryolite is not shown because it is not widely used as an antireflection coating because of the reasons mentioned in 20.3.3.2.2. When plotted versus "g", the reflectivity has even symmetry about $g = 1.0$ (at normal incidence).

20.3.3.2.6 Several examples are given on how these curves are used to compute the reflectivity at a wavelength λ of a single-layer coating which has $n_1 t_1 = \lambda_o/4$.

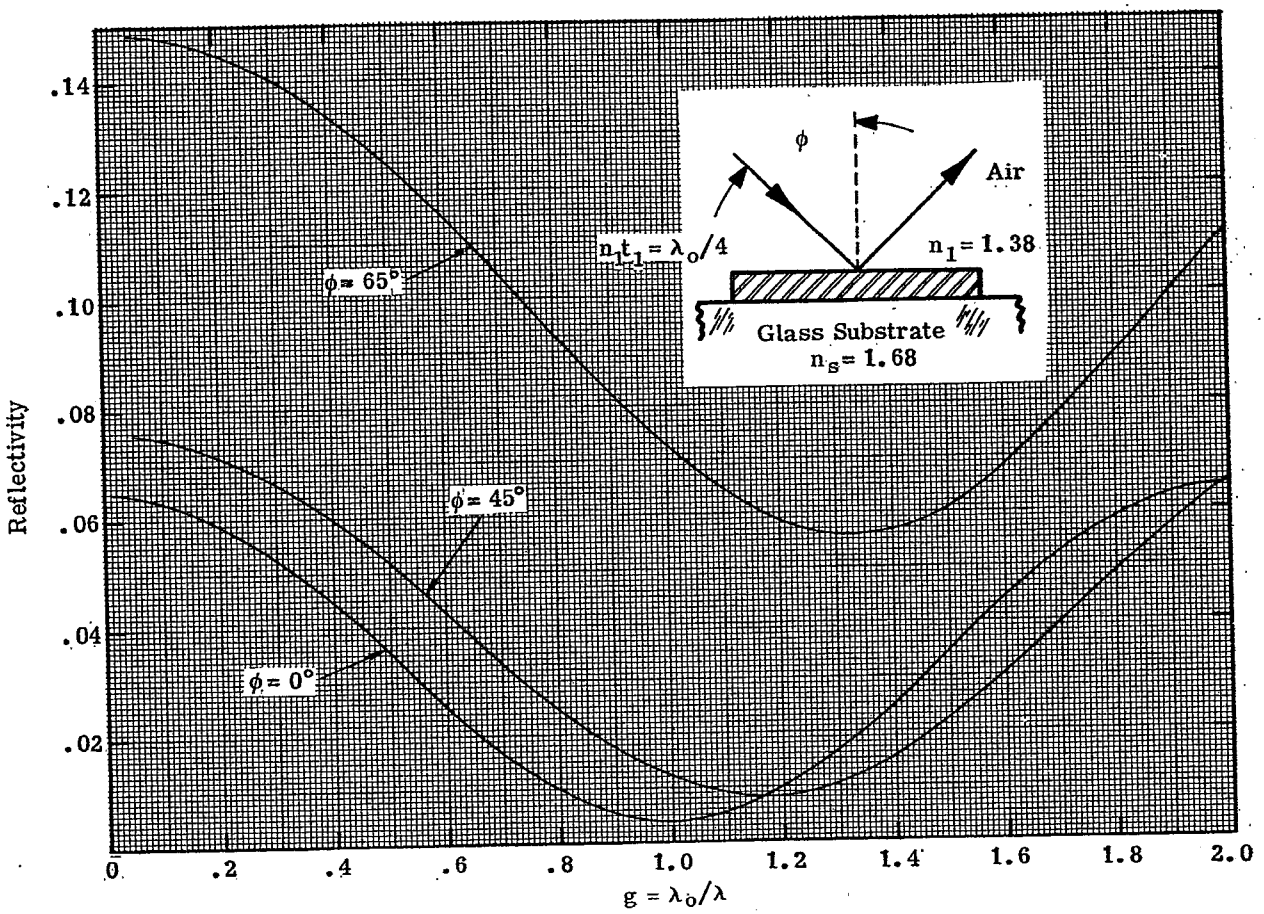

Figure 20.18 - Computed spectral reflectivity at various angles of incidence of a single-layer antireflection coating.

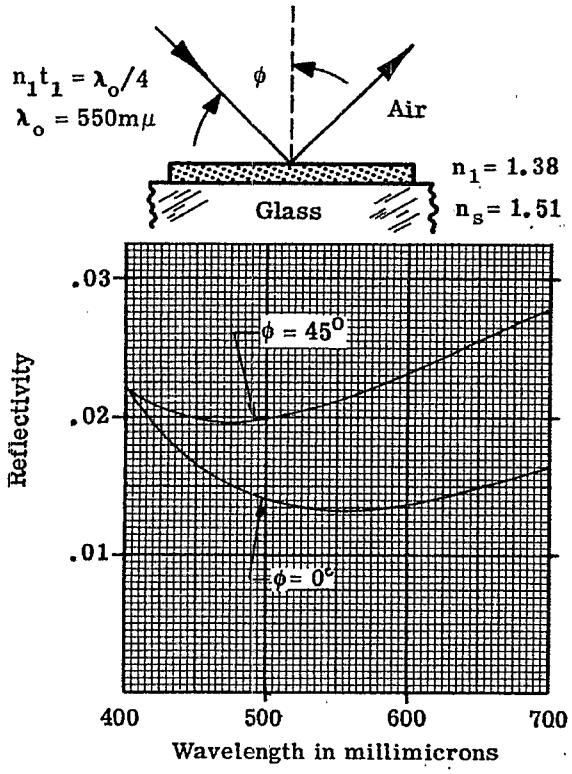

Figure 20.19 - Computed spectral reflectivity of a single layer at $\phi = 0$ and $\phi = 45^\circ$.

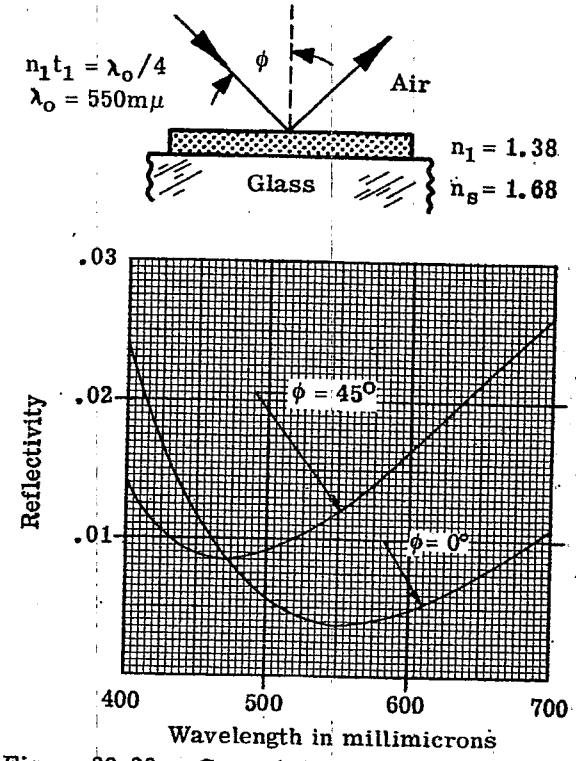

Figure 20.20 - Computed spectral reflectivity of a single layer at $\phi = 0$ and $\phi = 45^\circ$.

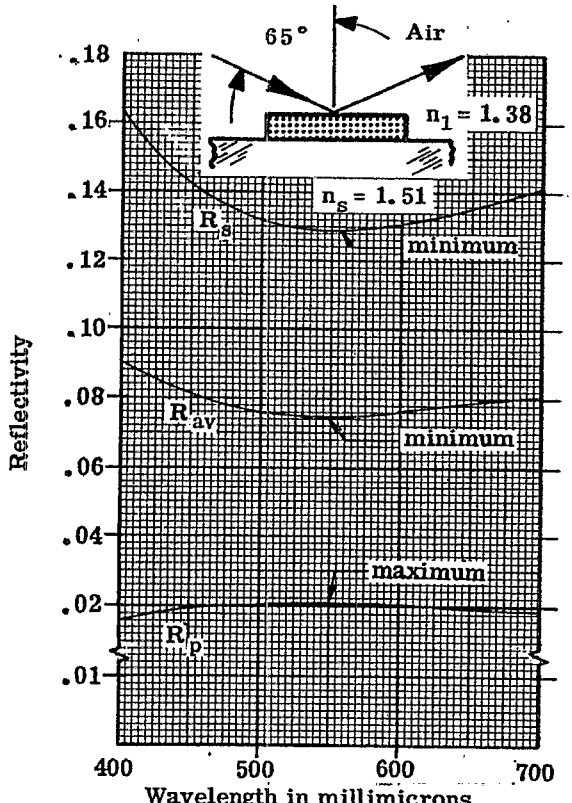

Figure 20.21 - Computed R_s, R_p, and $R_{av} = 1/2\ (R_p + R_s)$ at $\phi = 65^\circ$. The scale of the ordinate changes at 0.02.

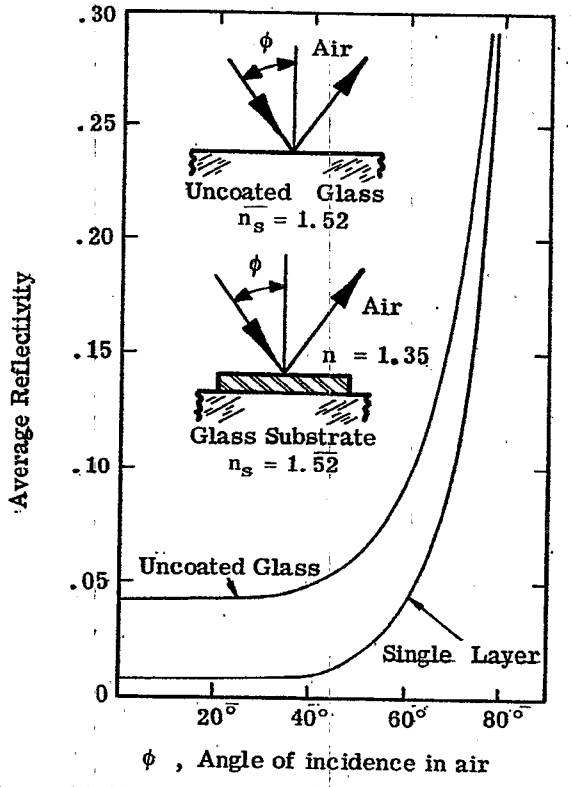

Figure 20.22 - Angle of incidence ϕ versus R_{av} of uncoated glass and the minimum R_{av} of the same glass coated with a single layer.

Example (a) A glass substrate of index 1.51 is coated with a single-layer magnesium fluoride antireflection coating with a minimum reflectivity at 700 mμ. What is the reflectivity at 950 mμ?

Solution: A quarter-wave film with λ_o = 700 mμ, has a minimum R at λ_o. Then at λ = 950 mμ, $g = \lambda_o/\lambda$ = 700/950 = 0.737. From Figure 20.16, at g = .737 R = .017.

Example (b) For the same coating and substrate, what is the reflectivity at 400 mμ?

Solution: Here $g = \lambda_o/\lambda$ = 700/400 = 1.75, and from Figure 20.16, R = .038.

20.3.3.2.7 The reflectivity versus "g" curves are periodic and at normal incidence the curve repeats at g = 2.0, 4.0, 6.0, etc. This fact can be used to find the reflectivity at values of "g" outside the range of the graphs. Example: For the thin film coating described in Paragraph 20.3.3.2.6, what is the reflectivity at 300 mμ? Here $g = \lambda_o/\lambda$ = 700/300 = 2.33. Due to the periodicity, the reflectivity at g = 2.33 is the same as at g = 0.33 and from Figure 20.16 the reflectivity is 0.035.

20.3.3.3 Coatings for substrates with low refractive index, at non-normal incidence.

20.3.3.3.1 As is discussed in Section 20.1.6, Equations (23), (24), and (26) can be used at non-normal incidence, provided that an effective thickness is substituted for the optical thickness and the effective index appropriate to each plane of polarization is used. Regardless the angle of incidence, the reflectivity curve still has either a maxium or a minimum when the phase of retardation of the layer δ_1 = 90°, 270°, etc. Because of the reasons cited in 20.1.6.4.2, the minimum in reflectivity curve shifts towards shorter wavelengths (i.e. the blue). This shift of the minimum reflectivity to shorter wavelengths is illustrated in Figures 20.19 and 20.20, which depict the spectral reflectivity of a layer of magnesium fluoride, ($n_1 t_1 = \lambda_o/4$, λ_o = 550 mμ) on glass substrates of index 1.51 and 1.68 respectively. At non-normal incidence, R_{av} is shown. The minimum reflectivity shifts from 550 mμ at ϕ = 0 to λ_2 = 465 mμ at ϕ = 45°. This shift can also be determined from the graph of the effective thickness versus ϕ in Figure 20.8. From this graph we find that $(n\ t)_{effective} = n_1 t_1 \cos\theta_1 = 0.859\ n_1 t_1$ for a film index of 1.38. Given λ_o of 550 mμ, we determine that $\lambda_2 = (.859)(550) = .472$ mμ.

20.3.3.3.2 The effective indices at ϕ = 65° of the substrate, film, and incident medium of a single-layer MgF_2 coating on glass, are shown in Table 20.3. Its spectral reflectivity in each plane of polarization and the R_{av} is shown in Figure 20.21. The optical thickness of the film is made thicker than $\lambda_o/4$ at normal incidence so that at ϕ = 65° the minimum reflectivity occurs at λ_o = 550 mμ. It is interesting to note that R_p attains a maximum rather than a minimum at λ_o. The reason for this is seen in Table 20.3. The effective indices in the "p" plane of polarization do not satisfy the condition for a minimum stated in Equation (25). However, the R_s curve drops to a sharp minimum at λ_o and hence the R_{av} has a minimum, rather than a maximum, at λ_o. Figures 20.16 and 20.18 show the average reflectivity at ϕ = 45° and ϕ = 65° of a film of refractive index 1.38 deposited on glass of index 1.51 and 1.68, respectively. The optical thickness is $\lambda_o/4$ at ϕ = 0. These curves have even symmetry about their minimum. For example, the curve in Figure 20.16 at ϕ = 65° has a minimum at g = 1.32 and hence the reflectivity is the same at g = 2.12 and g = 0.52.

20.3.3.3.3 Graphs of the average reflectivity, such as are shown in Figures 20.16, 20.18, 20.19 and 20.20, are useful in the case where the incident light is unpolarized and where the detector is not sensitive to polarization, as for example a photographic plate. If the incident light is polarized, or if polarization has been introduced by other elements of an optical system, such as prisms and beam splitters, then it is necessary to compute the reflectivity in each plane of polarization separately, as in Figure 20.27.

20.3.3.3.4 Single-layer antireflection coatings (which satisfy Equation (25)) on glass always decrease the average reflectivity to lower values than the uncoated surface. This is illustrated in Figure 20.22 which shows a plot of the angle of incidence versus R_{av} of an uncoated glass surface, and the minimum reflectivity of the same substrate covered with a single layer of refractive index 1.35. At any angle of incidence, whether it be 20° or 80°, the coated surface has a lower R_{av} than the bare substrate. This subject of antireflection coatings at non-normal incidence is treated in more detail in references 25 and 26.

20.3.3.4 Coatings for substrates with a higher refractive index.

20.3.3.4.1 Single-layer antireflection coatings for substrates with a higher refractive index are considered, which includes materials which are used principally in the infrared, such as arsenic trisulfide glass (index 2.40), silicon (index 3.48), and germanium (index 4.045). The refractive index of all of these materials changes with wavelength. The foregoing values are representative of some mean values in the infrared and even though the calculations do not account for the dispersion in the refractive index, they give some idea of what can be accomplished in the way of antireflection coatings for these materials.

LAYER	INDEX AT NORMAL INCIDENCE	EFFECTIVE INDEX AT $\phi = 65^\circ$	
		POLARIZATION P	POLARIZATION S
Incident medium (Air)	1.00	2.366	0.423
Magnesium fluoride	1.38	1.83	1.041
Glass substrate	1.51	1.89	1.208

Table 20.3 - The effective indices at $\phi = 65^\circ$ incidence of a single-layer antireflection coating.

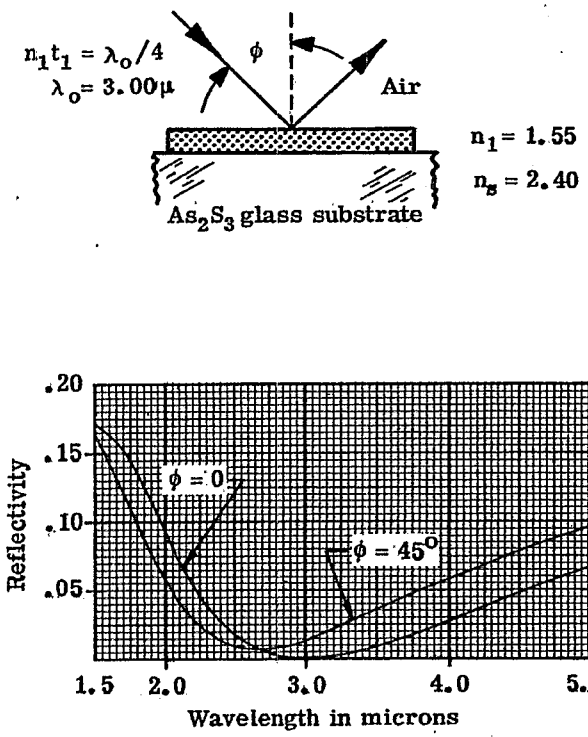

Figure 20.23 - Computed spectral reflectivity of a single-layer antireflection coating at $\phi = 0$ and $\phi = 45^\circ$.

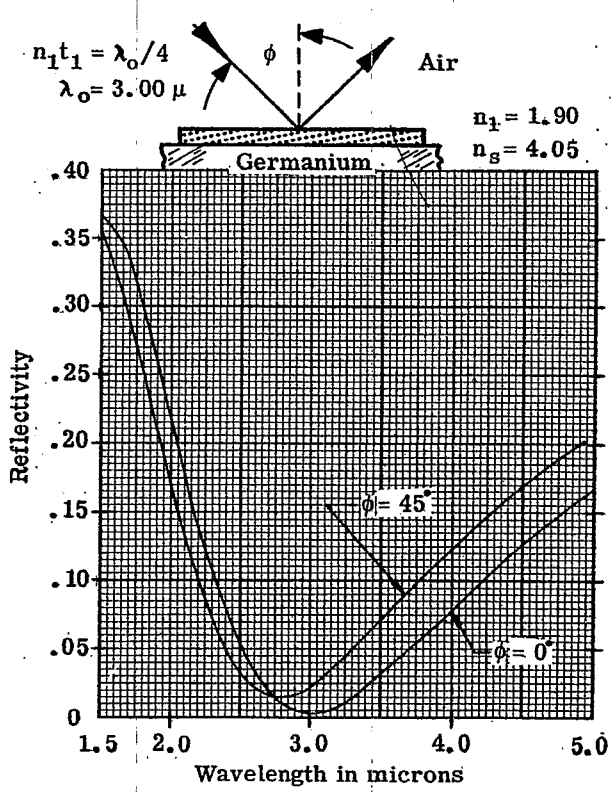

Figure 20.24 - Computed spectral reflectivity of a single-layer antireflection coating at $\phi = 0$ and $\phi = 45^\circ$.

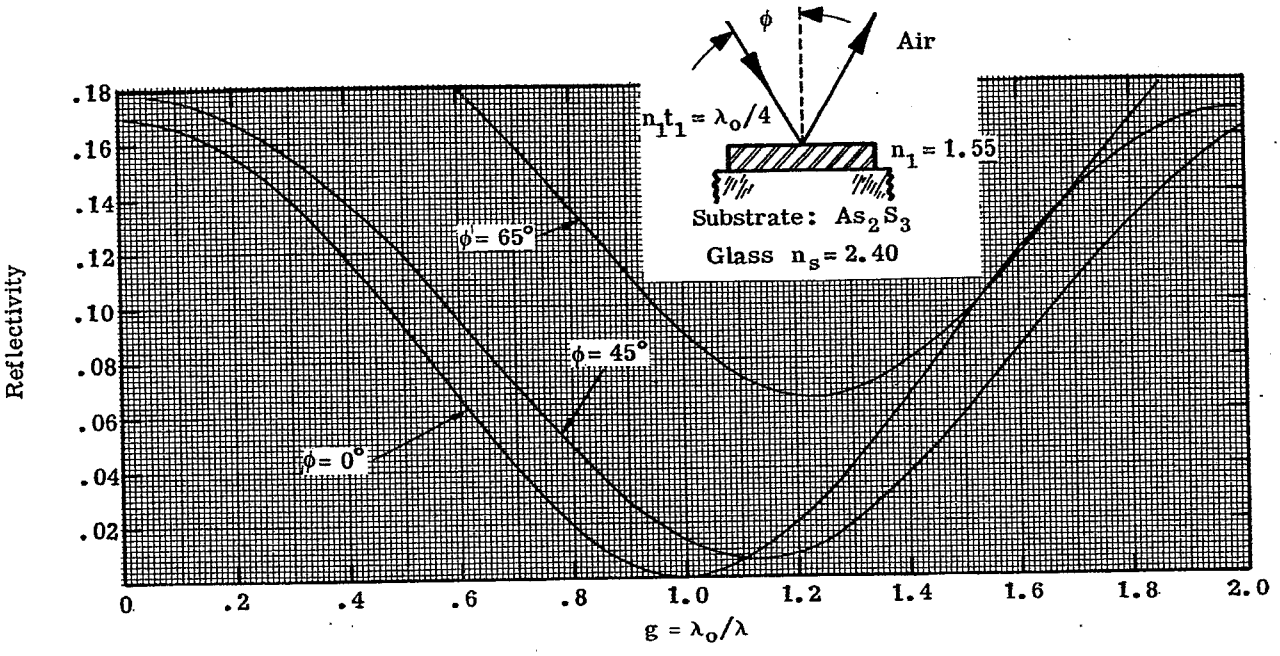

Figure 20.25 – Computed spectral reflectivity of a single-layer antireflection coating at ϕ = 0, 45° and 65°.

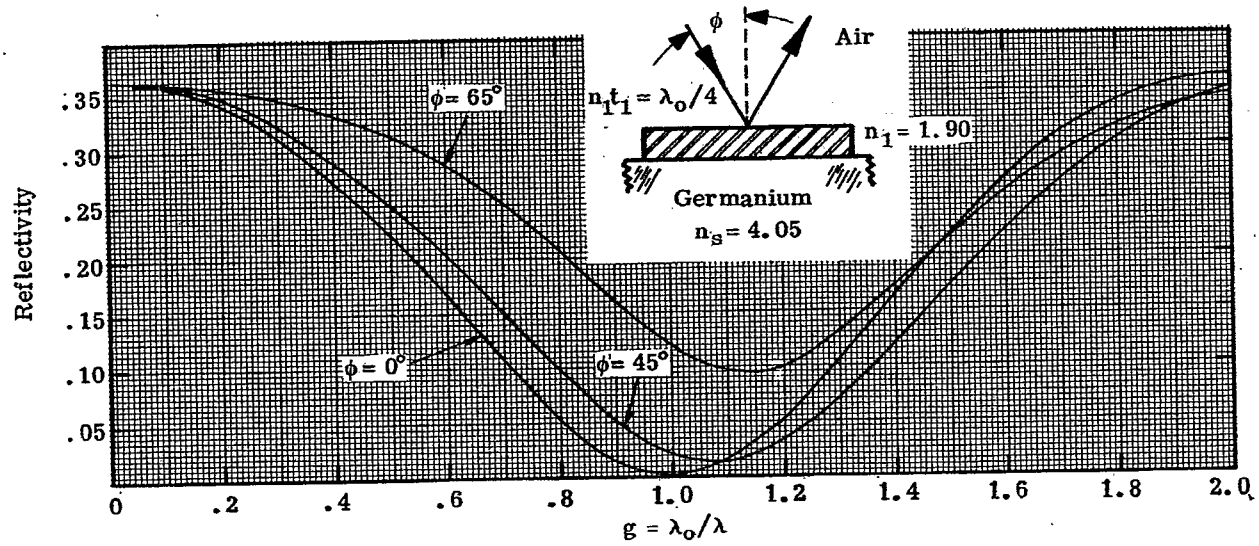

Figure 20.26 – Computed spectral reflectivity of a single-layer antireflection coating at ϕ = 0, 45° and 65°.

20.3.3.4.2 The difference between the coatings for low-index substrates and these higher index materials is that in the latter case thin film materials are available which satisfy Equation (26). Thus the antireflection layer on arsenic trisulfide glass should have a refractive index of $(2.40)^{1/2} = 1.55$, and so on for the other substrates. Figures 20.23 and 20.24 show single layer antireflecting coatings with a quarter-wave optical thickness of 3.0 μ, on substrates of arsenic trisulfide glass and germanium. The reflectivity of the uncoated surface is 0.17 and 0.364 respectively. It should be noted that in practice the reflectivity curve in Figure 20.24 is higher than shown in the region from 1.5 to 1.8 μ, because the absorption constant of the germanium is increasing. Figures 20.25 and 20.26 show a plot of the reflectivity versus "g". In each case the optical thickness of the films is $\lambda_o/4$. These curves can be used to find the reflectivity at various wavelengths of a film which has a quarter-wave optical thickness, say at 4.0 μ, in the manner described in Section 20.3.3.2.6.

20.3.3.5 Coatings for substrates with a higher refractive index, at non-normal incidence.

20.3.3.5.1 The behavior at non-normal incidence of coatings for substrates with a low refractive index was discussed in 20.3.3.3. That discussion applies equally well to these coatings for high-index substrates. The main difference is that the angle shift of the reflection minima to shorter wavelengths is considerably less for the high-index coatings. This is merely a manifestation of the fact that the change in the effective thickness is much less for high-index films than for the low index films, as one can see from Figure 20.8.

20.3.3.5.2 Figure 20.27 shows the spectral reflectivity at 65° in the two planes of polarization and also the R_{av} of a single layer coating on germanium. As in the case of the film shown in Figure 20.21, the effective indices of the incident medium, film, and substrate in the "p" plane of polarization do not satisfy Equation (25) and hence the reflectivity attains a maximum rather than a minimum. However, in the case of the germanium film, R_s is less than R_p. This means that at $\phi = 65°$ the polarizing effect of this coated plate is exactly opposite to that produced by an uncoated dielectric surface, which satisfies the condition that $R_s > R_p$, for all values of $\phi > 0$. This coating on germanium could be used to compensate for the polarization introduced by other uncoated surfaces in an optical system. Figures 20.25 and 20.26 show the average reflectivity of these coatings at various angles of incidence. Hass[27,28] and his co-workers have measured the transmittance in the infrared of some antireflected high-index substrates.

20.3.3.6 Coatings with a higher order of interference. As was pointed out in 20.3.3.1.2, a minimum in the reflectivity of a single-layer coating occurs when the optical thickness of the coating is $\lambda/4$, $3\lambda/4$, $5\lambda/4$, $m\lambda/4$, where the order number "m" is an odd integer. Hitherto we have only shown coatings which show a first-order interference minimum, that is, for $m = 1$. A minimum reflectivity will also occur for higher order interference coatings, such as films which have an optical thickness of three-quarter or five-quarter waves. Figure 20.28 shows the spectral reflectivity of these thicker films deposited on a glass substrate. As one might expect, the reflectivity rises sharply on either side of the minimum at 550 mμ. Hence, there is little advantage to using such higher order interference coatings, with the following exception. In an infrared optical system which is designed to transmit a narrow band of wavelength, some additional attenuation of wavelengths outside of the desired range could be obtained by using higher order interference antireflection coatings.

20.3.3.7 Analogy with electrical transmission lines. In this section we have considered the problem of light impinging upon a substrate of index n_s from an incident medium of index n_o. The problem has been to select the film of proper optical thickness and refractive index so that the reflectivity is reduced to zero. The analogous problem in transmission line theory to match a load of admittance n_s to a transmission line of characteristic admittance n_o so that there will be no standing waves. It is shown in many texts on transmission line and microwave theory that a "quarter-wave transformer" or "quarter-wave matching line" is required to do this. The electrical length of the line should be a quarter-wave and the admittance, n_1, of the line should satisfy Equation (26).

20.3.4 Double-layer coatings.

20.3.4.1 Types of coatings. It is often desirable to use double-layer antireflection coatings because in certain cases these coatings have a lower reflectivity over a wider spectral region than do single-layer coatings. The following types of coatings will be considered:

(1) Double-quarter, single minimum.

(2) Double-quarter, double minimum.

(3) Quarter-half.

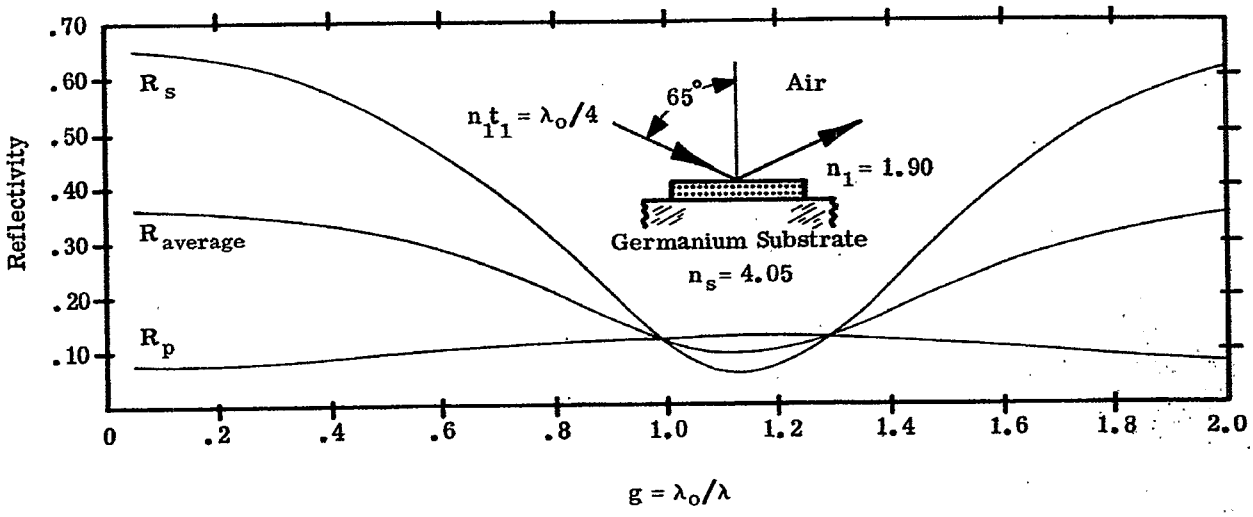

Figure 20.27 Computed R_s, R_p and $R_{av} = 1/2\ (R_s + R_p)$ at $\phi = 65°$.

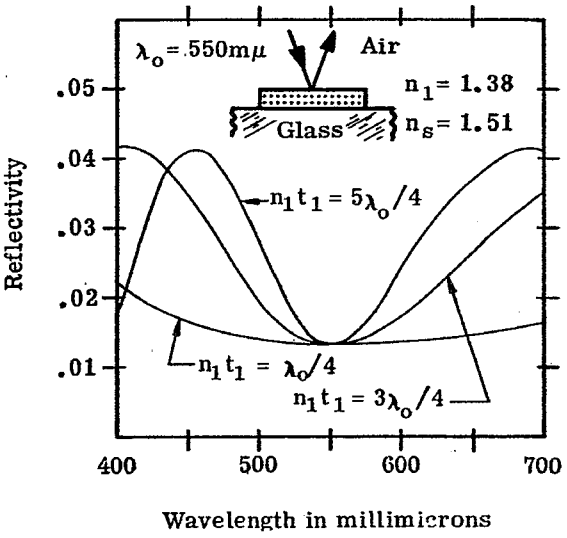

Figure 20.28 Computed spectral reflectivity of single-layer antireflection coatings of various thickness.

Type of Coating	n_1	n_1t_1	n_2	n_2t_2
Single Quarter	1.38	$\lambda_o/4$	—	—
Double Quarter	1.38	$\lambda_o/4$	1.70	$\lambda_o/4$
Quarter-Half	1.38	$\lambda_o/4$	1.80	$\lambda_o/2$

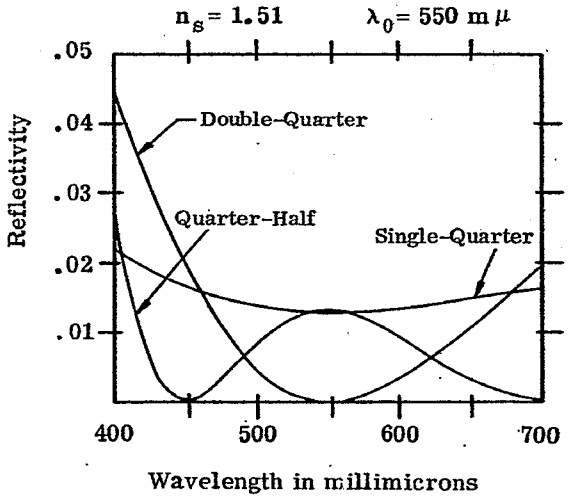

Figure 20.29 Computed spectral reflectivity of single and double-layer antireflection coatings on a glass substrate.

20.3.4.2 Basic equations.

20.3.4.2.1 It is possible to write an equation for the reflectivity of a double-layer coating, but there is little advantage because the equation is lengthy and cumbersome.[29] For our purposes, it is preferable to use the vector addition of amplitude or the characteristic matrix method to compute the reflectivity.

20.3.4.2.2 In the special case where the optical thickness of each film is a quarter-wavelength, that is $n_1 t_1 = n_2 t_2 = \lambda/4$, then $\delta_1 = \delta_2 = 90°$ and the characteristic matrices (Equation (6)) have non-zero elements only along the antidiagonal. The matrix product (Equations (7), (8)) becomes:

$$\begin{bmatrix} A & jB \\ jC & D \end{bmatrix} = \begin{bmatrix} 0 & jn_1^{-1} \\ jn_1 & 0 \end{bmatrix} \begin{bmatrix} 0 & jn_2^{-1} \\ jn_2 & 0 \end{bmatrix} . \qquad (29)$$

After taking the matrix product and substituting into Equations (9) and (10), we obtain for the minimum (or maximum) reflectivity

$$R = 1 - T = \left[\frac{n_o n_2^2 - n_s n_1^2}{n_o n_2^2 + n_s n_1^2} \right]^2 . \qquad (30)$$

Thus for R to be zero, the condition must be satisfied that:

$$\left(\frac{n_2}{n_1}\right) = \left(\frac{n_s}{n_o}\right)^{1/2} . \qquad (31)$$

The condition for zero reflectivity of a double quarter, single minimum type of coating only involves the ratio of the indices of the two films. For example, suppose glass of index 1.51 is coated with a double-quarter-wave coating with the following indices:

$$n_1 = 1.38 \qquad n_2 = 1.69 \qquad (32a)$$

$$n_1 = 1.65 \qquad n_2 = 2.03 \qquad (32b)$$

In both cases Equation (31) is satisfied and the reflectivity is zero at $\lambda = \lambda_o$. However, it can be shown that the reflectivity rises quite sharply on either side of the minimum in the case of Equation (32b), whereas the spectral range over which the reflectivity has a low value is much larger in the case of Equation (32a), and thus Equation (32a) is the better coating to use. Hence it is preferable to use as low index materials as possible.

If the indices satisfy Equation (31), then this is called a double-quarter, single minimum coating. The single minimum means that it has only one reflectivity minimum for a given order of interference. For example, the plot of the reflectivity versus λ_o/λ of the double-quarter coating (curve I in Figure 20.30) has one minimum for the first order interference for $0 \leq g \leq 2.0$, another minimum in the second order for $2.0 \leq g \leq 4.0$, and so on.

20.3.4.2.3 Another type of coating which contains quarter-wave layers has a maximum R at λ_o and two minimum symmetrically spaced about λ_o on a frequency scale. Such a coating is called a double-quarter double minimum coating. A reflectivity curve for a typical coating is shown in Figure 20.35. There are several methods of determining the relationship between the indices of the films of such a coating, such as the solution of complicated algebretic equations [27], [29], [30] or alternatively the use of vector diagrams, as done in Figure 20.5. One type of double-quarter double minimum coating is obtained when the indices satisfy the equations

$$n_1^3 = n_o^2 n_s , \qquad n_2^3 = n_o n_s^2 . \qquad (33)$$

The foregoing equations can be reduced to

$$n_1 n_2 = n_o n_s . \qquad (34)$$

Equations (33) and (34) are derived by Berning [30].

20.3.4.2.4 The spectral reflectivity curve of the quarter-half coating is similar to the curve of the double-quarter, double minimum coating mentioned in the foregoing paragraph, to the extent that it has a maximum at λ_o and two minimum spaced equally about λ_o on a frequency scale. The spectral reflectivity curve of such a coating is depicted in Figure 20.30 (curve III). It is required that the half-wave layer must have a

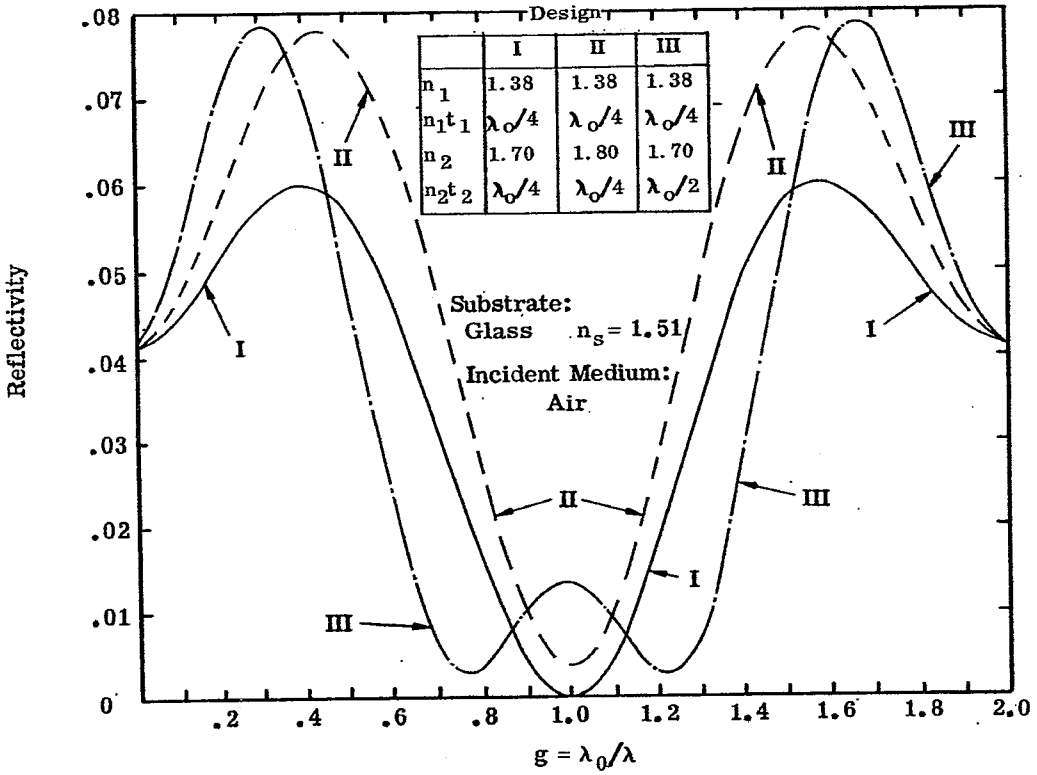

Figure 20.30 – Computed spectral reflectivity of single and double-layer antireflection coatings on a glass substrate.

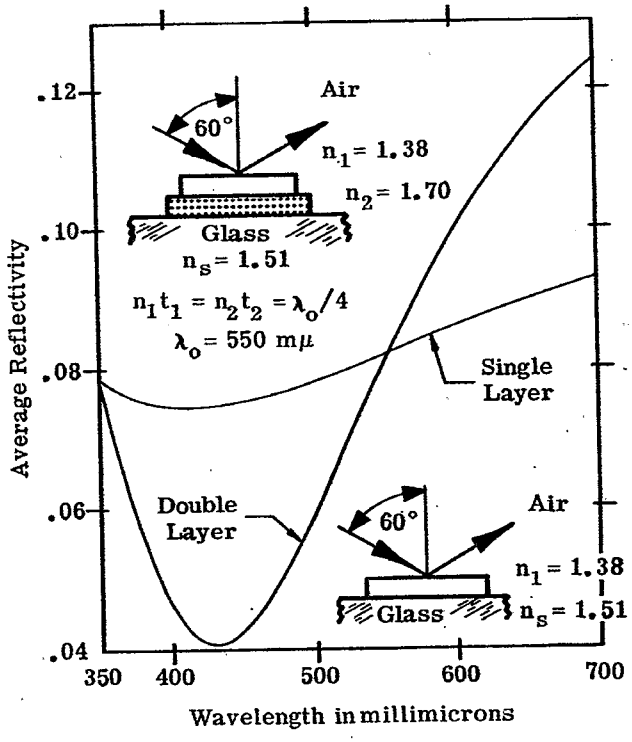

Figure 20.31- Computed average spectral reflectivity of a single-layer and a double-layer coating at $\phi = 60°$.

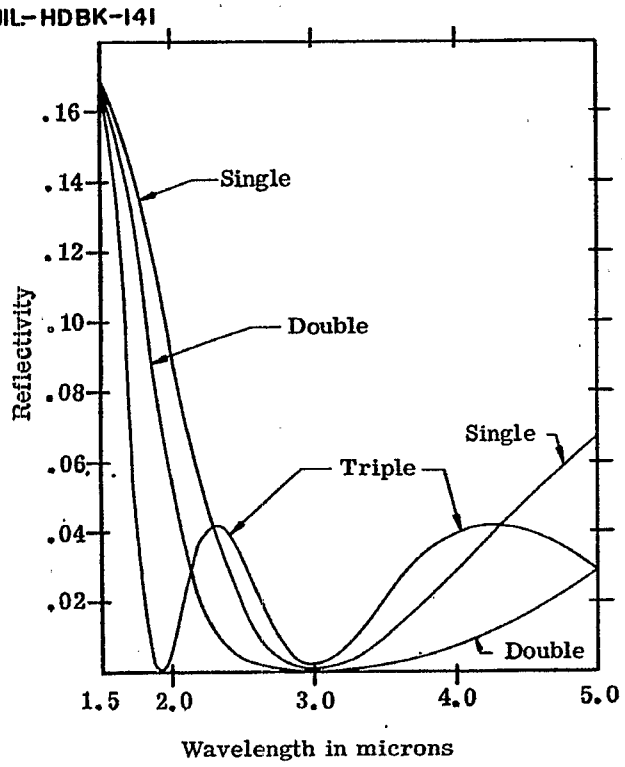

Figure 20.32 — Computed spectral reflectivity of the antireflection coatings whose designs are depicted in Fig. 20.33.

All layers have a quarter-wave optical thickness at $\lambda_0 = 3.0\mu$

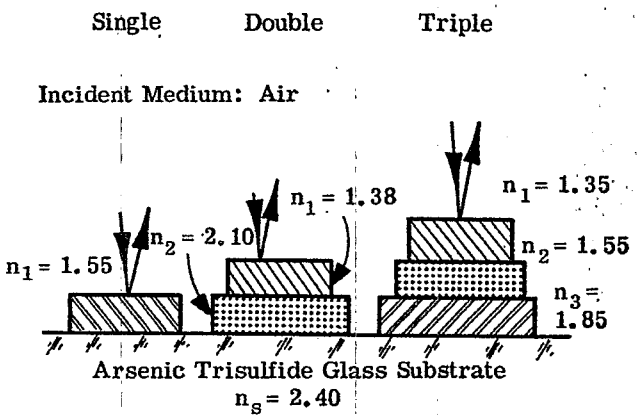

Figure 20.33 — The designs of single, double, and triple-layer antireflection coatings whose reflectivity curves are shown in Figure 20.32.

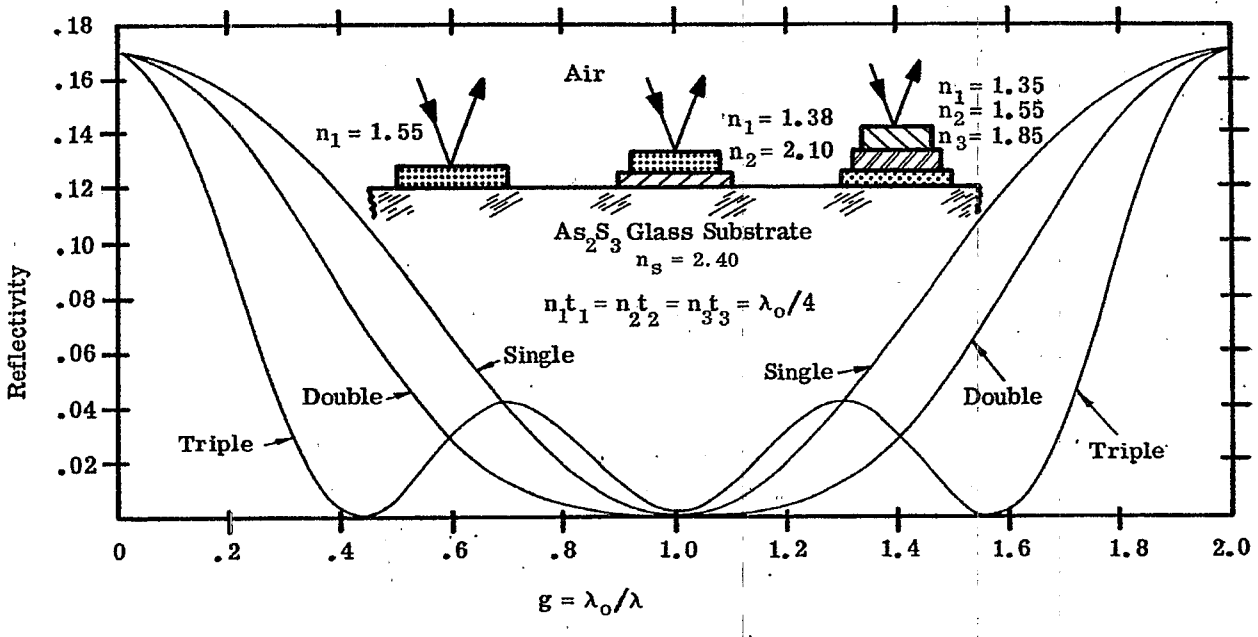

Figure 20.34 — Computed spectral reflectivity of antireflection coatings at normal incidence.

higher refractive index than the substrate. The refractive indices of the two layers can be determined either from a vector diagram (i.e. Figure 20.5) by adjusting the lengths of the vectors so that the vector polygon should close at some value of δ_1 and δ_2. The length of the vectors is proportional to the Fresnel amplitude coefficients and hence one can solve for the indices of the layers. The refractive indices can also be found by solving transendental equation.[29] Whatever indices are chosen, the reflectivity when $\lambda = \lambda_o$ is determined easily from Equation (24) because the half-wave layer is absentee.

20.3.4.3 Double-layer antireflection coatings for low index substrates.

20.3.4.3.1 In this subsection, the term low index substrate is used in the same sense as in 20.3.3.2. The fact that the lowest index film material which is available has an index of 1.35 means that double quarter, double minimum coatings cannot be produced for substrates in this index range.

20.3.4.3.2 The double quarter curve in Figure 20.29 is the spectral reflectivity of a double-quarter, single minimum coating on glass of refractive index 1.51. The optical thickness of the films is a quarter-wave at 550 mμ and because the indices satisfy Equation (31), the reflectivity at this wavelength is zero. Such a coating could be manufactured using magnesium fluoride as the low index film and silicon monoxide as the high index film. Unfortunately, when the index of the silicon monoxide is this large (see Note 4 in Table 20.2), it has a slight absorption in the blue and hence the films are yellowish in appearance. On the same graph is shown for comparison, the reflectivity of a single quarter-wave coating of magnesium fluoride. The reflectivity of the double-quarter coating is below the single layer in the green, but rises considerably above it at 400 mμ. Figure 20.30 shows the reflectivity of the double-quarter coating on a frequency scale. At certain wavelengths, the reflectivity is greater than that of uncoated substrates. Shown also in Figure 20.30 is the reflectivity of a double-quarter coating composed of films of indices 1.38 and 1.80. This shows what happens to the reflectivity when the relationship in Equation (31) are not precisely satisfied. Hass[29] shows many computed reflectivity curves in which variations have been made in both the thickness and refractive indices from the optimum condition specified in Equation (31).

20.3.4.3.3 Figure 20.29 shows the spectral reflectivity of a quarter-half coating. As was stated in 20.3.4.2.4, at λ_o (550 mμ) the half-wave layer is absentee and the reflectivity is the same as the single quarter-wave layer of index 1.38. Since the two minimum are equally spaced about the maximum on a frequency scale, they are unequally spaced on the wavelength scale. Figure 20.30 shows the spectral reflectivity of the same configuration, but on a λ_o/λ scale.

20.3.4.3.4 The limitation on the film index mentioned 20.3.4.3.1 means that the reflectivity of both the double-quarter and the quarter-half antireflection coatings exceeds the reflectivity of the uncoated substrate at some wavelengths, as is shown in Figure 20.30. This is not true of the single-layer low index coating, whose reflectivity never exceeds that of the uncoated substrate. The question as to which type of coating to use depends upon the range of wavelengths over which the reflectivity is to have a low value. If the range is narrow, a double-quarter coating might be preferable. However, if the range is quite large, then even though the single-layer coating does not achieve as low a reflectivity as the double-quarter coating in certain spectral regions, the better overall performance of the single layer over a wide range of wavelengths would make it preferable.

20.3.4.4 Double-layer antireflection coatings for low index substrates at non-normal incidence. At non-normal incidence the reflectivity of coatings which have two or more layers is influenced by the fact that if the optical thicknesses of the layers are matched at normal incidence, they are no longer matched at any other angle. This point is discussed in more detail in 20.1.6.3 and 20.1.6.4. If the layers are matched at some angle of incidence, ϕ, then one can compute the reflectivity at $\lambda = \lambda_o$ by substituting the effective index appropriate to each plane of polarization into Equation (30). In the case of double layer coatings, there are many possible combinations of incident angles and matched or mismatched layers which can be considered and hence a complete analysis of the behavior of the double-layer coatings of non-normal incidence would be quite lengthy. As an illustration of a typical case, Figure 20.31 shows the spectral reflectivity of a double-quarter coating on glass at 60° incidence. Both layers have a quarter-wave optical thickness at normal incidence at 550 mμ. The reflectivity minimum has shifted to the blue and notwithstanding the fact that the optical thickness of the layers is mismatched, the minimum reflectivity is still considerably lower than the minimum of the single-layer coating.

20.3.4.5 Double-layer antireflection coatings for high index substrates.

20.3.4.5.1 In this subsection, the term high index substrate is used in the same sense as in 20.3.3.4.1. For high-index substrates, coating materials are available which not only satisfy Equations (31), (33), or (34), but also the relationship:

$$n_o < n_1 < n_2 < n_s . \qquad (35)$$

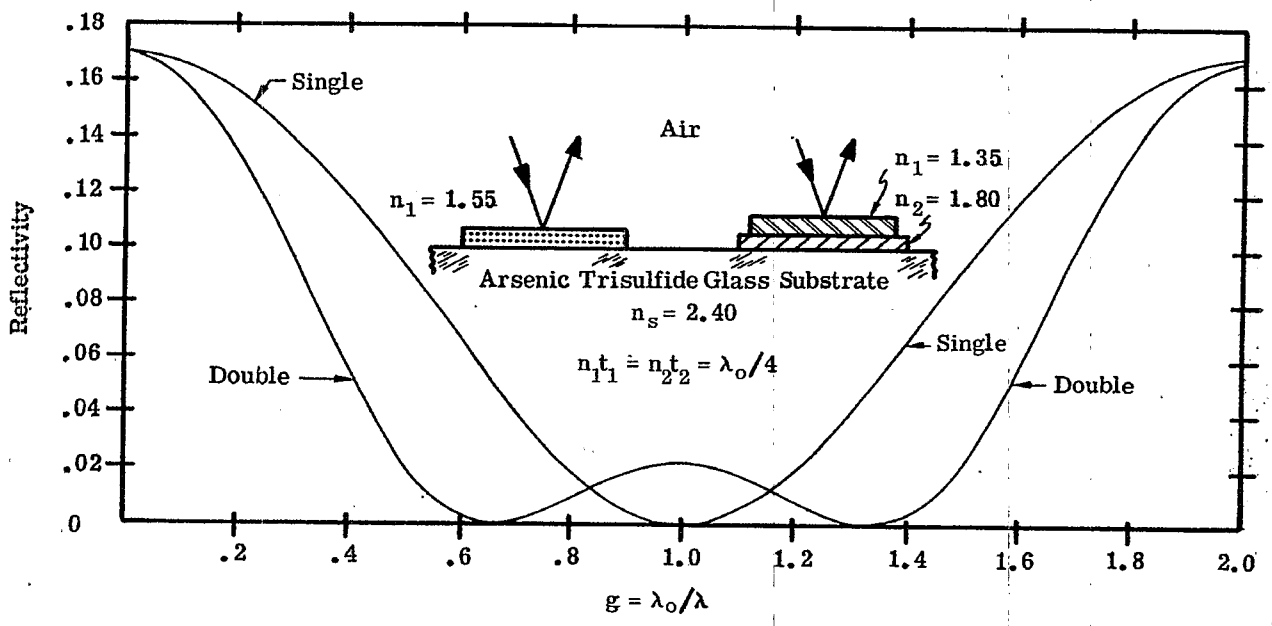

Figure 20.35 – Computed spectral reflectivity of antireflection coatings at normal incidence.

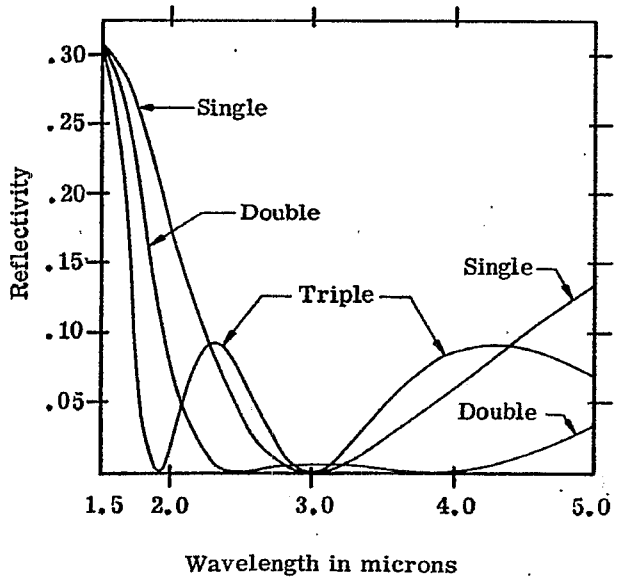

Figure 20.36 – Computed spectral reflectivity of the antireflection coatings whose designs are depicted in Fig. 20.37.

All layers have a quarter-wave optical thickness at $\lambda_0 = 3.0\mu$

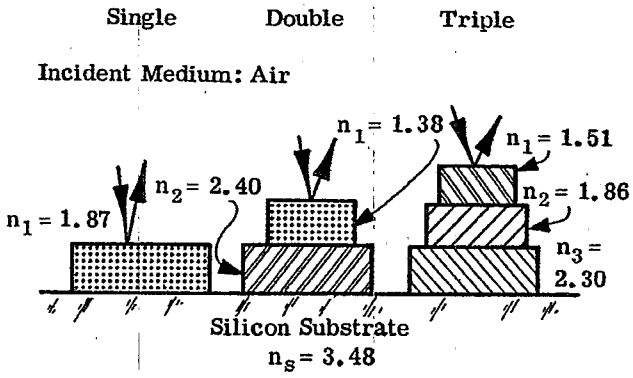

Figure 20.37 – The designs of single, double, and triple-layer antireflection coatings whose reflectivity curves are shown in Figure 20.36.

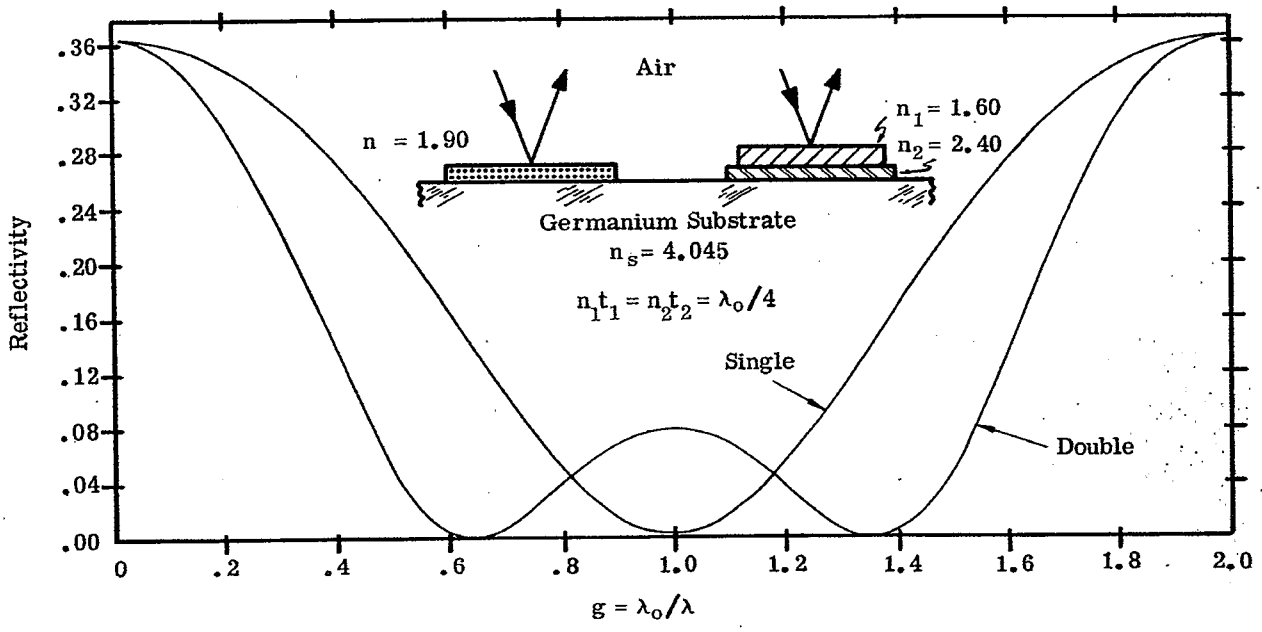

Figure 20.38 – Computed spectral reflectivity of antireflection coatings at normal incidence.

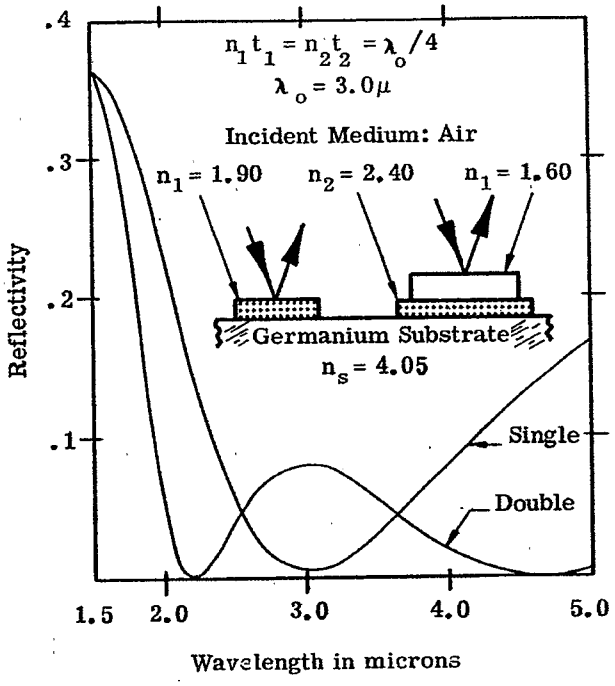

Figure 20.39 – Computed spectral reflectivity of antireflection coatings at normal incidence.

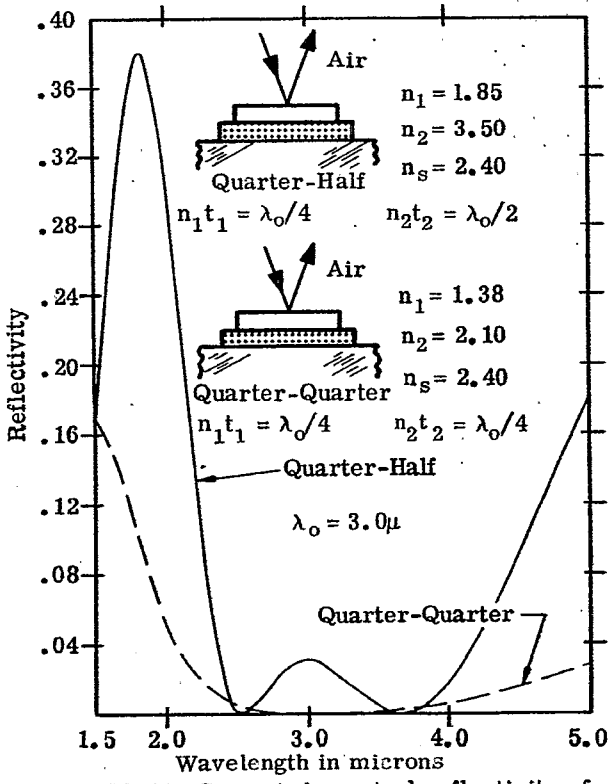

Figure 20.40 – Computed spectral reflectivity of antireflection coatings at normal incidence.

In this case a wide region of low reflectivity is achieved and the reflectivity does not exceed the reflectivity of the uncoated substrate. This fact is illustrated in Figure 20.34, which depicts a double-quarter, single minimum coating on a substrate of arsenic trisulfide glass.

20.3.4.5.2 With higher index substrates it is possible to use film materials which satisfy Equation (33) and hence it is possible to produce double-quarter, double minimum coatings. Figure 20.35 shows the spectral reflectivity of such a coating on arsenic trisulfide glass; the indices of the layers satisfy Equations (33) and (34). Figure 20.36 shows a double-quarter, double minimum coating on a silicon substrate in which the indices of the films satisfy Equation (34) to a fair approximation. Figures 20.38 and 20.39 show the spectral reflectivity of a double-quarter, double minimum coating on a germanium substrate. The indices of the films in this coating satisfy Equations (33) and (35).

20.3.4.5.3 Figure 20.40 shows the spectral reflectivity of a half-quarter coating on a substrate of arsenic trisulfide glass. The layer with the half-wave optical thickness is silicon, which has a higher refractive index than the substrate. The reflectivity rises considerably above that of the uncoated substrate and hence there seems to be little advantage of this type of coating over the double-quarter coatings.

20.3.4.5.4 Figure 20.41 shows the spectral transmittance of a germanium plate with both sides antireflected by a two-layer coating.[28] With the double-quarter single minimum coating, the ratio of the index of the silicon film to the index of the didymium fluoride film closely approximates the ratio specified in Equation (31). Figure 20.42 shows the transmittance of a silicon plate which has been coated in a similar manner.[28] The index of the cerium dioxide film and the magnesium fluoride film of this double-quarter double minimum coating satisfy Equation (34). The double reflectivity minimum of this type of coating are manifested in the transmission maxima at 1.8 and 2.7 μ. The bump in the curve near 3 μ is due to the water adsorbed on the coating. In both cases, the spectral region in which the transmission exceeds 0.9 is wider for these double-layer coatings than for a single layer coating.

20.3.5 Triple-layer antireflection coatings.

20.3.5.1 Types of coatings. The number of types of three-layer antireflection coatings which can be produced is legion, because there are six parameters which can be varied - three thicknesses and the three refractive indices. The discussion is confined to two types of coatings:

(1) The quarter-half-quarter.

(2) The triple-quarter, triple minimum.

20.3.5.2 Basic equations. Triple-layer coatings are usually designed by the use of vector diagrams (Section 20.1.5) or with the more sophisticated methods of Section 21.7.4. A few of the many conditions for zero reflectivity of three-layer coatings are derived by Berning.[30] One of the conditions for a stack of three quarter waves to attain a triple reflectivity minimum is:

$$n_1 n_3 = n_o n_s \qquad (36a)$$

$$n_2^2 = n_o n_s \ . \qquad (36b)$$

20.3.5.3 Triple-layer coatings for substrates with low refractive index. In this subsection, the term low index substrate is used in the same sense as in 20.3.3.2.1. For such substrates, a quarter-half-quarter coating is quite effective in reducing the reflectivity to below .005 throughout the entire visible spectral region. The computed spectral reflectivity of such a coating on a glass substrate of index 1.51, is shown in Figure 20.43. The reflectivity of single-layer, double-quarter, and quarter-half coatings are also shown for purposes of comparison. The reflectivity of the triple-layer coating is well below the reflectivity of the single-layer coating over an octave (i.e. from $g = 0.6$ to $g = 1.2$). However, outside of this region, the reflectivity rises to quite large values. Hass[31] presents a detailed study of this type of coating and shows how the spectral reflectivity is altered as the refractive index and the thickness of each layer is varied. Figures 20.44, 20.45, 20.46, and 20.47 show the measured spectral reflectance of glass covered with this type of triple-layer coating.

20.3.5.4 Triple-layer coatings for substrates with high refractive index. The term high refractive index is used in the same sense as in 20.3.3.4.1. For such substrates, it is possible to use coating materials whose refractive indices satisfy

$$n_o < n_1 < n_2 < n_3 < n_s \ . \qquad (37)$$

Figures 20.32 and 20.34 show the spectral reflectivity of a triple layer coating on a substrate of arsenic trisulfide glass whose refractive indices satisfy Equations (36) and (37). The reflectivity does not exceed

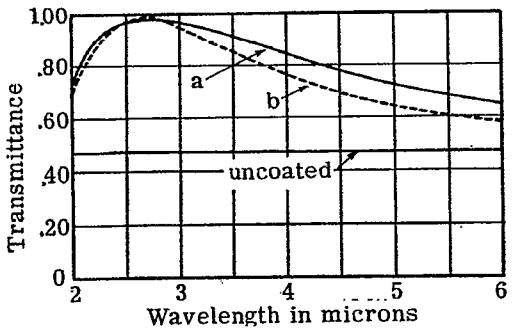

Figure 20.41 – Measured transmittance of Ge plate with antireflection coatings of (a) Si + didymium fluoride, and (b) SiO; (nt = $\lambda/4$ at 2.7 μ). From ref. 28 .

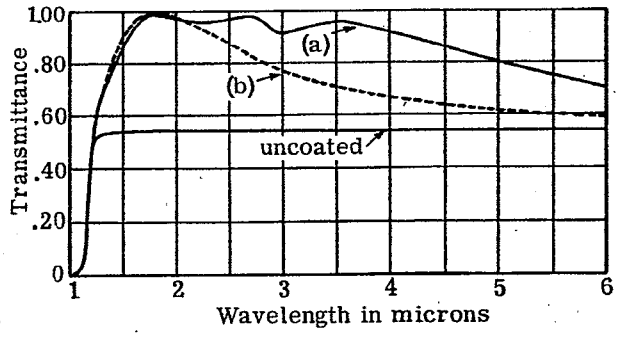

Figure 20.42 – Measured transmittance of Si plate with antireflection coatings of (a) CeO_2 + MgF_2 (nt = $\lambda/4$ at 2.2 μ), and (b) SiO (nt = $\lambda/4$ at 1.8 μ). From ref. 28.

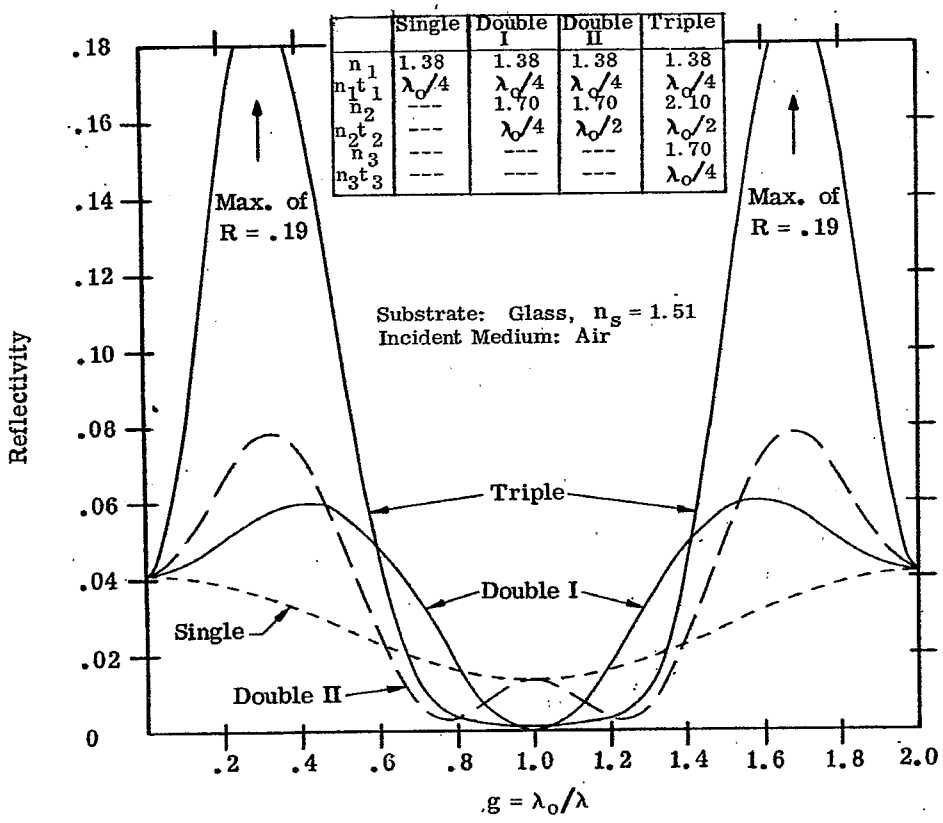

Figure 20.43 – Computed spectral reflectivity of antireflection coatings at normal incidence.

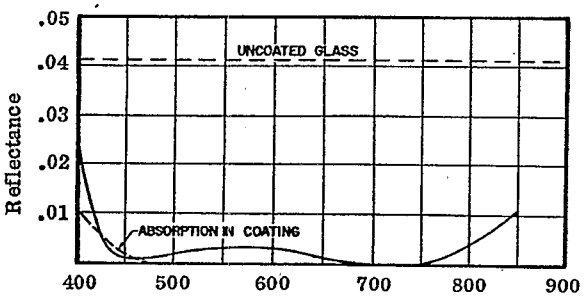

Figure 20.44 - Measured reflectance of a quarter-half-quarter antireflection coating consisting of MgF_2 + ZrO_2 + CeF_3 on glass. From ref. 31.

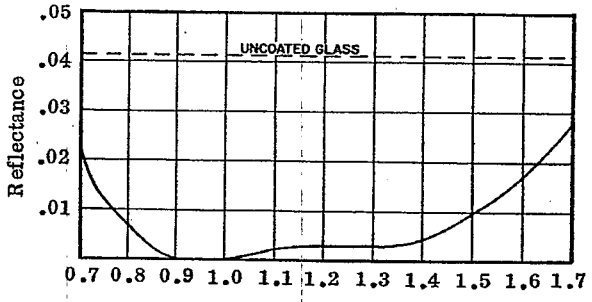

Figure 20.45 - Measured reflectance of a quarter-half-quarter antireflection coating consisting of MgF_2 + Nd_2O_3 + CeF_3 on glass. From ref. 31.

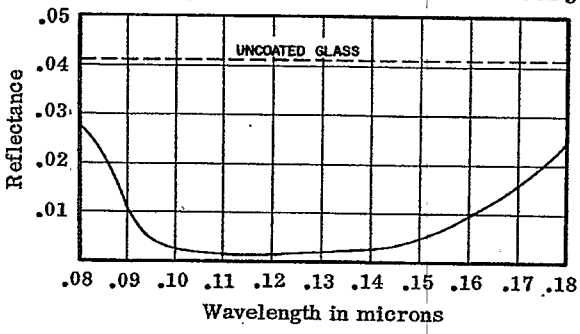

Figure 20.46 - Measured reflectance of a quarter-half-quarter antireflection coating consisting of MgF_2 + SiO + CeF_3 on glass. From ref. 31.

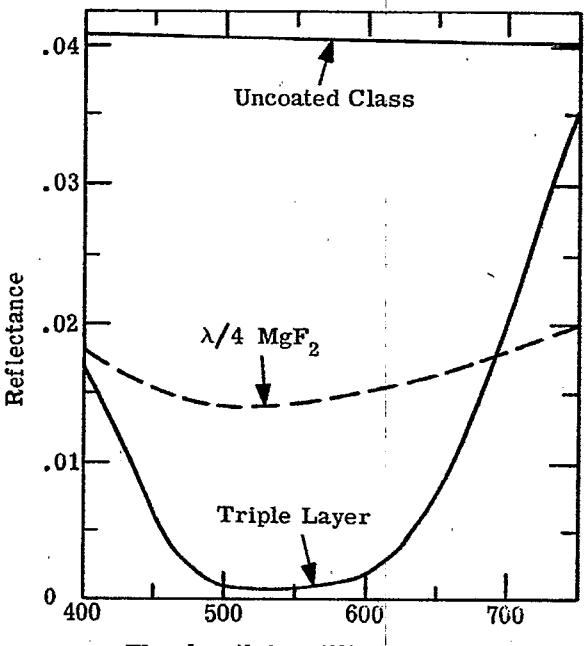

Figure 20.47 - Measured spectral reflectivity of single and triple-layer antireflection coatings. Courtesy of Fish-Schurman, Corporation.

.005 over a frequency range of more than two octaves. Silicon monoxide and chiolite could be used as films in such a coating. Figure 20.36 shows a coating of similar design on a silicon substrate.

20.4 THE REFLECTIVITY OF MULTILAYERS WITH PERIODIC STRUCTURE

20.4.1 The quarter-wave stack.

20.4.1.1 The basic period.

20.4.1.1.1 Before delving into the subject of multilayer mirrors, color filters, beam splitters, etc., it is helpful to understand some of the basic concepts relating to the propagation of light in a multilayer stack with a periodic structure.

20.4.1.1.2 The simplest type of stack with a periodic structure is a quarter-wave stack, which consists of layers with the same optical thickness, but alternating between two refractive indices, n_a and n_b. A diagram of a quarter-wave stack consisting of eight layers is shown in Figure 20.48. At some wavelength λ_o, the optical thickness of each layer is $\lambda_o/4$, that is

$$n_i \; t_i = \lambda_o/4 \qquad (38)$$

for all values of i. The basic period of the quarter wave stack consists of two layers: HL, using the notation of Section 20.1.3.5. The design of the stack depicted in Figure 20.48 can be written:

Glass LHLHLHLH Air .

The foregoing design can also be written:

Glass $(L\,H)^4$ Air

or as

Glass $(L\,H)^m$ Air, where $m = 4$,

to emphasize the fact the basic period, L H, is repeated "m" times.

20.4.1.2 Reflectivity of a typical quarter-wave stack. Figures 20.49 and 20.50 show the computed reflectivity versus $g = \lambda_o/\lambda$ of a quarter-wave stack with the same n_a and n_b but with different numbers of periods. The following observations are made:

(1) The reflectivity in the range of g within the crosshatched area monotonically increases, as the number of basic periods, m, increases from 2 to 5. This region is called the high-reflectance zone.

(2) The reflectivity outside of the high reflectance zone is an oscillating function. By this we mean that for any arbitrary value of g (outside of the high-reflectance zone) the reflectivity can either increase or decrease if two addition layers (i.e. L H) are added to the stack so that m increases to $m + 1$.

(3) In the region between $g = 0$ and the edge of the high-reflectance zone, there are $m - 1$ maximum and $m - 1$ minimum in the reflectivity.

20.4.1.3 Properties of an infinite stack. It is of interest to consider the limiting case where the number of periods, m, becomes infinite. This is called the infinite stack. The statements in 20.4.1.2 can be generalized to include any quarter-wave stack:

(1) The reflectivity in the high-reflectance zone approaches 1.0 as m becomes infinite. As the number of periods becomes large, the reflectivity curve in the high-reflectance zone becomes very flat. Regardless of the number of periods the reflectivity attains a maximum value R_{max} at the center of the zone at $g = 1.0$. The width of the high-reflectance zone depends only on the index ratio, n_a/n_b.

(2) The reflectivity curve in the region outside of the high-reflectance zone oscillates between maximum and minimum values. The number of oscillations between $g = 0$ and the edge of the high-reflectance zone depends upon the relationship between n_o, n_s, n_a, and n_b, but is proportional to m for $m >> 1$.

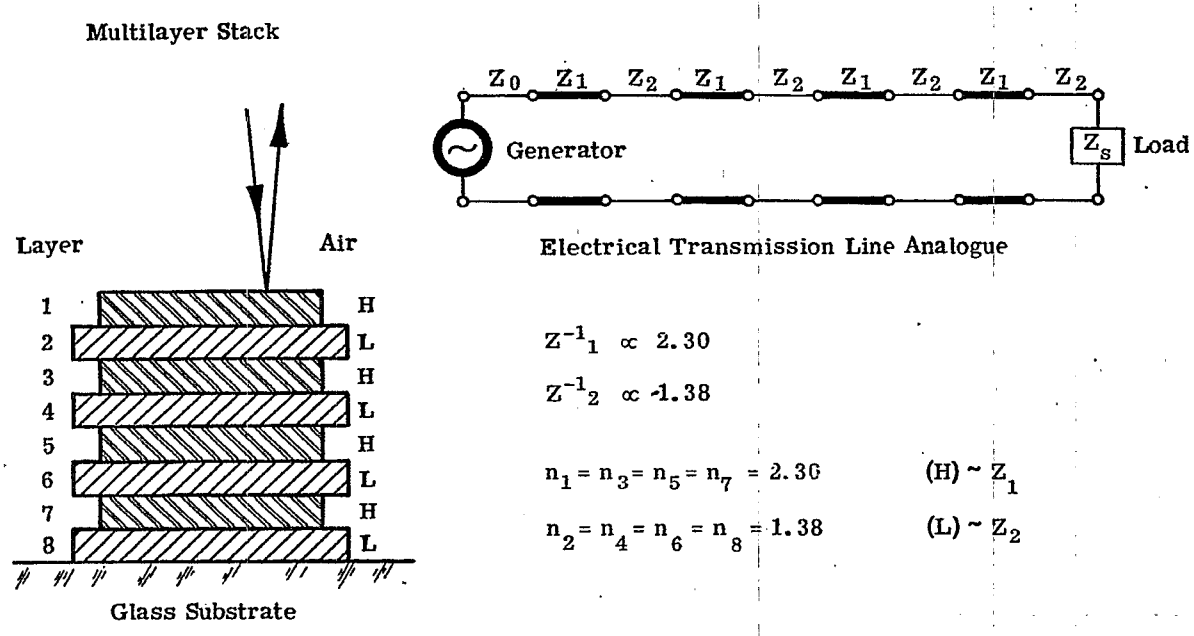

Figure 20.48 - Diagram of a quarter-wave stack and its transmission line analogue.

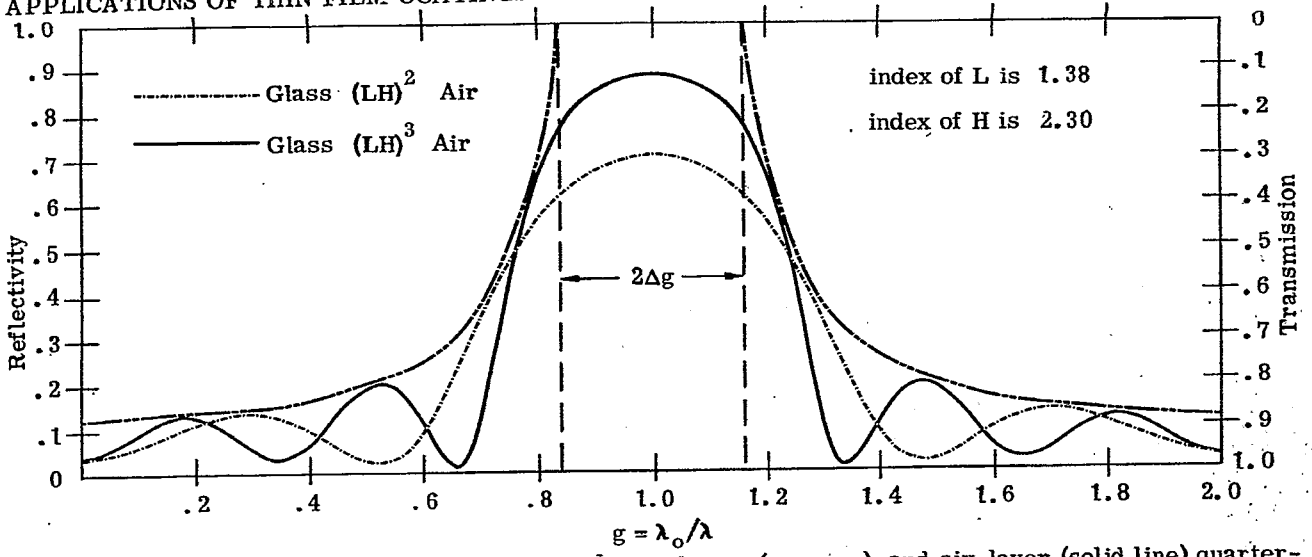

Figure 20.49 - Computed spectral reflectivity of a four-layer (----------) and six-layer (solid line) quarter-wave stack and the envelope of maximum reflectivity (----------).

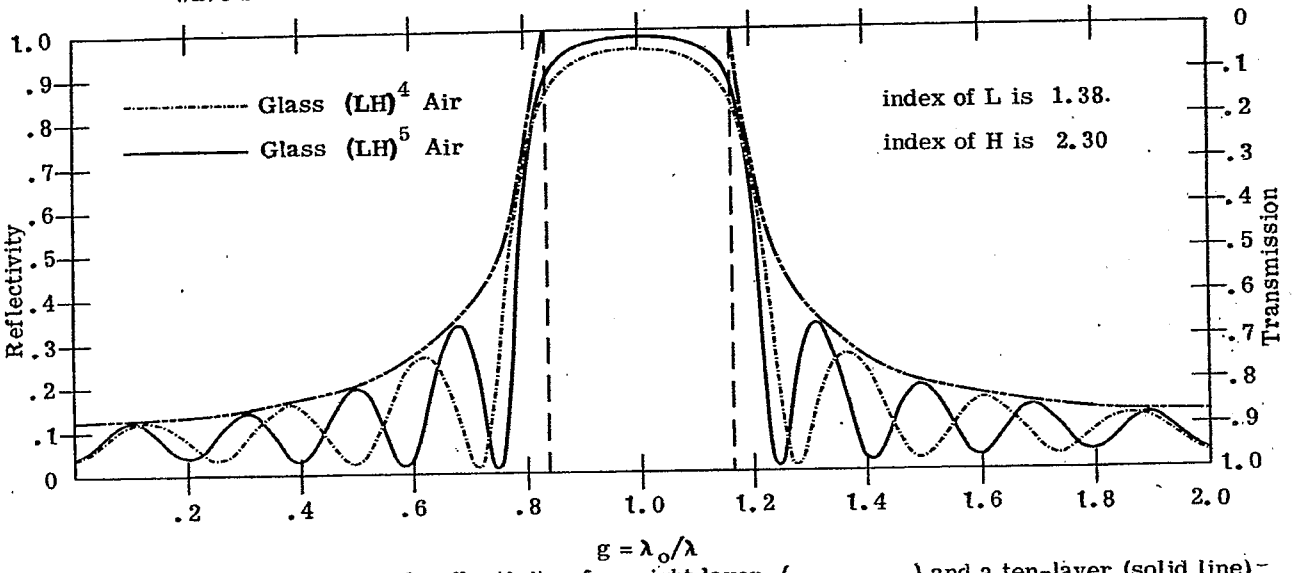

Figure 20.50 - Computed spectral reflectivity of an eight layer (----------) and a ten-layer (solid line) quarter-wave stack, and the envelope of maximum reflectivity (----------).

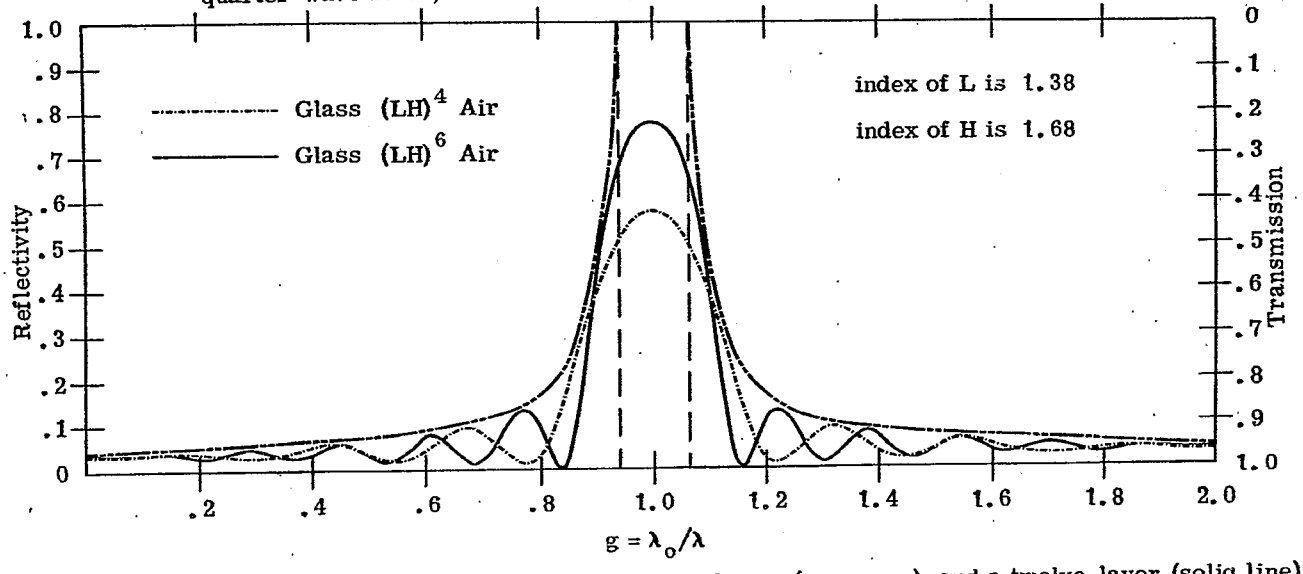

Figure 20.51 - Computed spectral reflectivity of an eight-layer (----------) and a twelve-layer (solid line) quarter-wave stack, and the envelope of maximum reflectivity (----------).

The reflectivity oscillates between two envelope curves. The reflectivity maximum envelope curve is shown as dashed line ———— in Figures 20.49 to 20.52. Both the maximum and minimum envelope curves are shown in Figure 20.53.

(3) The reflectivity of a multilayer with a periodic structure is adequately described by plotting the width of the high-reflectance zone and the maximum and minimum reflectivity envelopes, as is shown in Figure 20.54.

20.4.1.4 Width of the high-reflectance zone. The high-reflectance zone is symmetrical about $g = 1.0$. In the case of a quarter-wave stack, there is a simple expression for the distance Δg from the center of high-reflectance zone at $g = 1.0$ to its edge:

$$\Delta g = \frac{2}{\pi} \arcsin \left| \frac{1 - n_a/n_b}{1 + n_a/n_b} \right| \tag{39}$$

where the $|\ |$ denotes an absolute value; the principal value of the arcsin is to be used. The total width of the high-reflectance zone is $2\Delta g$. For example, the quarter stacks shown in Figures 20.49 and 20.50 have $n_a = 1.38$ and $n_b = 2.30$; from Equation (39) we find that $\Delta g = 0.161$. As another example, consider the quarter-wave stacks shown in Figures 20.51 and 20.52. The index ratio, n_a/n_b of these stacks is approximately the same, although the stack in Figure 20.51 is composed of low-index layers, while the latter stack has high-index layers. As one might expect, the width of the high-reflectance zone of the two stacks is essentially equal. The index ratio n_a/n_b is large for the stack shown in Figure 20.53 and consequently the high-reflectance zone is quite wide. This large index ratio can only be attained with materials such as germanium and chiolite in the infrared.

20.4.1.5 Maximum reflectivity of a quarter-wave stack. Consider a more general type of quarter-wave stack in which the optical thickness of each of the layers is $\lambda_o/4$, but the refractive index, n_i, of each of the layers can be different. From Equations (5), (7), (9) and (10), it follows that the transmission T_{min} and reflectivity R_{max} at $g = 1.0, 3.0, 5.0$, etc. is

$$R_{max} = 1 - T_{min} = (P + P^{-1} - 2)(P + P^{-1} + 2)^{-1} \tag{40}$$

$$T_{min} = 4/(P + P^{-1} + 2) \tag{41}$$

where the variable P is defined as

$$P = \left[\frac{n_\ell}{n_{\ell-1}} \frac{n_{\ell-2}}{n_{\ell-3}} \cdots \frac{n_4}{n_3} \frac{n_2}{n_1} \right]^2 \frac{n_o}{n_s} \tag{42}$$

when the total number of layers ℓ is even and

$$P = \left[\frac{n_\ell}{n_{\ell-1}} \cdot \frac{n_{\ell-2}}{n_{\ell-3}} \cdots \frac{n_3}{n_2} \frac{n_1}{} \right]^2 \frac{1}{n_o\ n_s} \tag{43}$$

when ℓ is odd. From Equation (41) we see that as the number of layers becomes large, P also becomes large and $p >> p^{-1}$, $p >> 2$ and thus

$$T_{min} \sim 4P^{-1} . \tag{44}$$

Equations 40 to 43 are for a quite general type of quarter-wave stack, and can be easily applied to specific cases. For example, P for the stack in Figure 20.48 is:

$$P = \left[\frac{n_b}{n_a} \right]^8 \frac{n_o}{n_s} . \tag{45}$$

In the case where the stack has many layers and hence the index ratio n_a/n_b is raised to a large power, T_{min} is a very sensitive function of this ratio.

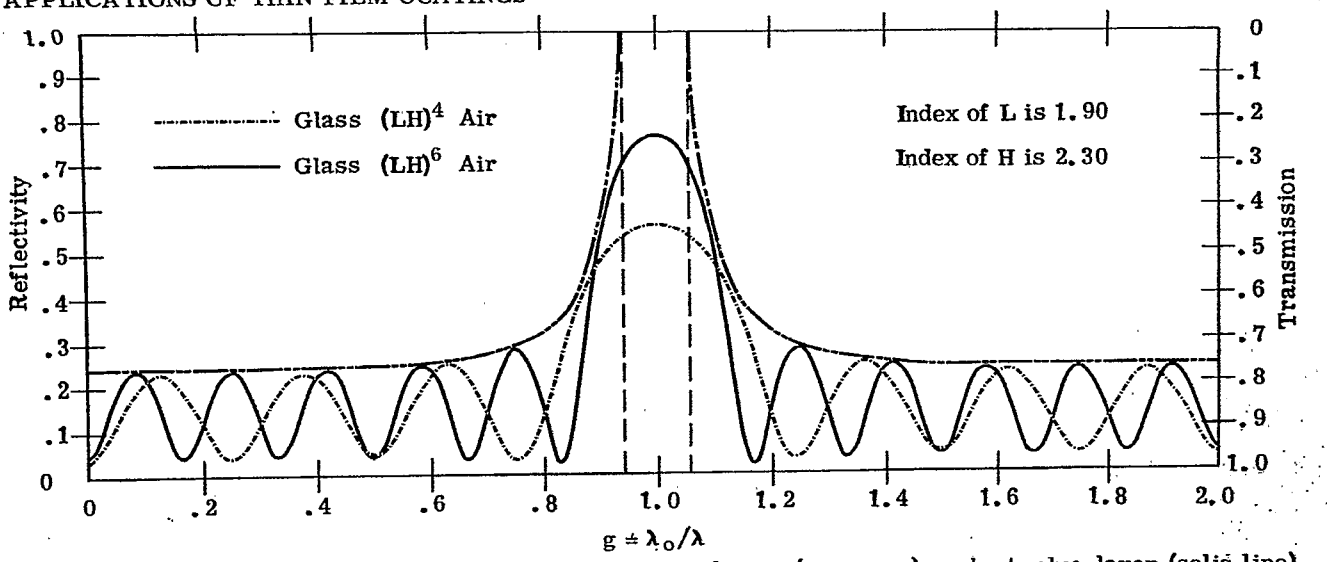

Figure 20.52 - Computed spectral reflectivity of an eight-layer (----------) and a twelve-layer (solid line) quarter-wave stack, and the envelope of maximum reflectivity (----------).

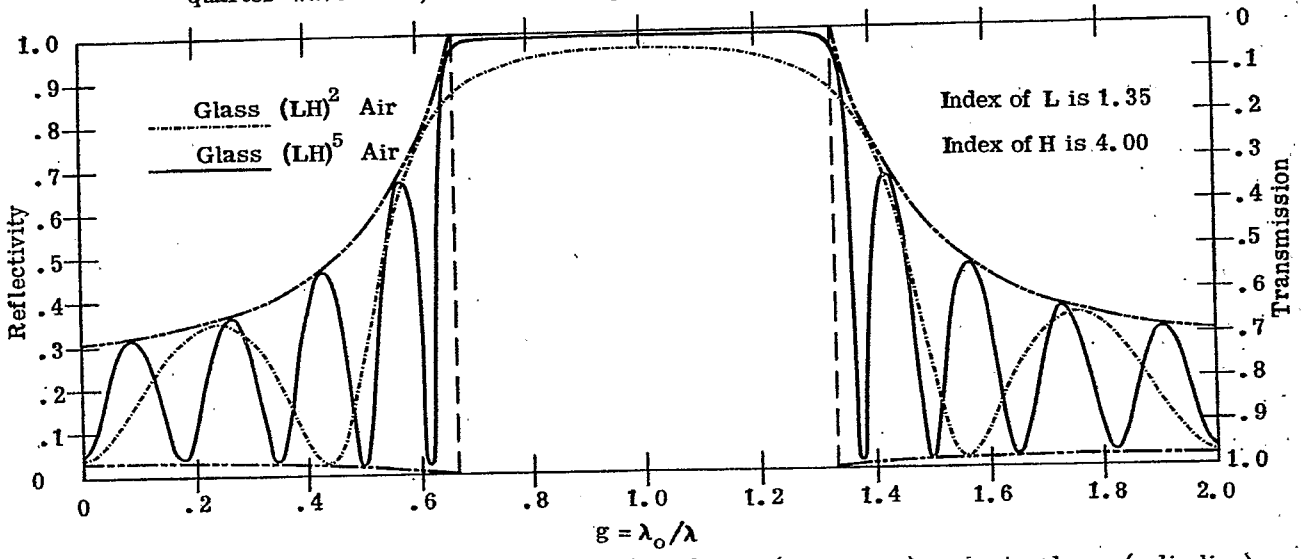

Figure 20.53 - Computed spectral reflectivity of a four-layer (----------) and a ten-layer (solid line) quarter-wave stack, and envelope of maximum reflectivity (----------).

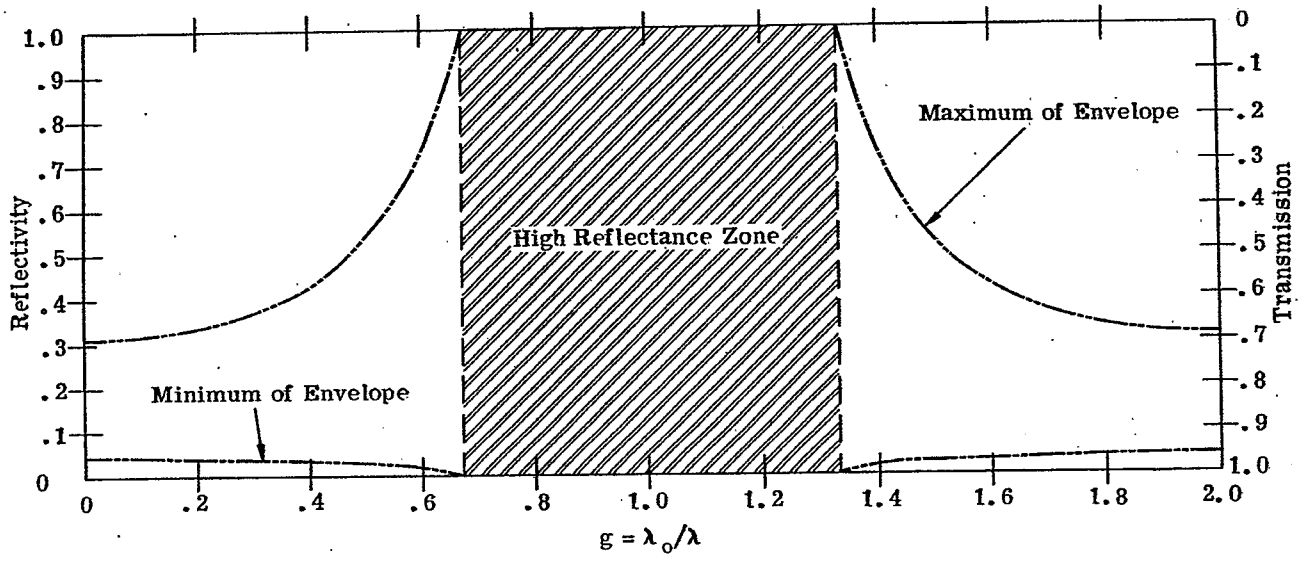

Figure 20.54 - Showing the high-reflectance zone, and the minimum and maximum of the reflectivity envelope of the quarter-wave stacks shown in Fig. 20.53

Type of Stack	g = 1.0	g = 2.0	g = 3.0	g = 4.0	g = 5.0	R_{max}, First Order, m=4
Quarterwave Basic Period L H	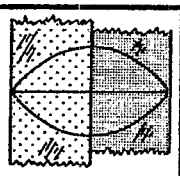	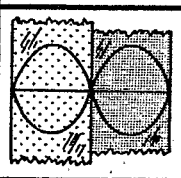	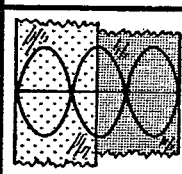	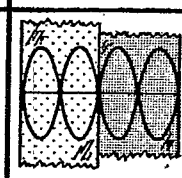	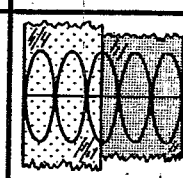	.957
2 : 1 Basic Period L' L' H'	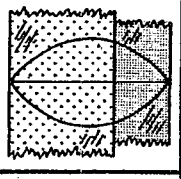	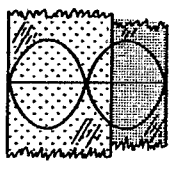	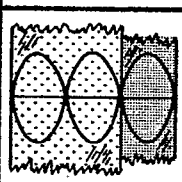	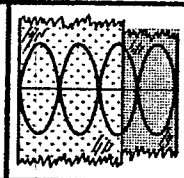	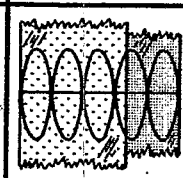	.925
3 : 1 Basic Period L'' L'' L'' H''	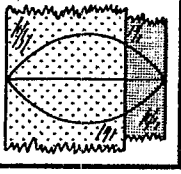	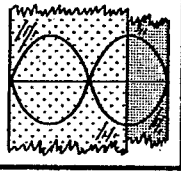	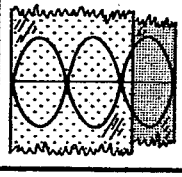	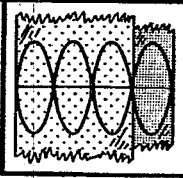	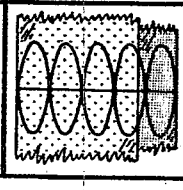	.858

Figure 20.55 A comparison of the wavelength (in vacuo) with the optical thickness of a basic period of a multilayer with a periodic structure, for various orders of interference.

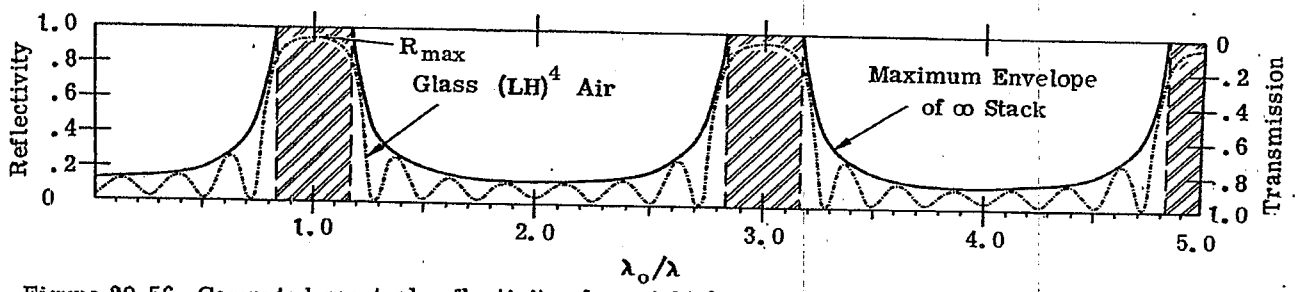

Figure 20.56 - Computed spectral reflectivity of an eight-layer quarter-wave stack (- - - - - - - -) and its envelope of maximum reflectivity (solid line). $n_H t_H + n_L t_L = \lambda_o/2$

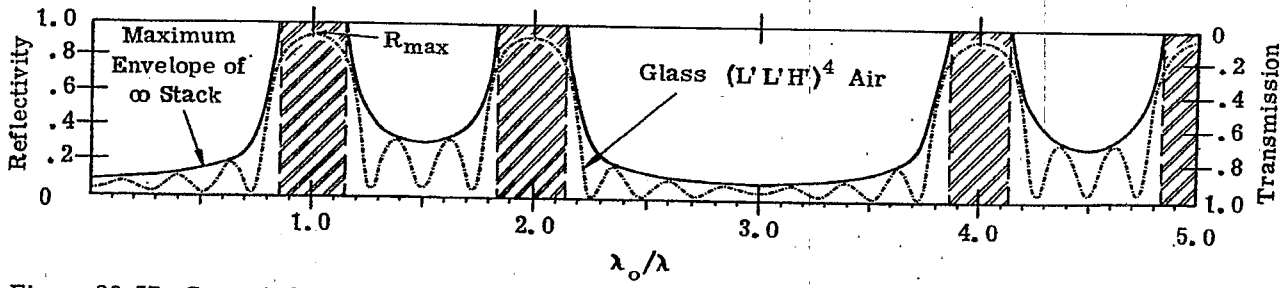

Figure 20.57 - Computed spectral reflectivity of an eight-layer 2:1 stack (- - - - - - - -) and its envelope of maximum reflectivity (solid line). $2\ n_L t_L + n_H t_H = \lambda_o/2$

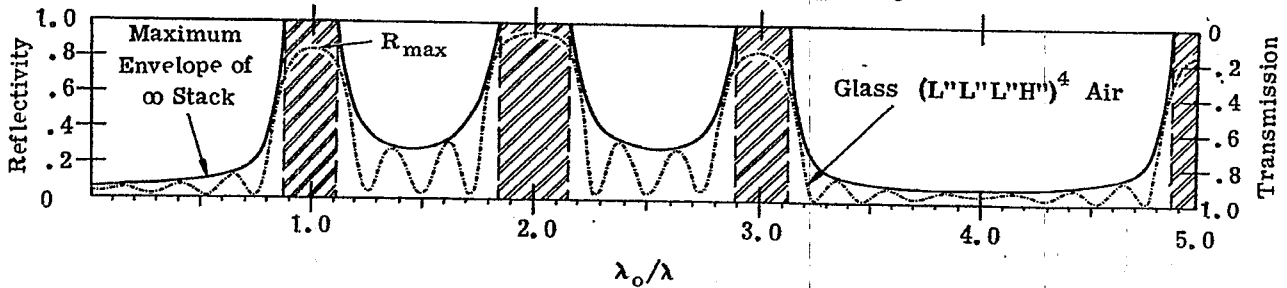

Figure 20.58 - Computed spectral reflectivity of an eight-layer 3:1 stack (- - - - - - - -) and its envelope of maximum reflectivity (solid line). $3\ n_L t_L + n_H t_H = \lambda_o/2$

20.4.2 Stacks with unequal thickness ratios.

20.4.2.1 General analysis.

20.4.2.1.1 Thus far we have considered the reflectivity properties of only a very specialized type of multilayer with a periodic structure, namely the quarter-wave stack, in which the two layers in a basic period have equal optical thickness. The high-reflectance zone occurs when the optical thickness of each layer is $\lambda_o/4$. Another way of stating this is to say that the high-reflectance zone occurs when the optical thickness of an entire period, LH equals $\lambda_o/2$. As is shown schematically in Figure 20.55, the high-reflectance zone occurs when a half-wave length fits into a basic period of stack. Consider the more general case where the two layers which compose the basic period of the stack do not have equal optical thickness, as for example, the stack

$$\text{glass } (HL')^6 \text{ air}$$

where the optical thickness of the L' layer is arbitrarily chosen to be 23% greater than the H layer. Does such a stack possess a high-reflectance zone ? The answer is yes. The position of the high-reflectance zones in any multilayer with a periodic structure can be found with the aid of the rule stated in the following paragraph.

20.4.2.1.2 A necessary but not sufficient condition for a high-reflectance zone to occur at a wavelength λ_o in a stack with a periodic structure is

$$\sum_i n_i t_i = q \frac{\lambda_o}{2} \qquad (46)$$

where q is an integer and the summation is over the basic period of the stack. Stated in other terms, the sum of the optical thicknesses of the layers comprising a basic period should equal an integral number of half wavelengths. This fact and the concept of an absentee layer (see Section 20.1.5.2.2) enables one to determine where the pass bands and high-reflectance zones of multilayer with a periodic structure occur.

20.4.3 Quarter-wave stack. Figure 20.56 shows the envelope function of the same quarter-wave stack shown in Figure 20.50, but over a larger range of g. Equation (46) is satisfied at $g = 1.0$ and hence this is in a high-reflectance zone. When $g = 2.0$, the optical thickness of the basic period LH is two half-waves and Equation (46) is satisfied for $q = 2$. Hence a high-reflectance zone could exist, but does not, because each of the layers in the stack is an absentee layer. Thus the reflectivity at $g = 2.0$ is the same as that of uncoated glass, namely .041. When $g = 3.0$, the total optical thickness of the basic period LH is three half-waves, and another high-reflectance zone occurs. When $g = 4.0$, the optical thickness of each layer is two half-waves and consequently all of the layers are absentee. Another high-reflectance zone occurs at $g = 5.0$, when the total optical thickness of the basic period LH is five-half waves. In the quarter-wave stack, high-refeitance zones occur at $g = 1, 3, 5, 7, 9, \ldots$ that is at odd integers. The high-reflectance zone which occurs at $g = 3$ is the third harmonic of the high-reflectance zone which occurs at $g = 1$, or to use the terminology of physical optics, this is a third-order interference peak. This is analogous to an open-ended organ pipe, which can sustain only odd harmonics.

20.4.3.1 The 2:1 stack. Let us study the reflectivity properties of the 2:1 stack:

$$\text{glass } L'L'H' \quad L'L'H' \quad L'L'H' \quad L'L'H' \quad L'L'H' \text{ etc.}$$

which can also be written as

$$\text{glass } (L'L'H')^m \text{ air}$$

where m is an integer. Here we have used the primed superscript, i.e. L' and H', to show that the optical thickness of these layers is different from the L and H which were used in the quarter-wave stack described in Section 20.4.1. In both cases, the optical thickness of the layers has been chosen so that a first-order interference high-reflectance zone occurs at λ_o. One must remember that the combination L'L' represents a single layer because each L' layer has the same refractive index. Thus the optical thickness of the L'L' layer is twice that of the H' layer and hence this is called a 2:1 stack. The spectral reflectivity curve of a 2:1 stack and its maximum reflectivity envelope are shown in Figure 20.57. Applying the rule which was stated in Section 20.4.2.1, the first-order high-reflectance zone occurs at $g = 1.0$ when the total optical thickness of the basic period L'L'H' is $\lambda_o/2$, as is shown in Figure 20.55. The second-order high-reflectance zone occurs at $g = 2.0$ when the total optical thickness of the basic period is two half-waves of λ_o. One might expect another high-reflectance zone at $g = 3.0$, but the optical thickness of the H' layer is a half-wave and the optical thickness of the L'L' layer is two-half waves. Hence, at $g = 3.0$, all of the layers are absentee layers and the reflectivity is that of

uncoated glass. At $g = 4.0$ and $g = 5.0$, the total optical thickness of the basic period equals four half-waves and five half-waves, respectively and high-reflectance zones occur. In this example, we have chosen L'L'H' as a basic period in which the optical thickness of the low-index layer is twice that of the high-index layer. The width of the high-reflectance zone is the same as the 2:1 stack, H'H'L'. As is shown in 20.4.6 however, the reflectivity properties at non-normal incidence of the two types of 2:1 stacks are quite different.

20.4.3.2 The 3:1 stack.

20.4.3.2.1 As a final illustration, consider the properties of stack with a periodic structure in which the optical thickness ratio is 3:1 :

$$\text{glass } (\text{L''L''L''H''})^m \text{ air}.$$

The double prime superscripts, H'' and L'' are used to show that the optical thickness of the L'' and H'' layers are different from both the H and L layers in the quarter-wave stack and the H' and L' layers of the 2:1 stack. The optical thickness of the H'' and the L'' layers is chosen so that the total optical thickness of the basic period of the stack, L''L''L''H'' equals $\lambda_o/2$, as is shown in Figure 20.55. Figure 20.58 shows a spectral reflectivity curve and the reflectivity envelope of a 3:1 stack. A first-order high-reflectance zone occurs at $g = 1.0$ and high-reflectance zones also occur at $g = 2.0$ and $g = 3.0$ when the total optical thickness of the basic period is two and three half-waves of λ_o, respectively. However, when $g = 4.0$ the optical thickness of the L''L''L'' layer is three half-waves and the optical thickness of the H' layer is a single half-wave. Hence all of the layers are absentee layers and the reflectivity at $g = 4.0$ is the same as uncoated glass. At $g = 5.0$ the total optical thickness of the basic period is five half-waves and hence another high-reflectance zone occurs. Thus every fourth high-reflectance zone is missing. Another way of stating this is to say that high-reflectance zones occur at the 1, 2, 3, 5, 6, 7, 9, 10, 11th etc. harmonics of the frequency of the fundamental.

20.4.3.2.2 The reflectivity curves of the multilayers with a periodic structure have been plotted on a frequency scale. It is possible that many readers are more accustomed to thinking in terms of wavelength, and so in Figure 20.59 is depicted the reflectivity versus wavelength of the 3:1 shown in Figure 20.58 with λ_o chosen to be 2.0 μ. A first-order reflectivity peak occurs at the fundamental wavelength, 2.0 μ. A second-order peak occurs at 1.0μ, which is one-half the fundamental and a third-order peak occurs at 0.667 μ, which is one-third of the fundamental. A fourth-order peak does not occur at $2.0/4 = 0.5\ \mu$ because the layers are absentee. A fifth order peak occurs at $\lambda_o/5 = 0.400\ \mu$, and so on. In comparing Figures 20.58 and 20.59, we note that on a frequency scale, the width of the first and third order reflectivity peaks is the same, whereas this is not true on a wavelength scale.

20.4.4 The general p:q stack.

20.4.4.1 General properties. It is patent that the analysis which we have made on the properties of the 1:1 (i.e. quarter-wave stack), 2:1 and 3:1 stack could be easily extended to any stack in which the ratio of the optical thickness of the layers is p:q, where q and p are integers. The following comparisons can be made between stacks which have a periodic structure, but different thickness ratios:

(1) The high-reflectance zone of the quarter-wave stack has even symmetry about $g = 1.0, 3.0$ etc. This is not necessarily true for other types of stacks.

(2) For a stack composed of layers of alternating refractive index n_a and n_b the width of the high-reflectance zone for any given ratio of $n_a : n_b$ is the largest when the optical thickness is equal. In other words, the high-reflectance zone of the quarter-wave stack is wider than high-reflectance zone of 2:1, 3:1, 3:2, etc. stacks.

(3) The width of the high-reflectance zone of a quarter-wave stack is given by a rather simple expression (i.e. Equation (39)). No such simple equations exist for other types of stacks. For example, the width of the high-reflectance zone of a 2:1 stack is given by the roots of a cubic equation.

(4) In the spectral region outside of the high-reflectance zones, the number of oscillations of the reflectivity increases as the number of periods (and hence the number of layers) of the stack increases. In any case, the oscillations will lie between the maximum and minimum reflectivity envelope of the infinite stack. The shape of this envelope function depends upon:

(a) The ratio of the optical thickness of the layers in a basic period.

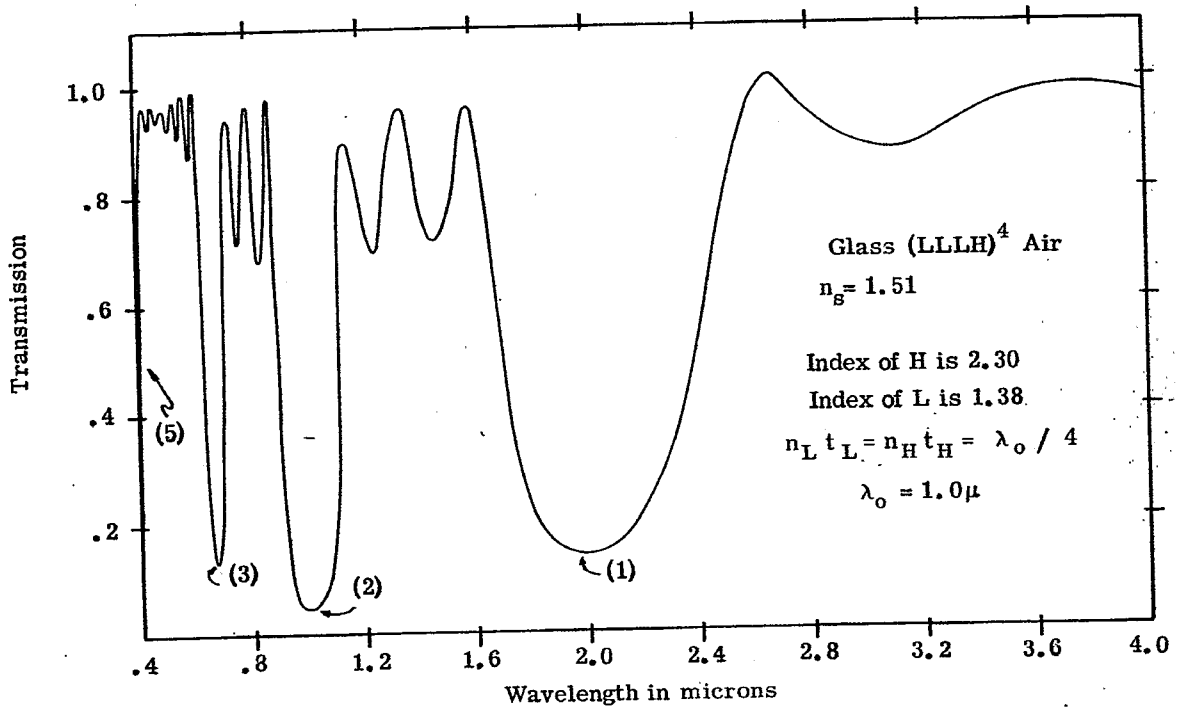

Figure 20.59 – Computed spectral transmission of an eight-layer 3:1 stack.

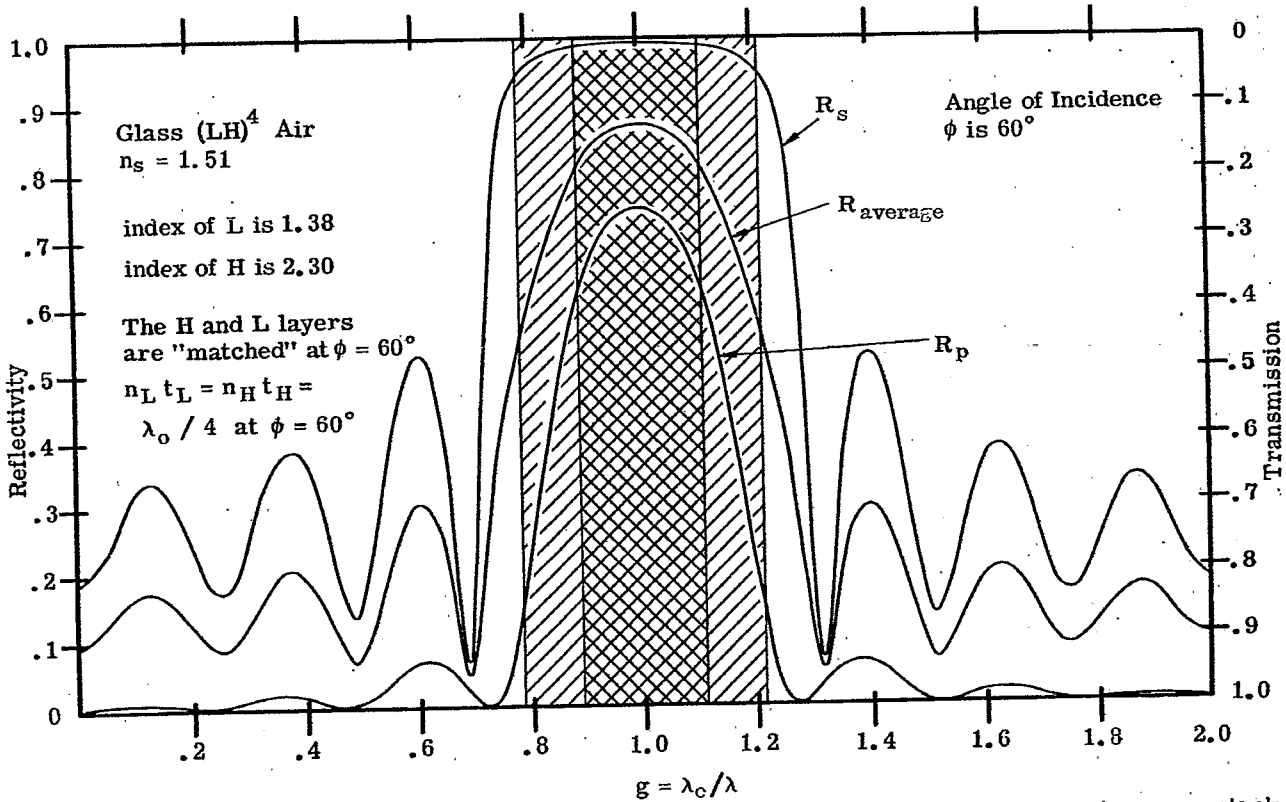

Figure 20.60 – Computed R_p, R_s, and $R_{av} = 1/2\ (R_p + R_s)$ of an eight-layer quarter-wave stack at $\phi = 60°$. The optical thickness of the H and L layers is matched 1:1 at $\phi = 60°$.

(b) The index of the two layers, n_a and n_b .

(c) The refractive index of the substrate, incident medium, and the refractive index and optical thickness of any layers which are added to the either end of the basic stack. This topic is discussed in Section 20.4.8.

(5) Given the indices n_o , n_s , n_a , n_b for any given order of interference the highest reflectivity for a given number of layers is obtained with a quarter-wave stack. This is illustrated in Figure 20.55, where the maximum reflectivity in the first order is listed for the quarter-wave, 2:1 and 3:1 stacks with an equal number of layers, with the same n_a, n_b, n_o, and n_s.

20.4.4.2 As an example of how the concept of absentee layers can be used to find the reflectivity at specific wavelengths, consider the ten-layer stack:

glass H'H'L' H'H'L' H'H'L' H'H'L' H'H'L' air

in which the optical thickness of the H'H' and L' layers has been chosen so that a first-order high-reflectance zone occurs at $g = 1.0$ as is shown in Figure 20.55. The problem is to find the reflectivity of this stack at $g = 1.5$. The optical thickness of each of the H'H' layers at $g = 1.5$ is a half-wave and hence each of these layers is absentee. Thus the stack reduces to:

glass L' L' L' L' L' air .

However, at $g = 1.5$ each of the L' layers is a quarter-wave in optical thickness and hence each pair of L' layers represents a half-wave. Thus four of the L' layers can be removed from the stack leaving:

glass L' air .

Thus the reflectivity of this ten-layer stack at $g = 1.5$ is the same as the reflectivity of a single quarter-wave layer on glass and can be readily computed from Equation (30).

20.4.4.3 The treatment given here of the propagation of waves in a medium with a periodic structure has been descriptive and qualitative. A rigorous mathematical treatment is given by Epstein[32], Brillouin[33], and Seitz[34].

20.4.5 Analogies.

20.4.5.1 Electrical transmission line. It is helpful to give some analogies between the propagation of light in a multilayer with a periodic structure and other fields, such as electrical engineering, x-ray crystallography, and solid state physics. Using the concepts which were presented in Section 20.1.4.1, the electrical transmission line shown in Figure 20.48 is the analogue of the quarter-wave stack shown in the same Figure. The transmission line consists of eight sections, each of which has an electrical length of a quarter-wave and which alternate between a high and low impedance. We recall that the load admittance of the transmission line is analogous to the refractive index of the substrate. As one can readily show by using a Smith chart, the load impedance is reflected back to the terminals of the preceeding section as a maximum value when the electrical length of the line is a quarter-wave. In this case the substitutional impedance at the input terminals is very large. Consequently there is large impedance mismatch between the characteristic impedance of the generator (which is 1.0) and the substitutional impedance of the line. This means that the voltage standing wave ratio is large and hence the voltage reflection coefficient to close to one.

20.4.5.2 Bragg reflection of x-rays. A beam of x-rays travels through a vacuum with the velocity of light. This velocity is pertubed slightly when the beam travels through a cloud of electrons, the amount of the perturbation being nearly proportional to the density of the electrons. In a crystal, there is a high density of electrons near each atomic lattice site. Since atoms are regularly spaced in a crystal, the x-rays travel through a periodically stratified medium. Although the change in the velocity is not abrupt, as it is for light propagating through a multilayer, nevertheless Bragg reflection of the x-rays is observed when the path difference between adjacent reflecting crystal planes is an integral number of wavelengths. This point is further amplified by Brillouin.[33]

20.4.5.3 The propagation of electrons in a crystal. The propagation of a single electron in a crystal is treated quantum mechanically by solving the Schrödinger equation, in which the electron is represented by a traveling wave with a deBroglie wavelength, λ_b . The velocity of the electron is perturbed by the electrostatic repulsion of electron cloud at each lattice site and consequently the electron moves in a potential which varies periodically. Regardless whether one chooses a simple one-dimensional periodical potential of Kronig and Penney, or a more sophisticated potential computed from atomic wave functions, the electron

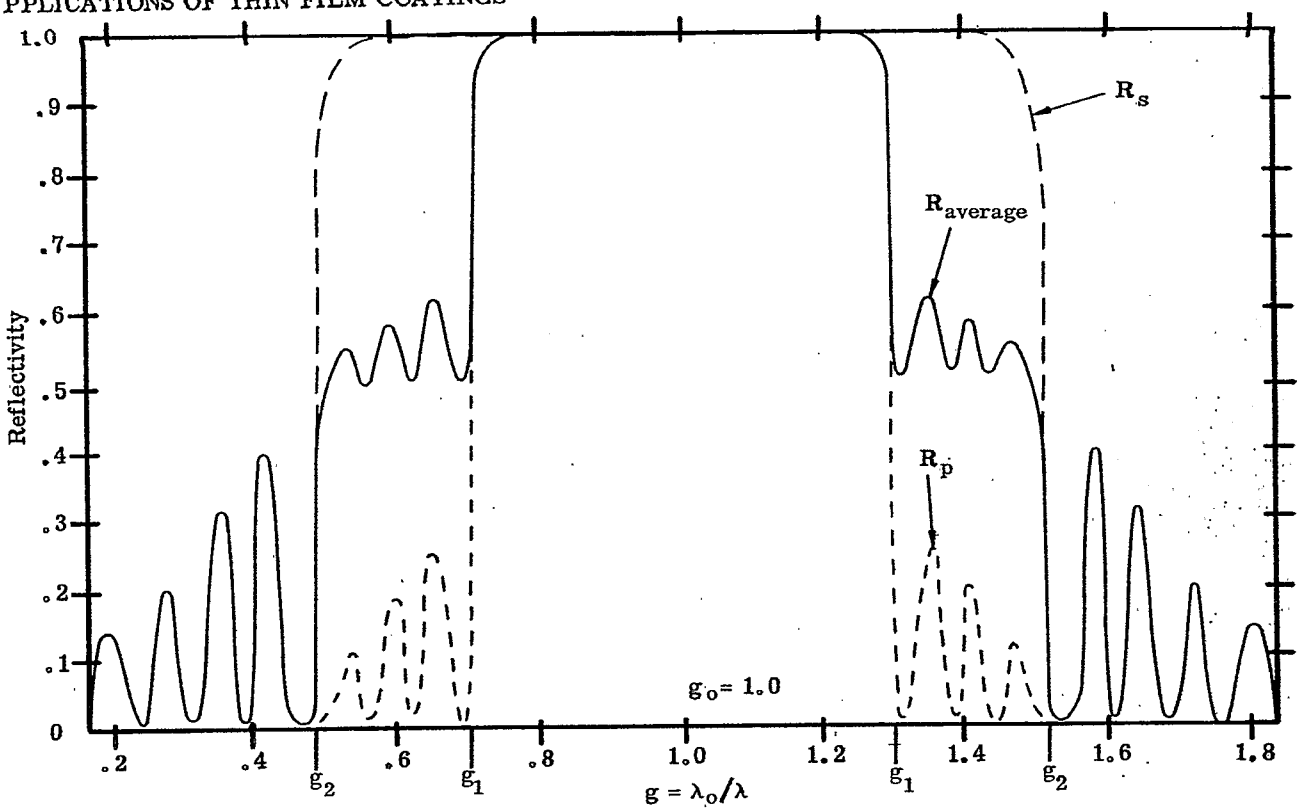

Figure 20.61 - R_p, R_s, and $R_{av} = 1/2 (R_p + R_s)$ at $\phi = \phi_o$ of a ficticious quarter-wave stack with the optical thicknesses of the layers matched 1:1 at ϕ_o.

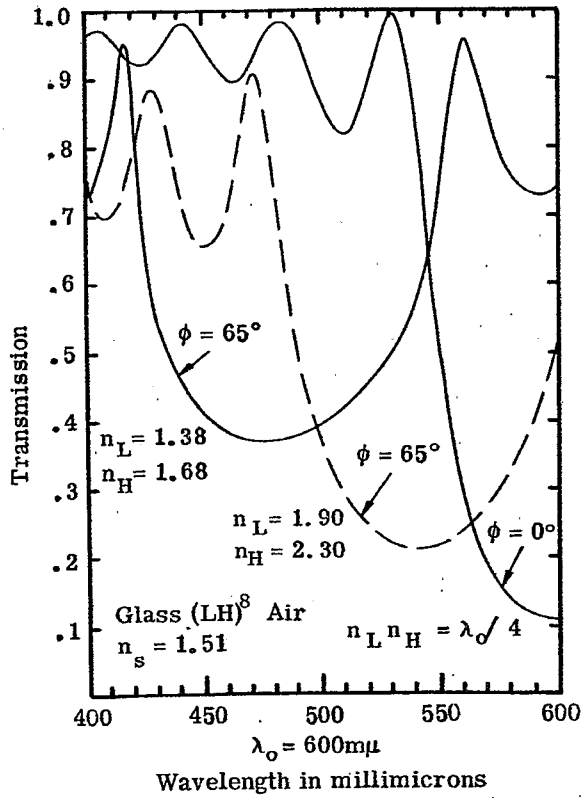

Figure 20.62 - Computed T_{av} at $\phi = 0$ and $\phi = 65°$ of sixteen-layer quarter-wave stacks with low index (solid line) and high index (dashed line).

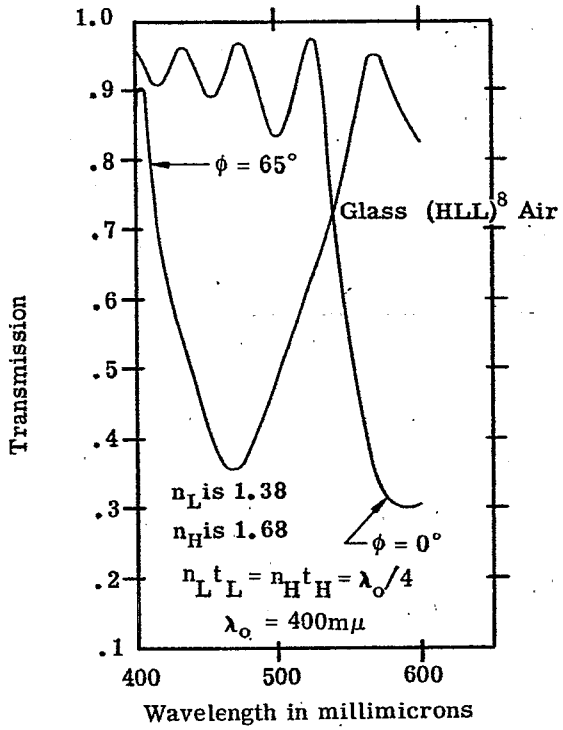

Figure 20.63 - Computed T_{av} at $\phi = 0$ and $\phi = 65°$ of a sixteen-layer 2:1 stack.

is reflected whenever $\lambda_b/2$ equals a multiple of the period of the lattice. An equivalent way of saying this is that the edge of the Brillouin zone occurs when the wave-vector $\underset{\sim}{K} = \pi/a$, where a is a lattice space in a particular direction and $\underset{\sim}{K}$ is wave-vector (Seitz)[34]. This is treated in detail by Brillouin [33], Seitz [34], and others.

20.4.6 The reflectivity of quarter-wave stacks at non-normal incidence.

20.4.6.1 Layers matched at angle. In considering the reflectivity of quarter-wave stacks at non-normal incidence, we must consider separately the case where thickness of the layers is matched (see Section 20.1.6.3, for a definition of this term) at normal incidence and the case where the layers are matched at a particular angle ϕ_o. In the latter case, the layers are deliberately mismatched so that at normal incidence the ratio of the optical thickness of the H and L layer is not 1:1, but the ratio is 1:1 at ϕ_o.

20.4.6.1.1 As an example of a match at angle, consider the eight-layer quarter-wave stack whose reflectivity curve is shown in Figure 20.60. The optical thickness of the low-index layer L has been made thicker than the high-index layer H in a ratio $n_H t_H : n_L t_L = 1.0 : 1.19$. In this case the layers are matched at $\phi_o = 60°$. Equation (39) can be used to compute the width of the high-reflection zone, using the effective index appropriate to each plane of polarization. For example, at $\phi = 60°$, in the "p" plane of polarization the effective index of the L layer is 1.773 and the effective index of the H layer is 2.483. From Equation (39) we find that the half-width, Δg, of the high-reflectance zone is 0.107. Similarly Δg in the "s" plane of polarization is 0.214, which is larger than the Δg at normal incidence, which is 0.161. The high-reflectance zones are shown in Figure 20.60 as cross hatched areas. The generalizations stated in 20.4.6.1.1 and 20.4.6.1.2 apply to quarter-wave stacks which matched at a particular angle ϕ_o, and are not confined to the eight-layer stack which has been used as an example.

20.4.6.1.2 The width of the high-reflectance zone increases in the "s" plane of polarization and decreases in the "p" plane of polarization. If many periods, say thirty or forty, are used in a stack, so that both R_p and R_s are close to 1.0 within their high-reflectance zones, the average reflectivity, $R_{av} = 1/2 (R_p + R_s)$ has the shape which is depicted in Figure 20.61. In the region between $g = 1.0$ at the center of the stack and g_1, a high-reflectance zone exists for both planes of polarization and hence R_{av} is close to 1.0. At g_1, the high-reflectance zone for the "p" plane of polarization ends and R_p fluctuates at low values outside of this zone. The high-reflectance zone for the "s" polarization extends to g_2 and in this intermediate region between g_1 and g_2 R_{av} attains a minimum value of 0.50. We observe that this shoulder on the R_{av} curve is due to the dissimilar width of the high-reflectance zones in the two planes of polarization. This shoulder has been somewhat exaggerated for purposes of illustration in Figure 20.61. The reflectivity curve of the eight-layer quarter-wave stack shown in Figure 20.60 does not show this shoulder, because the reflectance R_p does not drop to zero rapidly enough outside of the high-reflectance zone. If more periods were added to the stack, then eventually the R_{av} curve would show such a shoulder.

20.4.6.1.3 Maximum reflectivity. Since the thickness of the layers is matched at ϕ_o, the maximum reflectivity at $g = 1.0, 3.0, 5.0$, etc. can be computed in each plane of polarization from Equations (40) to (43), using the effective index appropriate to each plane of polarization.

20.4.6.2 Layers matched at normal incidence.

20.4.6.2.1 If a stack which is matched 1:1 at normal incidence is viewed at non-normal incidence, the position of the high-reflectance zone can be found by substituting effective thicknesses in Equation (46). The high-reflectance zone is no longer centered at a wavelength computed from Equation (46) and also the width of the zone (in each plane of polarization) is different than at normal incidence.

20.4.6.2.2 As an example of the application of Equation (46) to a stack at non-normal incidence, consider the 16 layer stack:

$$\text{glass} \quad (\text{LH})^8 \quad \text{air}$$

in which both the L and H have a QWOT of 600 mμ at normal incidence, that is,

$$n_i t_i = 150 \text{ m}\mu = 600 \text{ m}\mu/4 .$$

The transmission curve, shown in Figure 20.62, has a minimum at 600 mμ which is the center of the high-reflectance zone. Two cases are considered separately at $\phi = 65°$.

Case I $n_L = 1.90$, $n_H = 2.30$. From Figure 20.8 we find that the change in effective thickness is 0.92 for the H layer and 0.891 for the L layer, the latter value being found by linear interpolation.

Substituting these values for the effective thickness into Equation (46), we obtain

$$(.92)\ (150\ m\mu)\ +\ (.879)\ (150\ m\mu)\ =\ \frac{\lambda_1}{2}\ , \qquad (47)$$

whence $\lambda_1 = 540\ m\mu$. From Figure 20.62 we see that the minimum T_{av} at $\phi_o = 65°$ is very close to $540\ m\mu$.

Case II $n_L = 1.38$ and $n_H = 1.68$. The change in the effective thickness is found from Figure 20.9 to be 0.754 and 0.842. Solving an equation similar to Equation (47) gives the result that $\lambda_1 = 480\ m\mu$. Actually, Figure 20.62 shows that the wavelength at which T_{av} is a minimum is shifted to shorter wavelengths by about $10\ m\mu$.

20.4.7 Minimization of the angle shift.

20.4.7.1 The basic problem. The transmission curves of all multilayer filters change with the angle of incidence and usually exhibit a shift to shorter-wavelengths. This angle shift is of little importance if the multilayer filter is illuminated with collimated light at one angle of incidence. However, serious problems often arise when the light is highly convergent. For example, either of the multilayers shown in Figure 20.62 would attenuate the sodium yellow lines (at $589\ m\mu$) if used at normal incidence, but they would be quite ineffective at $\phi = 65°$. The problem of the angle shift of a multilayer filter is similar to the problem of the chromatic aberration of a lens. In either case, the effect is ubiquitous and at best the designer can only minimize it. Two methods of minimizing the angle shift are: (1) The use of high-index materials. (2) The use of more of the higher index material in the basic period.

20.4.7.2 The use of high-index materials. From the examples in 20.4.6.2.2, it is patent that the change in the effective thickness of each of the layers is much less for high-index layers than for low-index layers. Thus the angle shift of the quarter-wave stack with $n_L = 1.90$, $n_H = 2.30$ is much less than the stack with $n_L = 1.38$, $n_H = 1.68$, even though the width of the high-reflectance zone at normal incidence is the same because the index ratio n_L/n_H is the same. From this it follows that if a multilayer with a periodic structure is used as a "cutoff" filter - that is to pass, either in the long-wave or short-wavelengths region - it should contain high index materials if the angle shift is to be minimized. For example, an infrared filter which contains cryolite and germanium has a larger angle shift than a filter which contains zinc sulfide and germanium, because the refractive index of zinc sulfide is nearly twice as large as that of cryolite.

20.4.7.3 The use of more high-index material in a basic period. If only quarter-wave stacks were considered, then the discussion would terminate with 20.4.7.2. If, however, the optical thickness of the high-index material is different from the thickness of the low index material, such as occurs in a 2:1 or a 3:1 stack, then it is possible to reduce the angle shift below that of a quarter-wave stack (using the same materials) by using the high-index material in the thicker layer. That is to say, a $(LHH)^m$ stack has a lower angle shift than the stack $(HLL)^m$, even though the width of the high-reflectance zone at normal incidence of these two stacks is identical. Similarly, the stack $(LHHH)^m$ has a smaller angle shift than the stack $(HLLL)^m$. These facts are illustrated in Figure 20.63 which shows the spectral transmission of the 2:1 stack

$$\text{glass}\ (H\,LL)^8\ \text{air}$$

at normal incidence and at 65°. In this stack, the optical thickness of the low-index layer is greater than that of the high-index layer. The 2:1 stack whose transmission curve is shown in Figure 20.64 has more high-index material in the basic period:

$$\text{glass}\ (L\,HH)^8\ \text{air}.$$

In Figure 20.64 the T_{av} at 65° of the $(L\,HH)$ stack (shown as solid line) is compared with the H LL stack (dashed line). Although both stacks show a considerable angle shift to the blue, the shift of the LHH stack is definitely less. The angle shift of the HLL stack is considerably greater than the comparable quarter-wave stack shown in Figure 20.62 which uses the same refractive indices. Figures 20.79, 20.86, and 20.91 show the angle shift of transmission curve of various multilayers.

20.4.8 Variations on the basic periodic structure.

20.4.8.1 General considerations. Most of the quarter-wave stacks and other multilayers with a periodic structure shown in Figures 20.48 to 20.64 have been selected primarily as illustrations and should be modified slightly if they are used as practical filters. Additional layers can be added to these stacks for either

of two purposes:

(1) To increase the reflectivity in the high reflectance zone.

(2) To increase the transmission in the spectral region outside of the high-reflectance zone.

If a quarter-wave stack were used as a semi-transparent mirror coating for a Fabry-Perot interferometer, then primary objective would be to obtain a high reflectivity over a specific spectral region and little interest is paid to the transmission outside of this region. On the other hand, if a quarter-wave stack were used as a long-wave pass filter, then it is important to optimize the transmission in the long-wave region.

20.4.8.2 Increasing the reflectivity. It is evident from Equations (42) and (43) that a quarter-wave stack has a higher R_{max} when a high-index layer is next to both the substrate and the incident medium. The R_{max} of this odd-layered stack is greater than the R_{max} of an even-layered stack. This is illustrated in Figure 20.65, shows the computed reflectivity of a six-layer and a seven-layer stack which use the same n_a and n_b. Even though an additional H layer has been added to the basic stack so that its design can no longer be represented as $(HL)^m$, the seven-layer stack is still called a quarter-wave stack. It is evident that a considerable increase in the reflectivity has been achieved by the addition of the extra H layer. If an additional L layer were added so that the multilayer design is,

glass $(HL)^4$ air ,

the R_{max} would be less that of the seven-layer stack. An increase in the maximum reflectivity is also achieved if an odd number of layers are used rather than an even number in the 2:1 and 3:1 stacks shown in Figures 20.57 and 20.58 .

20.4.8.2.2 The effect on R of a mismatch in layer thickness. Closely allied to the problem of attaining the maximum reflectivity is the problem of a mismatch in the thickness of the layers. If the optical thickness of any one of the layers in a quarter-wave stack, or other type of multilayer with a periodic structure, deviates by a small amount from $\lambda_o/4$, then the reflectivity throughout the entire high-reflectance zone falls below the value which would be attained if all the layers were perfectly matched. For example, suppose that a quarter-wave stack is manufactured by evaporating each of the layers in a vacuum and that in this process errors of a random nature are made in controlling the thickness of each of the layers. Consequently, the optical thickness of each of the layers differs from $\lambda_o/4$ by a random amount. As long as these errors are not excessive, say greater than ten percent, the region of high-reflectivity about λ_o which is characteristic of a quarter-wave stack, is still observed. However, the R_{max} of such a multilayer is not as high as it would be for a perfect stack and also the cutoff at the edge of the high-reflectance zone is not as steep. The fact that rather large errors can be made in controlling the thickness of the layers without serious detrimental effects upon the reflectivity is the factor which permits certain types of band pass multilayer filters to be manufactured with relatively crude monitoring equipment to control the thickness of the layers.

20.4.8.3 Enhancing the transmission in the spectral region outside of the high-reflectance zone. Several methods are used to enhance the transmission in the spectral region outside of the high-reflectance zone:

(1) Additional layers of non-quarter-wave optical thickness can be added to the stack. This is discussed in 20.4.8.3.1.

(2) It is possible to vary the thickness of each of the layers by a small amount so that the transmission increases outside of high-reflectance zone. Since this method improves upon, or refines, an existing multilayer design, it is called the refining method. This is covered in 20.4.8.4.

20.4.8.3.1 An effective method of enhancing the transmission in the spectral region outside of the high-reflectance zone is to add additional layers to the basic stack (which has a periodic structure). For example, one could start with the twelve-layer quarter-wave stack

glass $(HL)^6$ air

and add several layers to either end of the stack:

glass $L_1\ H_2\ (HL)^6\ H_3\ L_4$ air

where the additional layers L_1 , H_2 , H_3 L_4 are tagged with subscripts to emphasize the fact that they do not necessarily have the same thickness or refractive index as the H and L layers in the

basic stack. As an example of this procedure, suppose that a quarter-wave stack is used as a short-wave pass filter which is intended to pass the blue and green, but attenuate in the yellow and red. A seven-layer stack of zinc sulfide ($n = 2.30$) and magnesium fluoride ($n = 1.38$) is considered:

glass H L H L H L H air .

The reflectivity versus frequency curve is shown in Figure 20.65, and has even symmetry about λ_o . The region of high reflectivity extending from $g = 0.8$ to 1.2 would attenuate the red and yellow, but this multilayer would be much more effective as a short-wave pass filter if the reflectivity peaks at $g = 1.39$ and 1.63 could be decreased. This accomplished if a low-index layer of eighth-wave optical thickness is added to each end of the stack:

glass $\frac{L}{2}$ H L H L H L H $\frac{L}{2}$ air .

The spectral transmission of such a stack with $\lambda_o = 700$ mμ is shown in Figure 20.66. The effect of adding the eighth-wave layers is to increase the transmission in the short-wave region. The reflectivity peak at $g = 1.39$ (at 504 mμ in Figure 20.66) has been decreased from 0.25 to 0.11 and the peak at $g = 1.63$ (430 mμ in Figure 20.66) is barely perceptible. The reflectivity in the long wavelength region has actually been increased slightly from .25 to .27 . The addition of the eighth-wave layers to the seven-layer stack has decreased R_{max} from .95 to .94 . Additional layers can be added to this nine-layer stack to increase the transmission even further in the short-wavelength region. Epstein[35] elaborates on methods of accomplishing this. As an example of how the transmission can be increased in the long-wave region, consider the multilayer

glass $\frac{H}{2}$ L H L H L H L $\frac{H}{2}$ air .

The spectral transmission of this multilayer is shown in Figure 20.67. The transmission in the red and infrared is quite high but the transmission in the near ultraviolet is considerably lower than that of a quarter-wave stack LHLHLHL . This is usually the case, that when the transmission is increased on the long-wave side of the high-reflectance zone, it is decreased on the short-wave side, and vice versa. In practice, the ultraviolet transmission of the stack shown in Figure 20.67 would be much lower than the computed values if zinc sulfide were used as the high-index layer material, since this material absorbs strongly below 400 mμ . The design of the multilayer shown in Figure 20.67 can also be written as:

glass $\left(\frac{H}{2} \; L \; \frac{H}{2} \right)^4$ air .

This can be regarded as a multilayer with a periodic structure with $\left(\frac{H}{2} \; L \; \frac{H}{2} \right)$ as a basic period. Equation (46) still applies and consequently a high-reflectance zone can occur when an integral number of half-waves fit into the basic period. When the design of the stack can be written in this manner, it can be shown that at any wavelength outside of the high-reflectance zone, it is possible to replace the entire stack of nine layers by a single layer with a ficticious index n_h and ficticious optical thickness τ . That is, for the purposes of computing the reflectivity (outside of the high-reflectance zone), the nine-layer stack is equivalent to a single-layer of index n_h and optical thickness τ . The index n_h is called the Herpin equivalent index. Space does not permit us to describe how the concept of the Herpin equivalent index is used to design multilayer combinations which have a high transmission outside of the high-reflectance zone. For further details, the reader can refer to Weinstein[5] or Epstein[35] . To cite some additional examples, eighth-wave layers of high-index material have been added to the quarter-wave stacks shown in Figures 20.73, 20.78, 20.80, 20.81,and 20.82 to increase the transmission in the long-wave region. The multilayers shown in Figures 20.82 and 20.83 are quarter-wave stacks modified so that the transmission is optimized in the short-wave region. An eighth-wave layer of low index material is added to one end of the quarter-wave stack (next to the incident medium), while a layer of optical thickness $1.28 \; \lambda_o/4$ is inserted between the quarter-wave stack and the substrate.

20.4.8.4 The refining method.[36] The refining method consists of varying by a small amount the thickness of each of the layers of a multilayer of specified design, so that the transmission is increased (or decreased, as the case may be) at certain specified wavelengths. This method can be used to increase the transmission of a quarter-wave stack on either the short-wave or long-wave side of the high-reflectance zone. As is mentioned in 20.4.8.1.1, the thickness of each of the layers can be changed by as much as 10% without seriously affecting the reflectivity in the high-reflectance zone. The refining method is similar to the relaxation method which is used to solve complex engineering problems. The computations are sufficiently lengthy and tedious that it is necessary to employ an electronic digital computer. As an example of the application of the refining method, suppose it is desired to increase the transmission of a quarter-wave stack which transmits in the blue but attenuates longer wavelengths. The computed reflectivity of a modified quarter-wave stack is shown in Figure 20.68. The effect of using a large number of layers is to achieve a high attenuation in the green and red ($T_{min} = .001$) and a sharp cutoff at

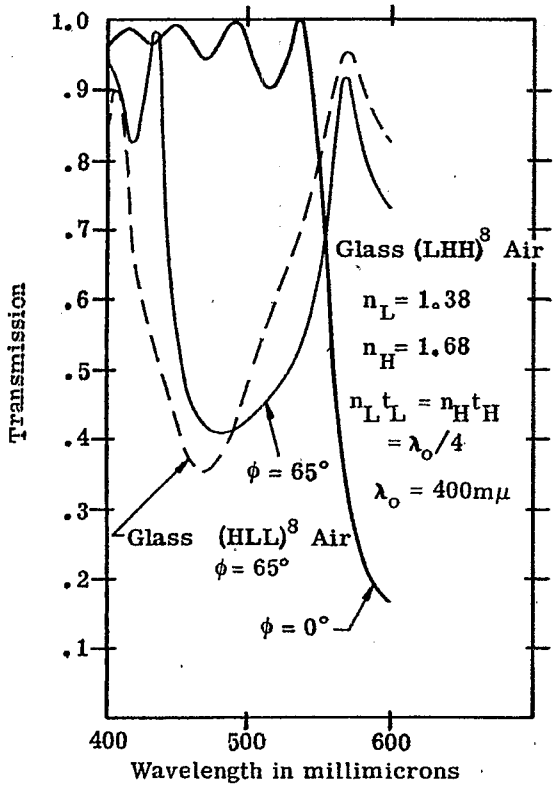

Figure 20.64- T_{av} of a sixteen-layer 2:1 stack at ϕ = 0 and 65°. The ϕ = 65° curve from Fig. 64 is shown as a dashed line.

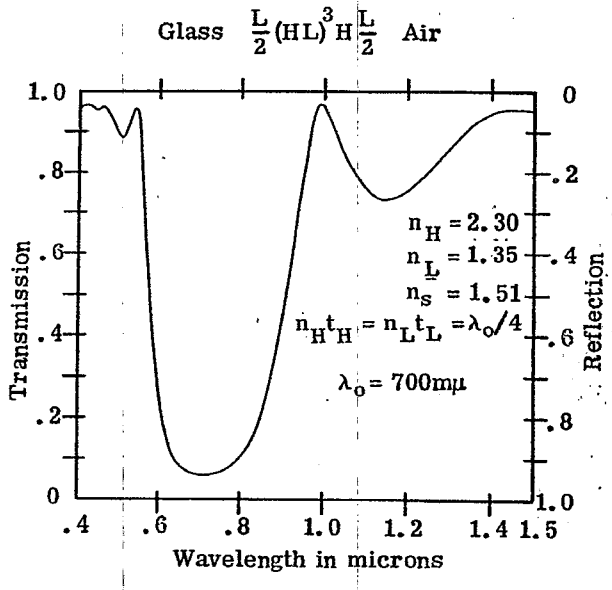

Figure 20.66- Computed spectral transmission of a short-wave pass filter consisting of a modified quarter-wave stack.

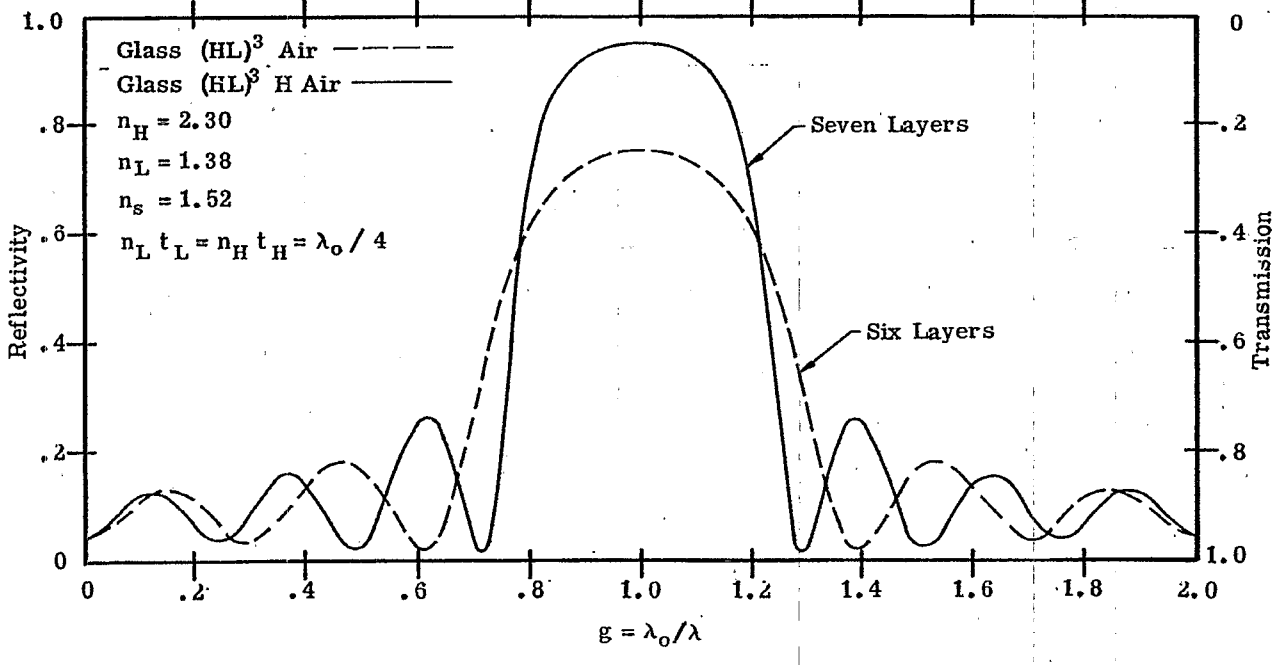

Figure 20.65- Computed spectral reflectivity of six-layer (dashed line) and a seven-layer (solid line) quarter-wave stack.

500 mμ . The reflectivity of the modified quarter-wave stack (DESIGN I) attains a maximum of .33 in this region. This multilayer would be much more effective as a blue pass filter if the undesirable peaks in the reflectivity at 484 mμ and 446 mμ could be eliminated. This is accomplished by varying the thickness of each of the layers by a relaxation process. Table 20.4 shows the quarter-wave optical thickness of each of the layers of the initial stack (Design I) and the refined design (Design II). The maximum change in the thickness of any of the layers is only 12% and the thickness of most of the layers has been changed by only a few percent. This mismatch in the optical thickness of the layers has caused the peak reflectivity to decrease from .9990 (in Design I) to .9988 (in Design IX). Also, the steepness of the transition from the high-reflectance zone to the pass region has been slightly decreased. As another example, the curve designated as Design III in Figure 20.69 depicts the spectral transmission of a quarter-wave stack composed of germanium and silicon monoxide which is used as a long-wave pass filter for the infrared. Table 20.4 shows the thickness of each of the layers (as a fraction $\lambda_o/4$) of the refined multilayer (Design IV) whose transmission curve is also shown in Figure 20.69 .

20.5 LONG-WAVE PASS FILTERS

20.5.1 General properties. From the discussion in 20.4 about the properties of a multilayer with a periodic structure, the method of designing either a long-wave or a short-wave pass filter is fairly obvious. One simply chooses a quarter-wave stack or other type of stack with periodic structure, so that the high-reflectance zone covers the region to be attenuated. It is necessary to choose the materials which are used in the stack and also the number of layers. This can be accomplished after the properties of the multilayer stack have been specified. In establishing the specifications of a long-pass, short-pass, or a band-pass multilayer filter, some of the following properties are considered:

(1) The optical density in the attenuation region. This is discussed in 20.5.1.1.

(2) The transmission in the pass region. In 20.4.8.3 two methods of enhancing transmission in the pass region are presented.

(3) The steepness of the cutoff.* This is discussed in 20.5.1.2.

(4) The change of the transmission with angle, i.e. the angle shift. If a minimum amount of angle shift is required, then high-index materials should be used in the stack, as is mentioned in 20.4.7.

(5) The change of transmission with temperature. In certain applications multilayer filters are used in environments which are either warmer or cooler than room temperature, and the shift of the spectral transmission must be taken into account. Multilayer filters are sometimes placed in thermal contact with an infrared detector which is cooled with liquid nitrogen. Figure 20.79 shows the shift with temperature of the transmission of an infrared filter.

20.5.1.1 The optical density in the attenuation region increases as the index mismatch between the layers of a stack increases and also as the total number of periods increases. In the special case of a quarter-wave stack, the maximum attenuation can be computed from Equations (41) through (43).

20.5.1.2 The sharpness or the steepness of the cutoff * is also an important parameter. The cutoff is the region in which the transmission drops from "high" values in the pass region to "low" values in the attenuation region (in the high reflectance zone). The words low and high in the preceeding sentence are enclosed in quotation marks because the criterion of what constitutes a low or high transmission is rather arbitrary. For example, in the multilayer shown in Figure 20.76 the high value is chosen as 0.70 and the low value as .05. Similarly, the wavelength at which the transmission has decreased to some arbitrary value is called the cutoff wavelength. For example, in Figure 20.79 the wavelength of the $T = .05$ point is chosen as the cutoff wavelength. Regardless of what criterion is chosen, the steepness of the cutoff increases as the number of periods increases. Let us apply as a criterion of the sharpness of the cutoff the wavelength difference $\Delta\lambda$ between the $T = 0.9$ point and $T = 0.1$. Each of the multilayers, whose transmission curves are shown in Figures 20.66 and 20.68, contain the same materials, but have a different number of periods. The $\Delta\lambda$ for the nine-layer stack (Figure 20.66) is 90 mμ, whereas the $\Delta\lambda$ for the seventeen-layer stack (Figure 20.68) is 20 mμ. Although the comparison does a slight unjustice to the nine-layer stack because its cutoff is at longer wavelengths, nevertheless this serves to illustrate the point that the steepness of the cutoff increases at the number of basic periods increases. The order of interfer-

* Some writers use the word "cuton" to denote the onset of the attenuation region and "cutoff" to denote the "cutoff" (or stopping) of the attenuation region. In section 20, this distinction is not made.

LAYER	INDEX OF LAYER	QUARTER-WAVE OPTICAL THICKNESS IN mμ		LAYER	INDEX OF LAYER	OPTICAL THICKNESS OF LAYER IN UNITS OF $\lambda_o/4$	
		DESIGN I	DESIGN II			DESIGN III	DESIGN IV
AIR	1.00	MASSIVE		AIR	1.00	MASSIVE	
1	1.38	300	306	1	4.00	0.5	0.419
2	2.30	599	639	2	1.80	1.0	1.181
3	1.38	599	630	3	4.00	1.0	1.272
4	2.30	599	610	4	1.80	1.0	0.967
5	1.38	599	606	5	4.00	1.0	0.879
6	2.30	599	597	6	1.80	1.0	1.060
7	1.38	599	582	7	4.00	1.0	1.194
8	2.30	599	573	8	1.80	1.0	1.023
9	1.38	599	577	9	4.00	1.0	0.874
10	2.30	599	589	10	1.80	1.0	0.961
11	1.38	599	596	11	4.00	1.0	1.143
12	2.30	599	590	12	1.80	1.0	0.979
13	1.38	599	585	13	4.00	0.5	0.405
14	2.30	599	601	GLASS	1.52	MASSIVE	
15	1.38	599	646				
16	2.30	599	672				
17	1.38	599	616				
GLASS	1.52	MASSIVE					

Table 20.4- The design of multilayer filters, whose transmission and reflectivity curves, are shown in Figures 20.68 and 20.69 .

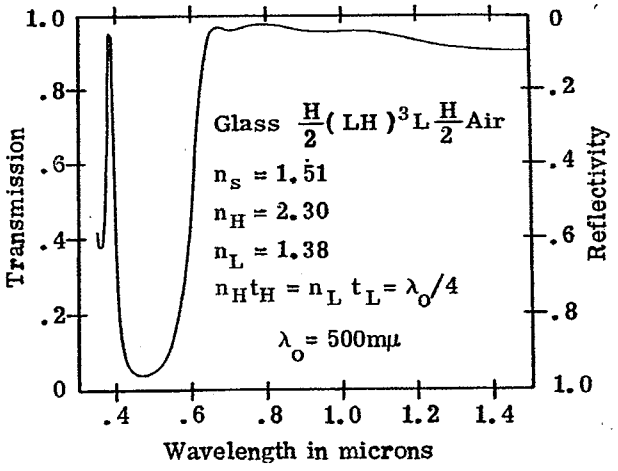

Figure 20.67- Computed spectral transmission of a long-wave pass filter consisting of a modified quarter-wave stack.

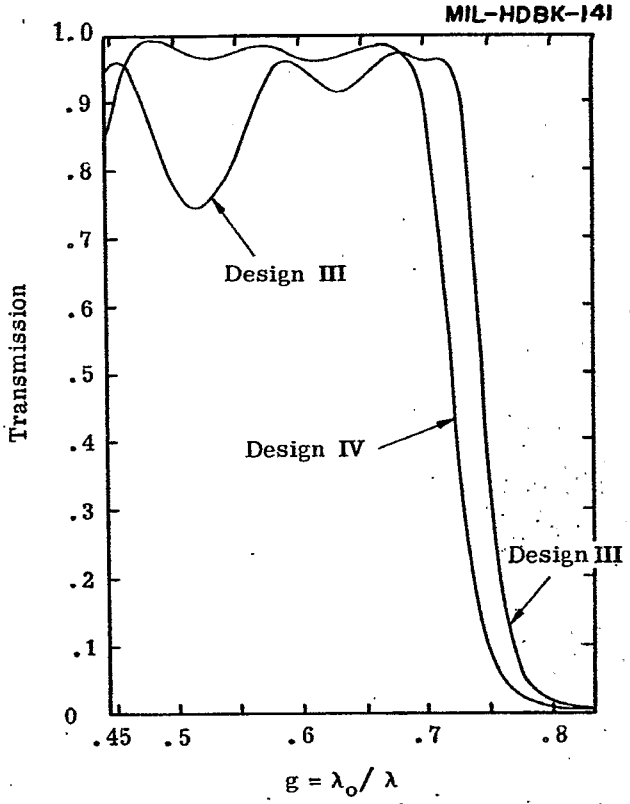

Figure 20.69- Computed spectral transmission of multilayers designated as Design III and Design IV in Table 20.4.

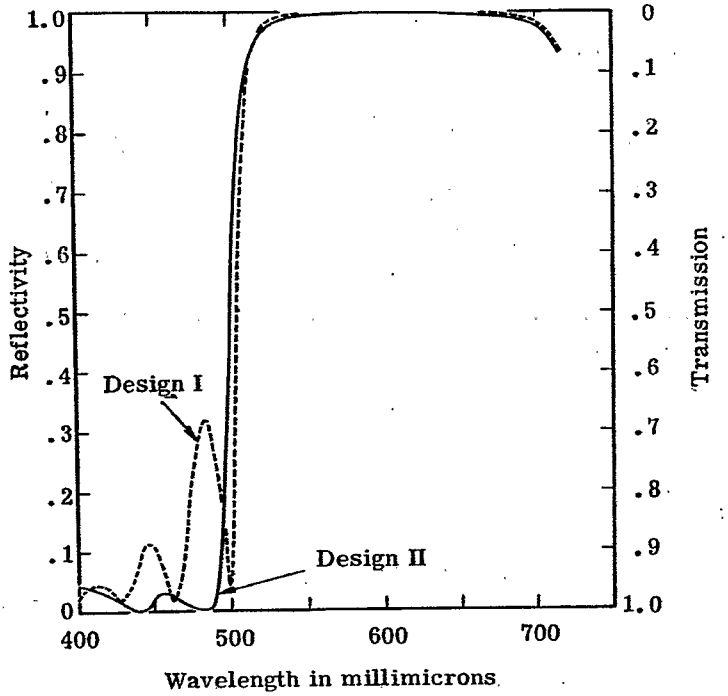

Figure 20.68- Computed spectral reflectivity of the multilayers designated as Design I (dashed line) and Design II (solid line) in Table 20.4.

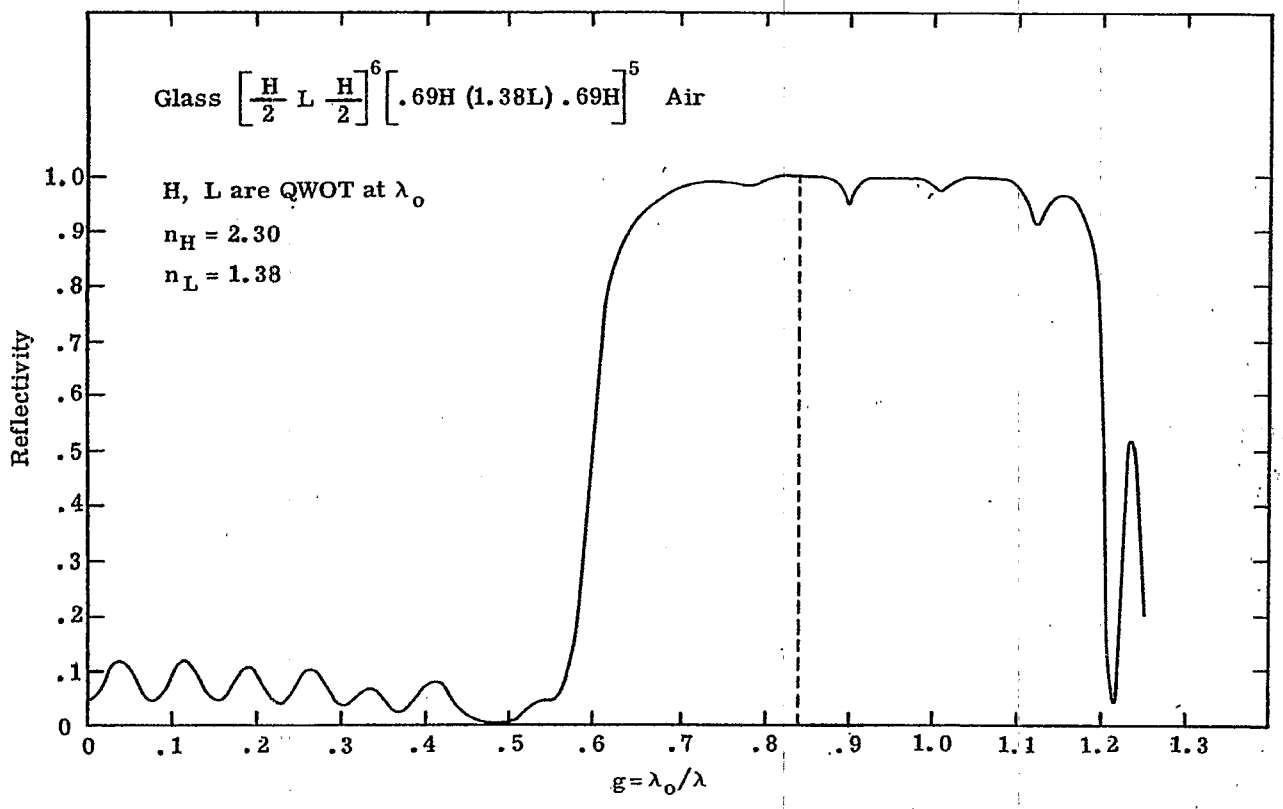

Figure 20.70- Computed spectral reflectivity of a multilayer consisting of an ensemble to two stacks.

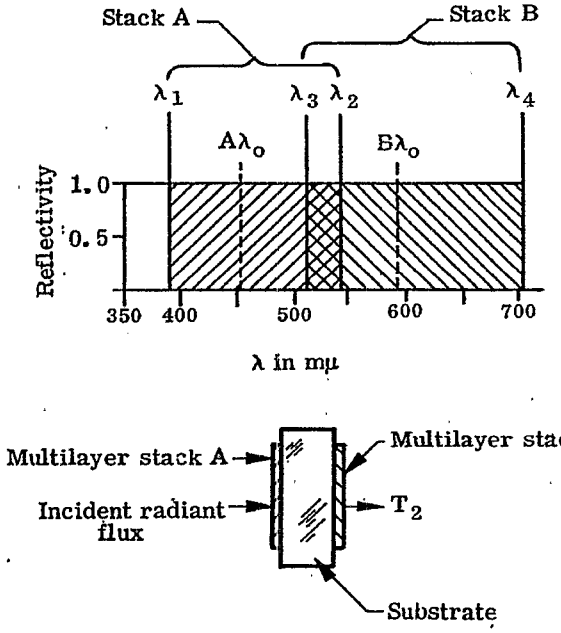

Figure 20.71- The positions of the high-reflectance zones of the two multilayers which constitute a composite filter.

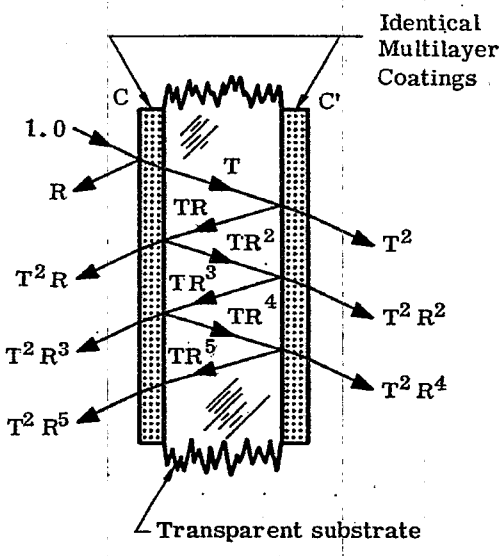

$$T_2 = T^2\left[1 + R^2 + R^4 + \ldots\right]$$

$$= \frac{T^2}{1 - R^2} = \frac{(1 - R)^2}{(1-R)(1+R)}$$

$$= \frac{1 - R}{1 + R} = \frac{T}{1 + R}$$

Figure 20.72- An illustration of the method of computing the total transmission, T_2 of a composite filter consisting of two identical non-absorbing coatings.

ence of the high-reflectance peak influences the steepness of the cutoff. At any given wavelength, a higher-order reflectance peak has a sharper cutoff than a first order peak. The disadvantage of using a higher-order reflectance peak is that the width of the region of high transmission at longer wavelengths is decreased. However, if a first-order high-reflectance peak is used to provide the attenuation region, then there are no regions of high-reflectivity between the long-wave cutoff and infinite wavelength. For example, reflectance peak at 500 mμ of the multilayer shown in Figure 20.67 is first order. In this case the computed transmission of this multilayer is greater than 0.85 mμ in the spectral region from 650 mμ to wavelengths as long as 50 μ in the infrared, or for wavelengths in the microwave region for that matter. Of course in practice the glass substrate and the materials in the multilayer would absorb strongly at wavelengths much shorter than 50 μ.

20.5.1.3 Attenuation over a broad spectral region. It was shown in 20.4.1.4 that the width of the high-reflectance zone is determined by the index ratio of the two materials which constitute the stack and hence the width of the high-reflectance zone is limited by the index of available thin film materials. The optimum width is achieved with a quarter-wave stack which has a large index mismatch. For example, in the region from 300 to 400 mμ the non-absorbing thin film materials have an index which does not exceed 2.10. The optimum width of the high-reflectance zone is achieved if this high-index material is used in conjunction with a low index material such as cryolite (index 1.35). Sometimes it is desired to attenuate a spectral region which is greater than this optimum width. One obvious solution is to combine two or more such stacks. The thickness of the layers in each of the stacks is chosen so that the high-reflectance zone of each one covers a different part of the spectral region to be attenuated. Here the term stack has been used to denote a group of films which have periodic structure. There are two ways of arranging the stacks so that a broad attenuation region is achieved.

(1) The stacks are deposited upon the same substrate, that is, they are piled on top of each other. Since this type of multilayer is an ensemble of individual stacks, it will be referred to as an ensemble multilayer.

(2) Each stack is deposited on a different surface. This configuration will be referred to as a composite filter.

20.5.1.3.1 Ensemble of stacks. As an example of a multilayer which is an ensemble of two individual (modified) quarter-wave stacks, consider

$$\text{glass} \quad \left(\frac{L}{2} \; H \; \frac{L}{2}\right)^6 \quad \left(\frac{L'}{2} \; H' \; \frac{L'}{2}\right)^5 \quad \text{air}$$

where the index of the L land H layers is 1.38 and 2.30, respectively. Using our terminology, the group of layers $(L/2 \; H \; L/2)^6$ constitutes one stack and the group $(L'/2 \; H' \; L'/2)^5$, another stack. If the optical thickness of the L, H and L', H' layers is chosen in the ratio of 1.38: 1, then the high-reflectance zones to the two stacks are contiguous. The reflectivity versus $g = \lambda_o/\lambda$ of this combination is depicted in Figure 20.70. The dashed line shows the boundary of the high-reflectance zones of each stack. The attenuation region covers nearly an octave. In general, two difficulties are encountered in constructing multilayers of this type. First, interference effects often occur between the various stacks and the ensemble filter acts like a Fabry-Perot type filter (described in 20.10), to the extent that narrow transmission bands appear in the attenuation region. Second, such filters are often difficult to manufacture. Each of the films in the filter has a small amount of mechanical stress (refer to 20.2.4.2.4) and if the number of layers is large, the total stress can build up to the point where the multilayer will no longer adhere to the substrate. Multilayers of this type which have a high-reflectivity over a wide spectral region are often called broad-band reflectors. The spectral reflectivity of such a reflector is shown as curve B in Figure 20.95.

20.5.1.3.2 The composite filter. The composite filter consists of two or more individual multilayers which are deposited on separate substrates and arranged so that the incident radiant flux passes through each one. Because the multilayers are on separate substrates, it is possible to separate them physically by a distance of many thousands of wavelengths, thus avoiding interference effects between the various multilayers. If only two multilayers are used in a composite filter, it is often convenient to deposit each multilayer on a side of the substrate, as is shown in Figure 20.71. As an example of this procedure, suppose a filter is required which attenuates the entire visible spectral region from 400 mμ to 700 mμ. Since a single quarter-wave stack of zinc sulfide and magnesium fluoride has a high-reflectance zone which covers approximately one-half of this region, a composite filter composed to two quarter-wave stacks is requisite. Each stack is deposited on a side of the glass substrate, as is shown in Figure 20.71. The high-reflectance zone of multilayer stack "A" extends from λ_1 to λ_2 and the zone of stack "B" from λ_3 to λ_4. Figure 20.71 shows how the high-reflectance zones are arranged so they not only cover the spectral region to be attenuated but also overlap in the center so that there is no possibility of a transmission leak. Stack "A" has a QWOT = 453 mμ and stack "B" a QWOT = 594 mμ. These values are chosen so that region

of attenuation extends from 390 mμ to 706 mμ. Having determined the QWOT and materials of the two stacks, the only remaining problem is to choose the number of periods. This number is determined by the amount of attenuation required, the steepness of the cutoff required at 700 mμ, or by economic considerations. The latter point should be considered if the filter is to produce in large numbers; the cost of manufacture depends upon the number of layers in the stack. It is noted that the transmission beyond 700 mμ would be enhanced if eighth-wave layers were added to each stack, so that stacks "A" and "B" are similar to the multilayer shown in Figure 20.67. The addition of these eighth-wave layers shifts the wavelength of maximum reflectivity of each stack, but does not affect the position of the high-reflectance zones.

20.5.1.4 Since the multilayers which are composed of dielectric materials have a negligible amount of absorption, the transmission properties of these filters, when placed in tandem, are considerably different from absorption-type filters. As an example, suppose that an absorption-type filter consisting of a slab of colored glass has a transmission T of 0.01 at some wavelength, say 610 mμ. If an identical filter is placed in tandem, then the transmission T_2 of the entire system is reduced to the low value of

$$T_2 = T^2 = 0.0001 .$$

Next, consider the case of a multilayer filter which is composed of dielectric (non-absorbing) layers, so that $T = 1 - R$. For purposes of comparison, suppose that this multilayer is designed so that it also has a $T = .01$ at 610 mμ. If an identical multilayer is deposited on the opposite side of the same transparent substrate, as is shown in Figure 20.72, then the total transmission T_2 of the tandem arrangement is close to 0.005, or more precisely:

$$T = (1 - R)/(1 + R)$$

$$\simeq T/2 \text{ as } R \rightarrow 1.0 \qquad (48)$$

The reason for this behavior can be seen in Figure 20.72, which shows identical multilayer coatings C and C' deposited on each side of the transparent substrate. Since the substrate is quite thick, interference effects can be neglected and the intensity of the beams which emerge can be added. As is shown in Figure 20.72, a radiant flux proportional to $T = 1 - R$ penetrates into the medium (i.e. the substrate) between the two multilayers. If the reflectivity is close to 1.0, then this flux is trapped and bounces back and forth between the two multilayers many times, decreasing in intensity only a small amount at each reflection. Eventually all of the flux escapes through interfaces C and C'. If R is close to 1.0, then approximately one half of it escapes through C and one-half through C'. Since T_2 is proportional to the radiant flux which penetrates C', T_2 is decreased by only a factor of two. The total transmission T_2 is decreased below the value given in Equation (48) if there is a small amount of scattering in the multilayers or if there is absorption in either the multilayer or the substrate. T_2 can also be decreased by using a wedge-shaped substrates so that the rays "walk off" the ends of the filter.

20.5.2 Long-wave pass color filters. From the discussion in 20.5.1 and 20.4.8.2.1, it is evident that it is a straightforward task to produce filters for the visible spectral region which pass in the long-wave region. However, it should be remembered that in the visible region there are many absorption filters of colored glass or organic dyes which rival multilayers in the sharpness of their cutoff, high attenuation in the short-wave region and high transmission at long wavelengths. Not only are these absorption filters often less expensive than a multilayer filter, but they have the additional advantage that they are virtually free from the variation of the transmission with the angle of incidence (i.e. the angle shift) which is inherent in multilayer filters. However, multilayer filters have the advantage that they can be manufactured to any specification so that the cutoff can be positioned at any wavelength, whereas the cutoff of glass and dye absorption filters is only at wavelengths which nature has provided. As an example of a long-wave pass color filter, Figure 20.73 shows the measured spectral transmittance of a modified quarter-wave stack composed of fifteen layers of zinc sulfide and magnesium fluoride. Eighth-wave layers of zinc sulfide on either end of the stack increase the transmission in the long-wave region. The transmittance of this filter is similar to the computed curve shown in Figure 20.67.

20.5.3 The cold mirror. The cold mirror is a multilayer composed of dielectric materials which has a high-reflectivity in the visible spectral region. The reflectivity drops abruptly at 700 mμ so that a high transmission is achieved in the near infrared. The discussion in 20.1.2.7 describes briefly how this cold mirror can be placed behind a light source in a projection system so that the light in the visible spectral region is deflected towards the lens, but the heat, (the radiant energy in the infrared), passes out of the system. There are many designs for cold mirrors; they usually consist of an ensemble of stacks, as described in 20.5.1.3.1. An effective cold mirror has a smooth reflectivity curve in the visible region so that the color of the reflected light is not altered. The sharpness of the cutoff at 700 mμ and the amount of transmission in the infrared are also important. A cold mirror which is used in conjunction with an arc lamp should have a sharp cutoff, since a typical arc lamp has a larger portion of its radiant energy concentrated in the region between 700 mμ and 800 mμ than does a tungsten filament. Since 85% of the radiant energy of

a tungsten incandescent lamp operated at 3350°K is outside of the visible region, a combination of a cold mirror and a heat reflector could theoretically reduce the heat six-fold. In practice, a two-fold to three-fold reduction is achieved by using a cold mirror and heat reflector in place of an aluminum mirror. Figures 20.74 and 20.75 depict the spectral transmittance and reflectance of some cold mirrors which are manufactured commercially. Both Dimmick[37] and Turner[38,39a] describe the use of cold mirrors in projection and illumination systems. A basic U.S. patent on the cold mirror has been issued to Koch[39b]

20.5.4 Long-wave pass filters for the infrared. Multilayer filters are used extensively in the infrared as components of missiles which have a heat-seeking guidance mechanism, infrared surveillance systems, and in the spectrochemical analysis of organic vapors. In the infrared, a limited number of absorption-type filters are available and hence multilayer filters are widely used. Infrared multilayers can be composed of the same materials which are used in the visible, such as zinc sulfide and chiolite. However, the use of certain materials is restricted by the stress in the films (see 20.2.3.2.4). Films of germanium can be used at wavelengths longer than 1.3 μ and lead telluride beyond 3.9 μ. Both of these materials have high refractive index. As is illustrated in Figure 20.53, a stack which has a quite broad high-reflectance zone is obtained when either of these materials is used in conjunction with a material of low refractive index, such as chiolite or silicon monoxide. The spectral width of the attenuation region can be increased by using two or more stacks, combined either as a ensemble (20.5.1.3.1) or as a composite filter (see 20.5.1.3.2). Figures 20.76 to 20.81 show the spectral transmittance of some long-wave pass filters which are manufactured by several commercial firms. It is interesting that the cutoff region of the stack shown in Figure 20.79 is provided by a 3:1 stack, which has the advantage of having a lower angle shift than the quarter-wave stack (see Section 20.4.7). It might be conjectured that the spike in the transmission at 3.8μ of the multilayer shown in Figure 20.80 is due to the fact that the edge high-reflectance zone occurs at this wavelength but that the transmission remains low because the lead telluride films are absorbing in this region. Using the refractive indices in Table II, from Equation (39) it is found that the ratio $\lambda_2/\lambda_1 = 1.66$, where λ_2 and λ_1 are the wavelengths at the long and short wave edge of the high-reflectance zone. From Figure 20.82 we see that $\lambda_2 = 6.5\ \mu$, and thus $\lambda_1 = 3.9\ \mu$; this conjecture is probably correct. The transmission peaks at shorter wavelengths in Figures 20.80 and 20.81 could be eliminated by depositing another long-wave pass multilayer on the opposite side of the substrate, thus forming a composite filter. The transmission in the long-wave region in both of these filters could be improved if an antireflection coating were deposited on the opposite side of the arsenic trisulfide glass substrate.

20.6 SHORT-WAVE PASS FILTERS

In Section 20.5.1, we enumerated some of the properties of long-wave pass filters, such as the attenuation, sharpness of the cutoff, angle shift, and so on. These general considerations apply equally well to short-wave pass filters, with the following important exception: The spectral width of the high-transmission region of a quarter-wave stack or other stack with a periodic structure is limited by the fact that at shorter wavelengths higher order high-reflectance zones always occur. For example, suppose that the 3:1 stack shown in Figure 20.59 is used to attenuate in the 1.8 μ to 2.2 μ region. Additional periods can be added to the stack if a higher attenuation in this region is required. The pass region on the short-wave side extends from 1.15 to 1.7 μ. At 1.15 μ the second-order high-reflectance peak occurs and the multilayer attenuates from 0.9 to 1.15 μ. It is evident from Figures 20.56, 20.57, and 20.58 that these higher order attenuation regions are not confined to the 3:1 stack, but occur in all stacks which have a periodic structure, regardless of the composition of the basic period. A comparison of Figures 20.56, 20.57, and 20.58 shows that the quarter-wave stack has the widest region of high transmission on the short-wave (high-frequency) side of the first order high-reflectance zone. The third-order high-reflectance zone occurs at one-third of the wavelength of the first order zone. The spectral width of high transmission of the 2:1 stack is somewhat smaller; the second-order high-reflectance zone occurs at one-half the wavelength of the first order zone. However, we have considered only the case where two layers are used in the basic period of the stack. If more than two layers are used in the basic period of a stack with a periodic structure, then a short-wave pass spectral region which is even wider than that of a quarter-wave stack can be achieved.[40] Regardless of whether a quarter-wave, 2:1 or 3:1 stack is used, it is desirable to add some additional layers to the stack to enhance the transmission in the short-wave region, as is shown in Figure 20.66.

20.6.1 Short-wave pass color filters. Multilayer filters are particularly useful as short-wave pass filters in the visible spectral region, because most of the colored glass and dyed gelatin filters have a low transmission in the pass region and a cutoff which is not sharp. For example, a typical blue glass absorption filter which transmits below 480 mμ has a peak transmission of 0.38 at 410 mμ and a bell-shaped transmission curve. Also, most absorption filters which transmit the blue and near ultraviolet have a leak- a transmission band in the red. Figures 20.66, 20.68, and 20.82 show the spectral transmission of some short-wave pass filters. The multilayer shown in Figure 20.82 is a quarter-wave stack with films added to enhance the transmission in the short-wave region, as described in 20.4.8.3.1.

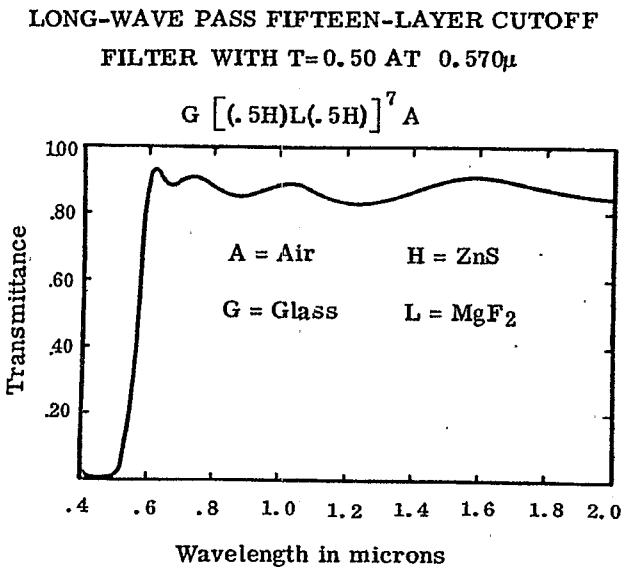

Figure 20.73- Measured spectral transmittance of a long-wave pass filter. Courtesy of Bausch and Lomb, Inc.

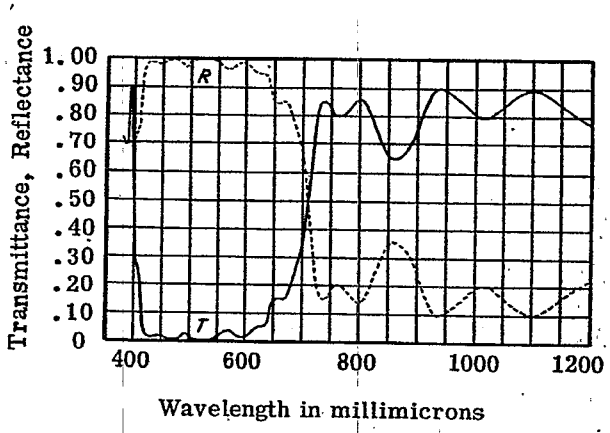

Figure 20.74- Measured reflectance and transmittance of a cold mirror multilayer coating. Courtesy of Balzers Aktiengesellschaft, Liechtenstein

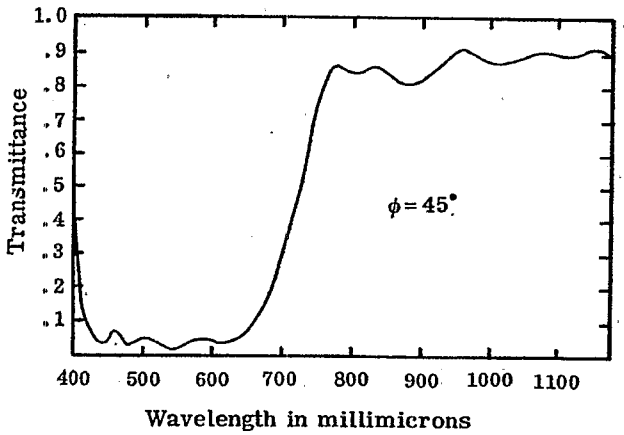

Figure 20.75- Measured spectral transmittance at $\phi = 45°$ of a cold mirror of unspecified design. Courtesy of Fish-Schurman, Corporation.

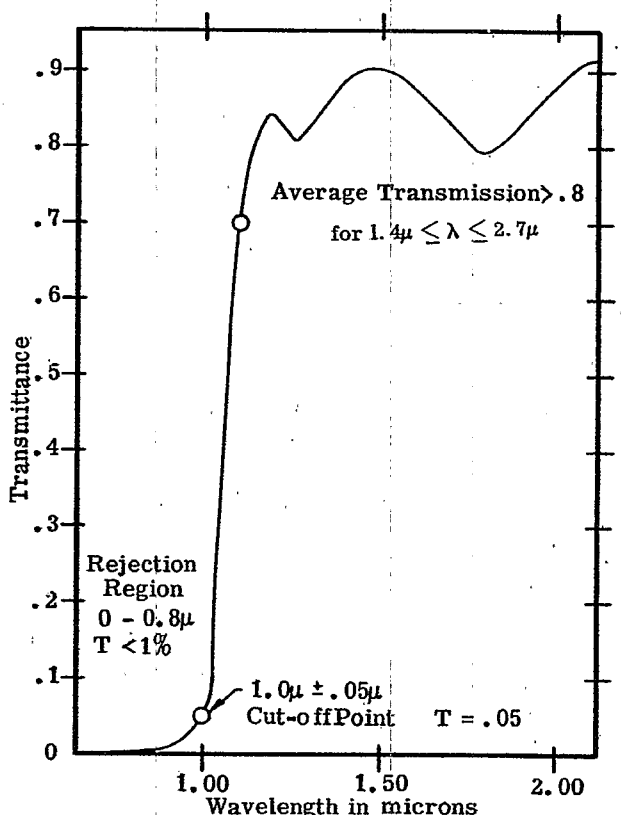

Figure 20.76- Measured spectral transmittance of a long-wave pass filter of unspecified design. Courtesy of Eastman Kodak Company.

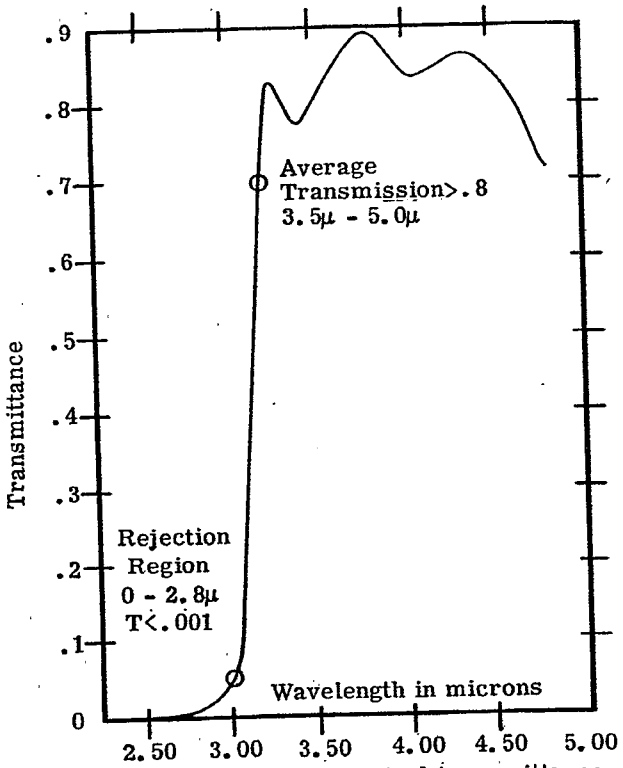

Figure 20.77- Measured spectral transmittance of a long-wave pass filter of unspecified design. Courtesy of Eastman Kodak Company.

MEASURED SPECTROPHOTOMETRIC TRANSMITTANCE OF A LONG-WAVE PASS ELEVEN-LAYER CUTOFF FILTER

G $[(.5H)L(.5H)]^5$ A

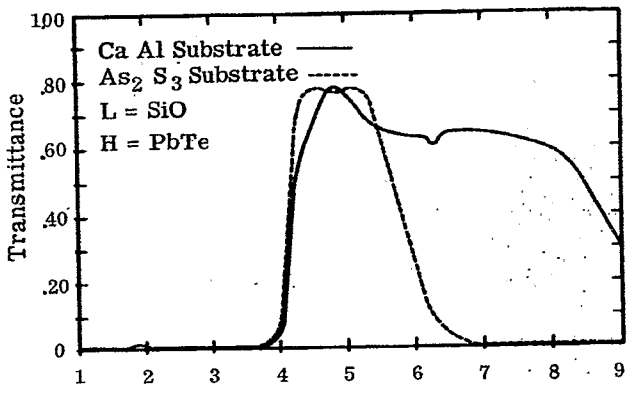

Figure 20.78- Measured spectral transmittance of a modified quarter-wave stack on two different types of substrate, namely As_2S_3 glass (solid curve) and calcium aluminate (dotted curve). Courtesy of Bausch and Lomb, Inc.

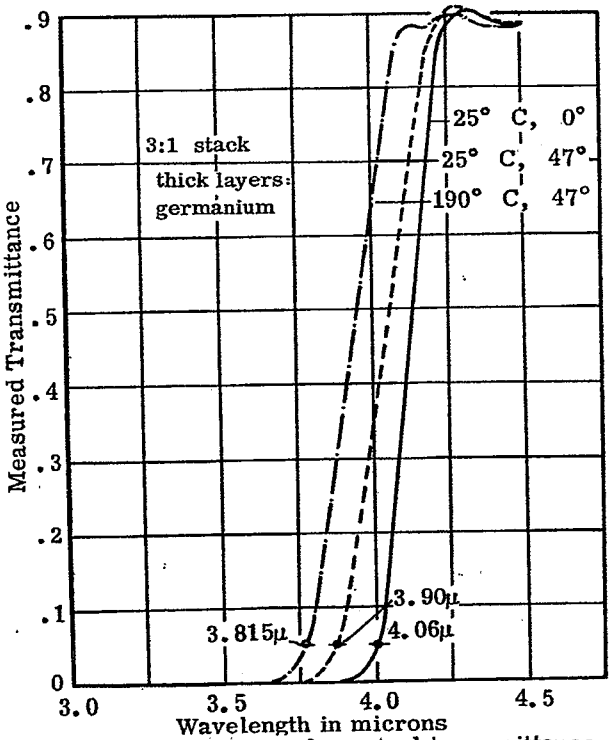

Figure 20.79- Measured spectral transmittance of a long-wave pass filter at ϕ = O and ϕ = 45° and at low temperature. The design is a modified 3:1 stack. Courtesy of Optical Coating Laboratory, Inc.

LONG-WAVE PASS NINE-LAYER CUTOFF FILTER AT 6.5 MICRONS

G $[(.5H)L(.5H)]^4$ A

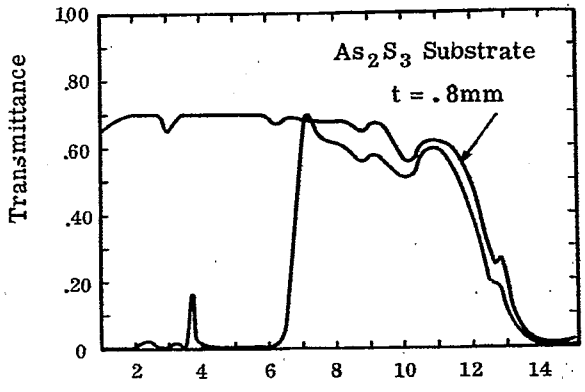

A = Air L = ZnS
G = As_2S_3 Glass H = PbTe

Figure 20.80- Measured spectral transmittance of a long-wave pass filter on an As_2S_3 glass substrate. The transmission of both the filter and the bare substrate would be improved if the substrate were antireflection coated. Courtesy of Bausch and Lomb, Inc.

20.6.2 Heat reflectors. Section 20.1.2.7 describes briefly how a multilayer heat reflector deflects the heat from a projection lamp away from the film gate. For many years heat absorbing glass has been used to absorb the radiant energy in the infrared, but this has the disadvantage that the heat must be removed from the glass by air cooling or other means. If this is not done, the glass becomes quite hot and often fractures. Multilayer heat reflectors have the advantage that they reflect, rather than absorb, the near infrared and thus remain comparatively cool. Figures 20.83, 20.84, 20.85, 20.86, and 20.87 show the spectral transmission of some infrared reflectors. The multilayer in Figure 20.83 is identical to that of Figure 20.82, with the exception that the QWOT of the former has been moved to longer wavelengths. The multilayer shown in Figure 20.84 attenuates far into the infrared, but unfortunately it also attenuates in part of the red spectral region. The width of the attenuation region in the infrared of the multilayer shown in Figure 20.85 is typical of what can be attained with a simple quarter-wave stack. The multilayer shown in Figure 20.86 not only reflects the infrared, but also has a higher order high-reflectance zone in the blue. Although the design of the multilayer is unspecified, the fact that the maximum of the red reflection band occurs at twice the wavelength of the blue reflection band leads one to suspect that this is a 2:1 stack. It should be pointed out that the heat reflector does not have to be used in conjunction with a cold mirror, as shown in Figure 20.82 Some advantage is gained if only a heat reflector is inserted into the beam at an angle.

20.6.2.1 Another type of heat reflector is used in conjunction with the solar energy cells which are used in satellites and space vehicles. The problem is that only the radiant energy in the range from 0.4 to 1.2 μ produces appreciable electrical energy. The radiant energy outside of this region merely heats the cell, thereby decreasing its efficiency. Therefore, solar cells used in space vehicles are usually protected with a short-wave pass filter which has a high-reflectivity from 1.2 μ out to longer wavelengths. The advantages of using these filters are discussed by Thelen.[41] It is remarked that heat reflecting mirrors are often called hot mirrors. It should be remembered that both the cold mirror (described in Section 20.5.3) and the hot mirror are made of non-absorbing materials. Thus neither of them absorbs an appreciable amount of radiant energy and thus they both remain comparatively cool.

20.6.3 Short-wave pass filters for the infrared. One difficulty which is encountered in using a multilayer as a short-wave pass filter for the infrared is that the spectral width of the pass region at short wavelengths is narrow, especially if high-index materials such as silicon, germanium, or lead telluride are used in the filter. In the latter case, the attenuation region is quite wide, and this width is at the expense of the width of the pass region. One way to avoid this difficulty is to use materials in the stack which have smaller ratio of refractive index, n_a/n_b. Another approach is to use a stack which has a basic period which contains more than two refractive indices.[40]

20.7 BEAM SPLITTERS

20.7.1 A beam splitter is used to divide a wavefront into two portions and direct each portion in a different direction. Beam splitters can be arbitrarily divided into two classifications:

(1) Achromatic, or neutral, beam splitters (see Section 20.7.2).

(2) Color selective beam splitters. These are sometimes called dichroic mirrors and are discussed in Section 20.7.3.

20.7.1.1 The properties of a beam splitter are usually specified by the average transmission, T_{av}, and average reflectivity, R_{av}, (defined in 20.1.3.7). However, as is shown in 20.7.1.2, it is often important to know T_s, T_p and R_s, R_p in the two planes of polarization so that the amount of polarization produced by the beam splitter can be determined. If the beam splitter is used as a component of an interferometer, such as a Michelson or Twyman-Green, then the variation with wavelength of the phase shift upon reflection should be considered, since the position of the fringes in the interferometer depends upon this phase shift. The phase shift of a silver film is shown in Figure 21.17.

20.7.1.2 Polarization effects. If T_s and T_p are unequal, or if $R_s \neq R_p$, then the beam splitter has a polarizing effect, which can be quite important. For example, a beam splitter which is used in a Michelson interferometer should divide the beam equally in order to produce fringes with maximum intensity. Thus a beam splitter composed of dielectric films which has an R_{av} of .50 might look attractive as a beam splitter for this purpose. However, it is important to know the R and T in each plane of polarization, since the beams interfere separately in each plane of polarization. For example, if a beam splitter for a Michelson interferometer has $R_{av} = 0.50$, but $R_s = 0.10$ and $R_p = 0.90$, then the fringe intensity, which is proportional to the product $R \cdot T$, is quite low. The dissimilarity of the reflectivity in the two planes of polarization can also affect other devices. For example, suppose a beam splitter in a glass cube is mounted behind the objective lens of a camera, as is shown in Figure 20.88. Such a beam splitter is manufactured by evaporating the multilayer coating onto the hypotenuse face of a 45-90-45 glass prism, and then cementing an identical prism onto it. The purpose of the beam splitter is to reflect 20% of the light into

MEASURED TRANSMITTANCE OF AN ELEVEN LAYER LONG-WAVE PASS FILTER ON As_2S_3 GLASS SUBSTRATE

G $\left[(.5H)L(.5H)\right]^5$ A

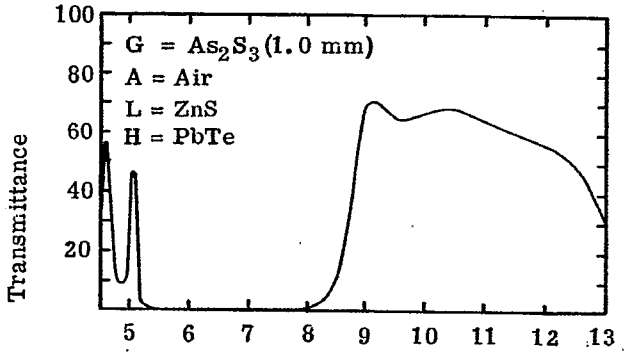

Figure 20.81- Measured spectral transmittance of a long-wave pass filter deposited on an As_2S_3 glass substrate. The transmission beyond 8 μ would improve if the "back" side of the substrate were antireflection coated. Courtesy of Bausch and Lomb, Inc.

SHORT-WAVE PASS THIRTEEN-LAYER CUTOFF FILTER WITH T=.5 AT .572μ

G (.78L) $\left[(.5L)H(.5L)\right]^6$ A

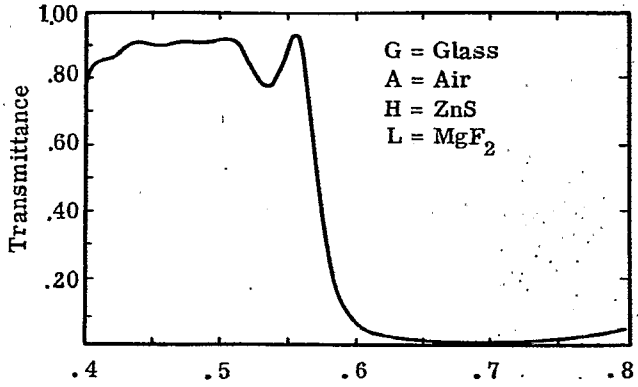

Figure 20.82- Measured spectral transmittance of a short-wave pass filter. Courtesy of Bausch and Lomb, Inc.

SHORT-WAVE PASS THIRTEEN-LAYER CUTOFF FILTER WITH T=.5 AT .80μ

G (.78L) $\left[(.5L)H(.5L)\right]^6$ A

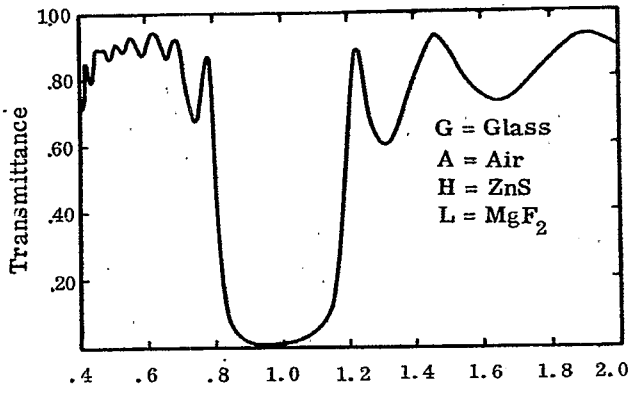

Figure 20.83- Measured spectral transmittance of a short-wave pass heat reflecting filter. Courtesy of Bausch and Lomb, Inc.

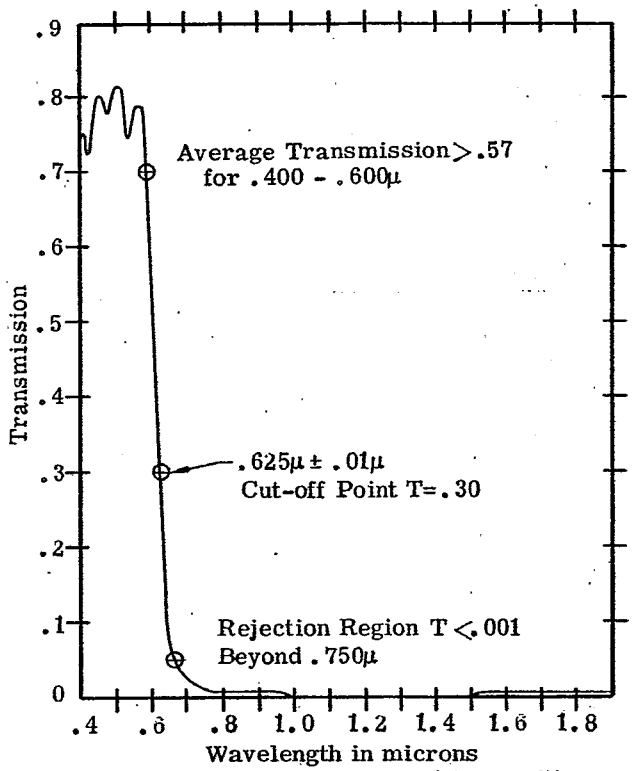

Figure 20.84- Measured spectral transmittance of a short-wave pass filter. Courtesy of Eastman Kodak Co.

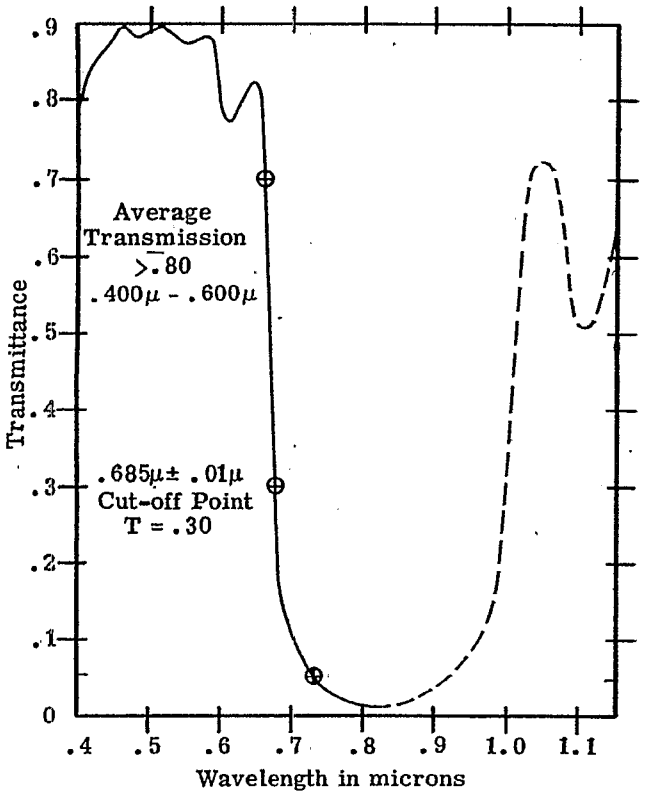

Figure 20.85- Measured spectral transmittance of a short-wave pass heat reflecting filter. Courtesy of Eastman Kodak Company.

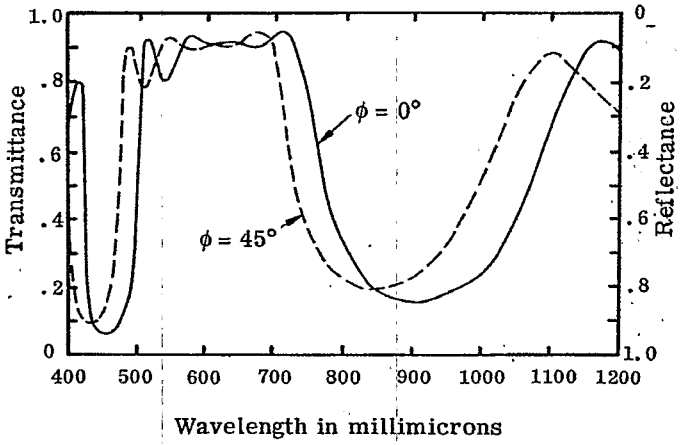

Figure 20.86- Measured spectral transmittance multilayer which reflects the blue and near infrared. Courtesy of Fish-Schurman, Corporation.

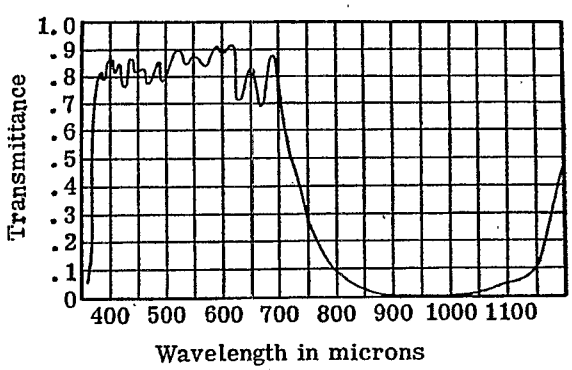

Figure 20.87- Measured spectral transmittance of a multilayer heat reflecting filter. Courtesy of Balzers Aktiengesellschaft, Liechtenstein.

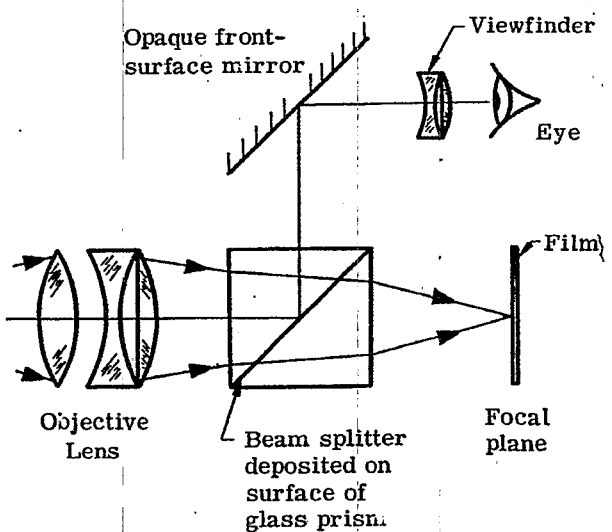

Figure 20.88- The utilization of a beam splitter in a camera to deflect an image into the view finder.

the view finder. As long as the light from the scene which is being photographed is unpolarized, then any beam splitter which has the specified $T_{av} = 0.80$ and $R_{av} = 0.20$ is satisfactory. However, suppose that $R_s = 0.08$ and $R_p = 0.32$ so that the beam splitter is polarizing. If a scene is photographed which produces polarized light, such as certain portions of the sky or the light which is reflected from a wet surface, then the brightness of the scene which is seen in the view finder and the scene which is recorded on the film are quite different. Another effect is that the brightness in the view finder changes as the camera is rotated about the axis of symmetry of the objective lens.

20.7.2 Achromatic beam splitters. An achromatic, or neutral, beam splitter should reflect and transmit equally at all wavelengths. In practice, the transmission of most beam splitters changes slightly with wavelength.

20.7.2.1 Silver films. Thin films of silver are widely used as beam splitters. For many years only chemical methods were used for depositing the films, but more recently superior quality silver films have been produced by evaporation in a vacuum. The optical constants, n and k, vary considerably with wavelength and consequently the R and T of a film of a given thickness also change. The R and T of silver films of varying thickness at a wavelength of 550 mμ is shown in Figure 21.16. Due to the dispersion of the optical constants, silver films which have a given value of t/λ have a much lower absorption in the red than in the blue. Silver films have the advantage that they are easy to prepare. The disadvantages are that they are less efficient than a dielectric beam splitter because they absorb part of the light and that they deteriorate after they are removed from the evaporator. A typical rule of thumb is that silver beam splitter which is designed to divide the light equally reflects 1/3, transmits 1/3 and absorbs 1/3. Sennett and Scott[42] have measured the transmission and reflectivity of some silver films. In the visible spectral region metals other than silver have a high absorption and are generally not used as beam splitters.

20.7.2.2 Dielectric films.

The simplest type of dielectric beam splitter is a single film of zinc sulfide or titanium dioxide deposited on a glass substrate. These beam splitters are neutral in color and divide the light in a ratio of $R : T = 0.4 : 0.6$. Figure 20.89 shows the spectral reflectivity and transmission at $\phi = 45°$ of a single film of TiO_2 on a glass substrate. The dispersion of the refractive index of the TiO_2 has been taken into account in this calculation. The curves in Figure 20.89 give some idea of the flatness of the reflectivity curve and also the amount of polarization which is produced by the beam splitter. Holland[43] describes in detail how beam splitters of this type are prepared. Figure 20.90 shows the spectral reflectivity and transmission at $\phi = 45°$ of two types of beam splitters which are produced commercially. It should be remembered that the uncoated side of the substrate of a beam splitter introduces a transmission loss and also some polarization into the beam. This effect is not large and is reduced even more if the opposite side of the substrate is covered with an antireflection coating.

20.7.3 Color selective beam splitters (dichroic mirrors). Color selective beam splitters are sometimes called dichroic mirrors. One of the definitions of the word dichroism refers to the selective absorption and transmission of light as a function of wavelength regardless of the plane of vibration.

20.7.3.1 It could be argued that section on dichroic mirrors logically belongs in Sections 20.5 and 20.6, which covered long-wave and short-wave pass filters. Actually, this is true, because any of the multilayers described in those chapters could be used a dichroic mirror simply by tilting them at an angle. The difference is that when these multilayers were used as pass filters, we were concerned only with the transmitted light and gave little attention to what happened to the reflected light. If the multilayer is used as a beam splitter, then the reflected light is utilized. Color selective beam splitters are used extensively in optical systems where different kinds of information are identified by a different color and combined so that they are projected simultaneously. Many thousands of such beam splitters are used in radar sets to superimpose the image of a cathode ray oscilloscope screen (which might be green) with a map of another color (magenta, for example). It is easy to see an additional color selective beam splitter could be added to the configuration shown in Figure 20.1 to form a three-color separation system which could be used in color photography or color television.[44] Figure 20.91 shows a measured transmission curve of a blue reflector, which is similar to the long-wave pass filter shown in Figure 20.73, but viewed at non-normal incidence. The transmission curves at various angles of incidence also illustrate the angle shift to shorter wavelengths as ϕ increases. Figure 20.92 shows the reflectivity of green reflector at 45° incidence. One method of achieving this narrow reflection band is to use a $3\lambda/4$ stack. This is illustrated in Figure 20.93, which shows the computed transmission of nine layers of zinc sulfide and magnesium fluoride which have an optical thickness of $3\lambda_o/4$ where $\lambda_o = 546$ mμ, matched at 60°. A first order reflectivity peak occurs at 3×546 mμ $= 1.64$ μ in the infrared. The third order high-reflectance zone is centered at 546 mμ. The use of high-order reflectivity peaks is an effective method of achieving a narrow reflection band.

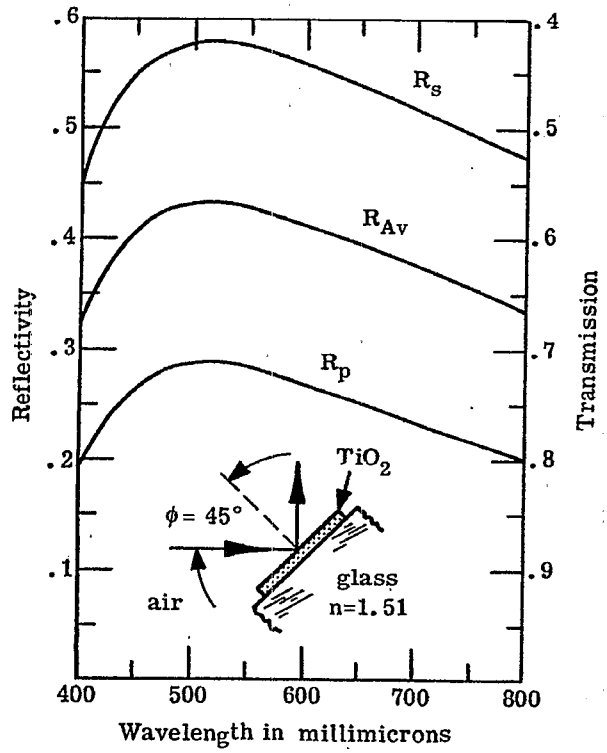

Figure 20.89- Computed R_p, R_s, and $R_{av} = 1/2 (R_p + R_s)$ of a single quarter-wave layer $Ti O_2$ at $\phi = 45$. The dispersion of the index of the $Ti O_2$ is taken into account.

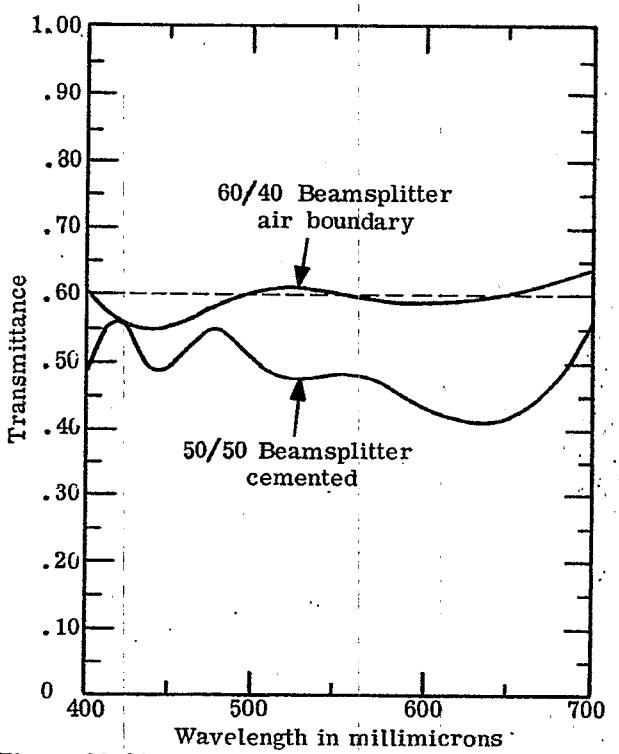

Figure 20.90- Measured transmittance of a 60/40 and a 50/50 multilayer beam splitter at $\phi = 45°$. R is nearly 1 - T. Courtesy of Fish-Schurman Corporation.

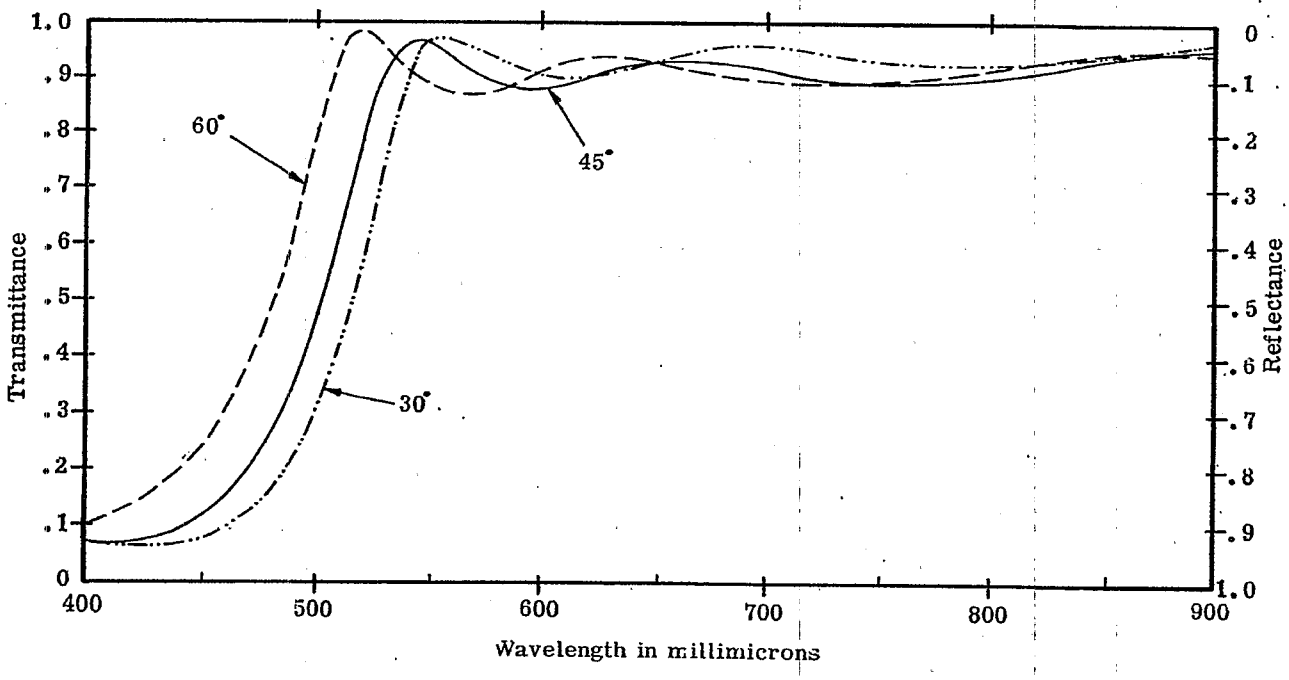

Figure 20.91- Measured spectral transmittance at various ϕ of a color-selective beam splitter. Courtesy of Fish-Schurman Corporation.

20.8 MIRRORS

The distinction between a mirror and a beam splitter is indeed tenuous. Some of the semi-transparent mirrors described in Section 20.8.2 could be used as color selective beam splitters if they were illuminated at non-normal incidence. Also, some of the long-wave and short-wave pass filters described in Sections 20.5 and 20.6 could be equally well used as semi-transparent mirrors. Thus the classification of a multilayer as a long-pass filter, color selective beam splitter, or a semi-transparent mirror depends upon its ultimate use and is not an inherent property of the device itself. Mirrors can be classified as either opaque or semi-transparent. Opaque mirrors are used if one is only concerned with the reflected light, whereas a portion of the light which is not reflected from a semi-transparent mirror, is transmitted.

20.8.1 Opaque mirrors. Silver, aluminum, and rhodium are commonly used as reflecting films in the visible spectral region. All three of these metals can be evaporated in a vacuum. An opaque coating is produced by a film 0.2 μ (eight millionths of an inch) thick. A freshly deposited film of silver has the highest reflectivity, particularly in the red, but the reflectivity deteriorates rapidly in air. An extremely thin, tough film of aluminum oxide forms naturally on the surface of an aluminum coating which protects it against further oxidation. Thus aluminum coatings last a long time under normal environmental conditions. The reflectivity of a rhodium coating is about 10% below that of aluminum. Rhodium is quite inert to attack from salt water and notwithstanding its lower reflectivity it is used in applications where the environmental conditions are severe. Gold films have a high reflectivity in the infrared. Hass [45] has published reflectivity data on the various metal coatings.

20.8.1.2 Protective coatings. A single layer of silicon monoxide(SiO) is often deposited on an aluminum film to protect it from abrasion and chemical attack. The addition of this layer does not alter the reflectivity of the aluminum if the optical thickness of the layer is either much smaller than the wavelength of the incident light or if its optical thickness is a half-wave, in which case it is absentee (see Section 20.1.5.2.2). The former condition can easily be obtained at long wavelengths in the infrared. Figure 21.14 shows the computed spectral reflectivity of aluminum overcoated with a single layer of silicon monoxide. At certain wavelengths the reflectivity of the aluminum is decreased from 0.90 to 0.78 by the addition of the protective overcoat.

20.8.1.3 Reflection enhancing overcoatings. The purpose of adding the single-layer overcoat described in the foregoing paragraph is to increase the resistance of the mirror to abrasion and chemical attack. It is also possible to overcoat a metal mirror with a multilayer coating in order to increase the reflectivity to values as high as .995. Such mirrors are useful in optical systems in which the light is reflected many times. Figure 20.94 shows the computed reflectivity of a bare aluminum mirror. It should be noted that the scale of the ordinate changes at 0.90. The dispersion of the optical constants is taken into account in the calculation; the reflectivity compares well with the published data of Hass [45] . On the same graph is shown the reflectivity of an aluminum mirror overcoated with a six-layer dielectric stack of magnesium fluoride and zinc sulfide. The dispersion of the refractive index of the latter material has also been included in the calculation. The computed reflectivity attains a maximum value of 0.996. Jenkins [46] measured accurately the reflectivity of such overcoated mirrors and found a maximum reflectivity of 0.994. Other types of overcoatings can be used to obtain a broader region of high reflectivity [46] , so that the reflectivity does not decrease in the blue, as it does in Figure 20.94.

20.8.2 Semi-transparent mirrors. The mirrors which are discussed in Section 20.8.1 are opaque - that is, the light which is not reflected is absorbed in the metal coating. There are some applications where mirrors are required which not only have a high reflectivity, but also transmit with a high efficiency the light which is not reflected. Such multilayers are useful as coatings for the plates of the Fabry-Perot interferometer and also as coatings for the ends of an optical maser (sometimes called a Laser).

20.8.2.1 Silver films. Silver films have been used for more than six decades as coatings for the Fabry-Perot interferometer. They have the advantage that the single film of silver can be deposited much more quickly and easily than the many films of a multilayer mirror. Kuhn and Wilson [47] measured carefully the R and T of layers of silver on a glass substrate and found that a freshly evaporated film has small absorption loss, particularly in the red spectral region. At a wavelength of λ = 680 mμ, typical values were R = 0.89, T = 0.08, and the remaining 3% is absorbed. However, in the blue (420 mμ) film with same transmission would absorb more than twice as much. The disadvantage of using silver films is that the reflectivity deteriorates in time. Multilayer coatings have the advantage that they have a lower amount of absorption and that a higher reflectivity can be attained.

20.8.2.2 Dielectric multilayers. Quarter-wave stacks and other types of multilayer coatings have been used quite successfully as semi-transparent mirrors, [46, 48, 49] principally for coating Fabry-Perot interferometers. Figure 20.95 shows the first-order high-reflectance peak of quarter-wave stacks consisting of five, seven, and nine layers of zinc sulfide and cryolite. For a given plate separation, the maximum resolution of a Fabry-Perot is limited by the flatness of the interferometer plates and increasing the reflec-

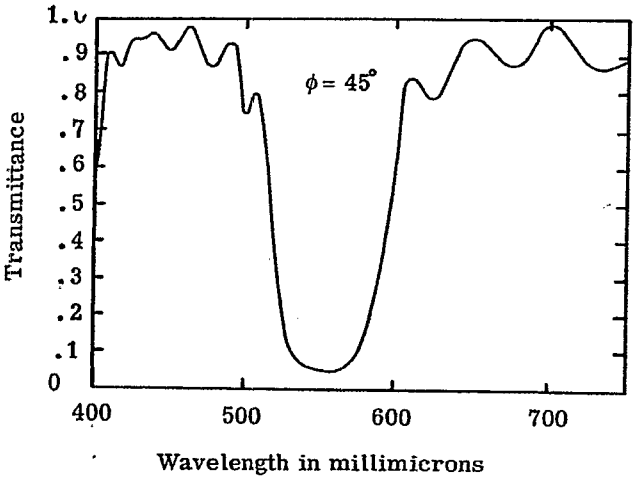

Figure 20.92- Measured spectral transmittance at $\phi = 45°$ of a color selective beam splitter which reflects the green. Courtesy of Fish-Schurman, Inc.

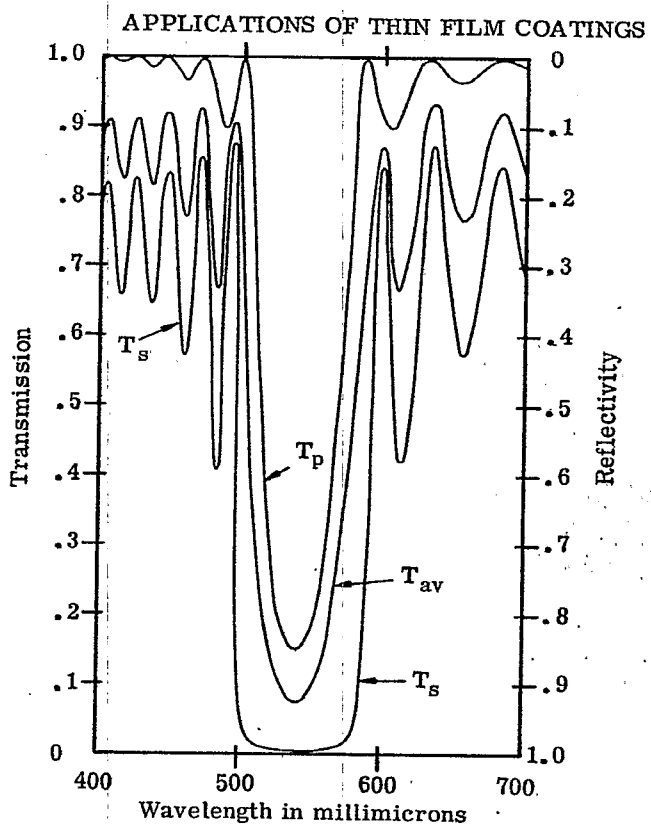

Figure 20.93- Computed T_p, T_s, and $T_{av} = 1/2 (T_p + T_s)$ of a color-selective beam splitter at $\phi = 65°$. The design is glass $H (LH)^4$ air, $n_L = 1.35$, $n_H = 2.30$, $n_L t_L = n_H t_H = \frac{3\lambda_o}{4}$ at $\phi = 65°$, for $\lambda_o = 550\ m\mu$.

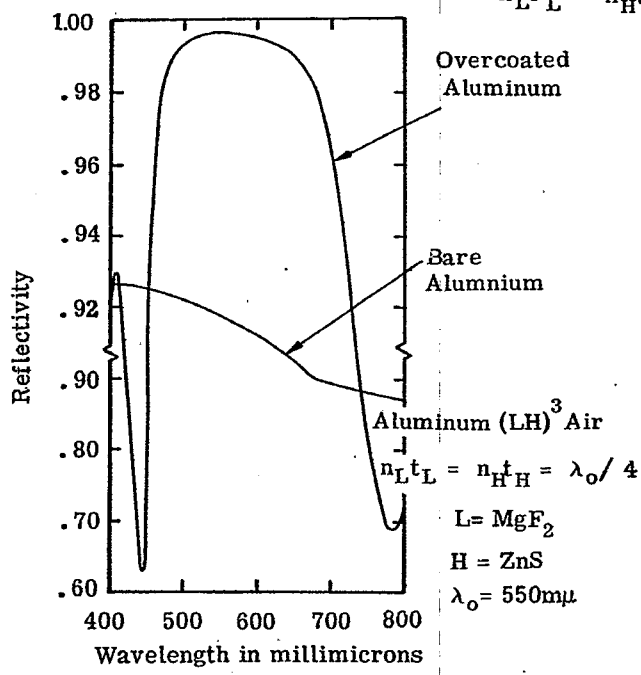

Figure 20.94- Computed spectral reflectivity of bare aluminum and aluminum overcoated with six dielectric layers. The scale of the ordinate changes at 0.90. The disperson of the optical constants is accounted for.

tivity over a certain value merely results in a loss of light without any gain in resolving power. Hence the seven-layer films are adequate for most plates. The advantage of using dielectric coatings over silver coatings is that the absorption loss of the former is quite low. A typical multilayer dielectric stack has an absorption of 0.005.[50] The disadvantage of using quarter-wave stack is readily apparent from Figures 20.71 or 20.95; the region of high reflectivity covers only about one-half of the visible spectrum. This difficulty is avoided if a broad-band reflector [49] is used, such as the one whose spectral reflectivity is shown as curve "B" in Figure 20.95. The design of this reflector is given in reference 49. The reflectance of this multilayer is close to 0.95 in the visible spectrum, which is the optimum value for most interferometer plates. The reflectivity of the cold mirror shown in Figure 20.74 is too high and would not be suitable for coating most interferometer plates.

20.8.2.3 From a theoretical point of view, (i.e. Equations (40) - (43)) the reflectivity of a quarter-wave stack can be made as close to 1.0 as we choose by simply using a sufficient number of layers in the stack. At the present state of thin film technology, it is found that the reflectivity of a $ZnS - MgF_2$ stack does not increase appreciably beyond fifteen layers. The fact which limits the ultimate reflectivity is that the layers are composed of small crystallites which are randomly oriented. This means that the layers have random fluctuations in their optical thickness and also that there are irregularities at the surfaces of the layers which scatter light. Giacomo [51, 52] has studied this problem in detail. As is discussed in 20.10.6.1, it is this scattering which limits the band width of dielectric interference filters. It is possible that in the future techniques will be developed to reduce this scattering, thereby making it possible to increase the reflectivity to values very close to 1.0 and consequently to produce multilayer interference filters with extremely narrow band widths.

20.9 BAND PASS FILTERS

A band pass filter is a multilayer which has a high transmission in a specific spectral region and attenuates in both the short and long wave regions on either side of the pass band. In a certain sense, all of the short-wave pass filters described in 20.6 are band pass filters, because the higher order high-reflectivity peaks limit the width of the short-pass region, although this is not the intent of such a filter. Included in the class of band pass filters are Fabry-Perot type filters or interference filters. This filter, which is discussed in 20.10, was the first type of filter whose transmission characteristics depended upon the interference of light, rather than the absorption of light. The name interference filter is retained for primarily historical reasons. Strictly speaking, every multilayer filter, from the single-layer coating to a sixty-layer stack, is an interference filter, in the sense that its transmission characteristics depends upon the interference of the light reflected from various layers within the filter. For reasons described in 20.10, we prefer to call this type of filter a Fabry-Perot type filter.

20.9.1 Filters with a wide pass band. From the discussion of long-wave and short-wave pass filters in 20.5 and 20.6, it is evident that a band pass filter can be constructed simply by combining a long-pass and short-pass filter. They can be either deposited on the same substrate or they can be deposited on separate substrates as a composite filter. The advantage of constructing a band pass filter in this manner is that width and position of the pass band can be changed at will by altering the cutoff of either the short or long-wave stack. Also, the amount of attenuation outside of the pass region can be easily controlled by changing the number of layers in either of the stacks. The width of the pass band is essentially independent of the attenuation outside the pass region. This is not true of the Fabry-Perot type filter described in 20.10. There are also other possibilities, such as combining a short-wave pass multilayer filter with a glass or dye absorption type filter which passes in the long-wave region. Figure 20.95 shows the spectral transmission of some assorted filters with a broad pass band in the visible and near ultraviolet spectral regions, while Figure 20.96 shows some similar filters for the infrared.

20.10 FABRY-PEROT TYPE FILTERS (INTERFERENCE FILTERS)

20.10.1 Basic concepts - the Fabry-Perot interferometer. In order to explain how an interference filter functions, it is first useful to understand how a Fabry-Perot interferometer works and to become familiar with such concepts as the "Q", free spectral range, order number, and so on. The basic idea of the interference filter has been known since the turn of the century, when two French physicists, C. Fabry and A. Perot, invented the interferometer which bears their name. Although this device is used mostly to measure fine details of emission line spectra, it can also be used as a filter with a very narrow pass band. The Fabry-Perot interferometer, which is shown in Figure 20.98, consists of two plates of glass or fused quartz which have been polished to a high degree of flatness. The plates are held apart by three separator pins so that the inner faces of the plates are parallel. These faces are coated with a semi-transparent mirror, such as the type described in 20.8.2. The transmission T_f of the interferometer is derived in most books on physical optics [53, 54] and in Section 5.17.

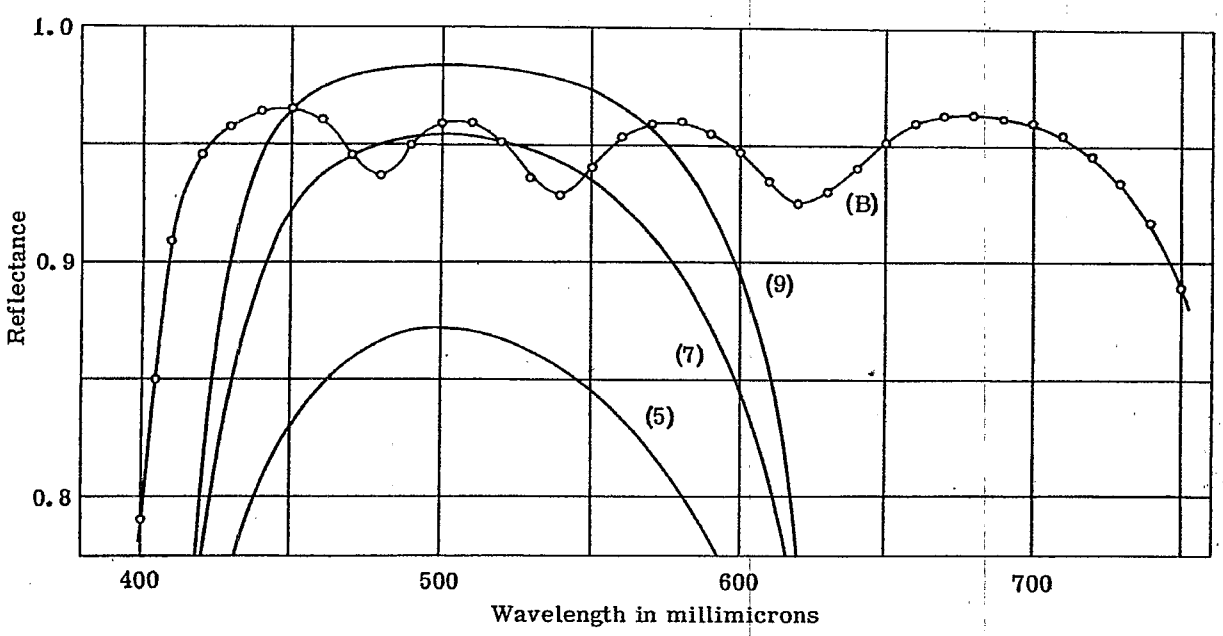

Figure 20.95- Measured spectral reflectivity of quarter-wave stacks with 5, 7, and 9 layers and also a broad-band reflector consisting of 15 layers of ZnS and cryolite. From ref. 49.

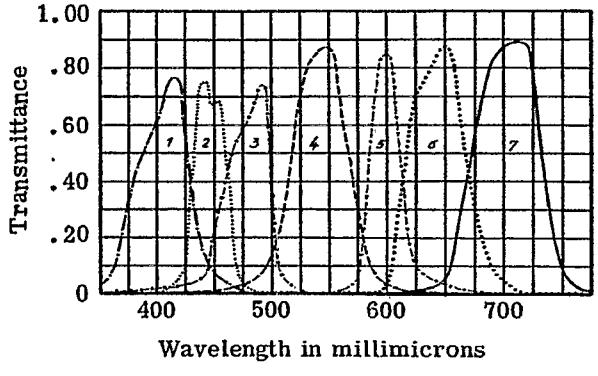

Figure 20.96- Measured transmittance of band pass filters which utilize both multilayer and glass absorption filters. Courtesy of Balzers Aktiengesellschaft, Liechtenstein.

MEASURED TRANSMITTANCE OF A SERIES OF BAND PASS FILTERS COMPLETE WITH AUXILIARIES

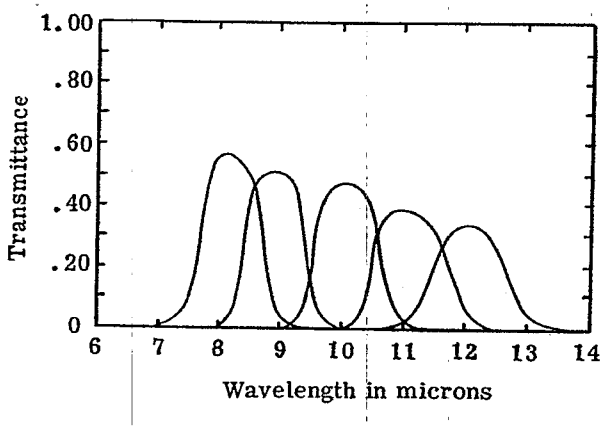

Figure 20.97- Measured spectral transmittance of some infrared band pass filters, complete with auxilliaries. Courtesy of Bausch and Lomb, Inc.

$$T_f = T_{max} \ (1 + F \sin^2 \eta)^{-1} \tag{49}$$

where

$$T_{max} = \frac{T_1 \ T_2}{(1 - R)^2} \ , \tag{50}$$

$$F = \frac{4R}{(1 - R)^2} \ , \tag{51}$$

$$R = \sqrt{R_1 R_2} \ , \tag{52}$$

and

$$\eta = 2\pi\sigma \ n_g \ t_g - \frac{\epsilon_1 + \epsilon_2}{2} \ . \tag{53}$$

T_1 , T_2 and R_1 R_2 are the reflectivity (measured on the side of the mirror coating facing the gap) and transmission of the semitransparent mirror coatings on each of the plates. The coatings need not have the same R and T, and can also be absorbing, so that $R + T \neq 1$. ϵ_1 and ϵ_2 are the phase shift upon reflection from each of the coatings, which is explained in Section 20.10.1.4. t_g is the physical separation of the plates, measured from the surface of the coatings and n_g is the refractive index of the medium in the gap, which is usually air or a vacuum. In the most general case, R_1, T_1, ϵ_1, R_2, T_2, and ϵ_2 all vary with wavelength.

Since the $\sin^2$ function in the denominator of Equation (49) is always a positive quantity, T_f attains a maximum value when $\eta = m\pi$; the integer m is called the order number. If we neglect for the moment the phase shifts, ϵ_1 and ϵ_2, in Equation (53), then T_f is a maximum when

$$m\pi = 2\pi\sigma \ n_g \ t_g \ , \tag{54}$$

or

$$m \ \frac{\lambda_o}{2} = n_g \ t_g \ . \tag{55}$$

Equation (55) states that the resonant, or maximum transmission condition, occurs when the separation of the plates is an integral number of half-waves. The Fabry-Perot interferometer can be considered as a resonant cavity for light waves. Similar resonance conditions occur when an integral number of half-waves fit into a microwave cavity or an organ pipe. One difference is that the resonance in microwave cavities is usually in the first or second mode, that is, $m = 1$ or 2. A very high mode - or to use the language of physical optics, a high order of interference - is obtainable in the Fabry-Perot interferometer. For example, a plate separation of $t_g = 1.0$ cm. is commonly used, in which case $m = 40{,}000$ at $\lambda = 500$ mμ; that is, 40,000 half-waves fit in between the plates.

20.10.1.2 Spectral transmission of F.P. interferometer. If the Fabry-Perot interferometer is illuminated with highly collimated light, as shown in Figure 20.99, then its transmission, T_f, as a function of wave number (frequency) consists of a series of transmission peaks which are equally spaced, as is shown in Figure 20.100. The spacing σ_f between adjacent transmission peaks is called the free spectral range of the interferometer and is inversely proportional to the separation of the plates:

$$\sigma_f = 1/2t_g \tag{56}$$

For most plate separations which are attainable, this free spectral range is rather small and hence many transmission peaks are packed close together. For example, suppose that two plates are separated by three thin pieces of metal foil which are a little less than one thousandth of an inch thick, so that $t_g = 0.0025$ cm. From Equation (56), we find that $\sigma_f = 200$ cm^{-1}. This means that in the green region of the spectrum, transmission maxima would occur at wave numbers of 20,000 cm^{-1}, 19,800 cm^{-1}, 19,600 cm^{-1}, and so on. Converting these wave numbers into wavelength (see 20.1.3.3), we find that transmission peaks occur at 500.00 mμ, 505.05 mμ, 510.10 mμ, and so on. Thus the separation of the peaks is about 5 mμ in this spectral region. If this interferometer were used to pass a spectrum line at 505.05 mμ, then it would be necessary to have an auxiliary blocking filter (a composite filter, to use the language of 20.5.1.3.2) to attenuate the unwanted transmission peaks at 500mμ, 510mμ, and at other wavelengths.

Figure 20.101 shows the shape of the transmission band of an F.P. interferometer whose plates are coated with highly-reflecting films so that $R_1 = R_2 = 0.95$. This is merely an enlarged view of one of the transmission bands shown in Figure 20.100, translated to a wavelength scale. The maximum transmission of the band is T_{max} and occurs at a wavelength λ_o. By definition, the total width of the band at $1/2\ T_{max}$ is $\Delta\lambda_{1/2}$ *. Thus $\Delta\lambda_{1/2}$ gives an indication of the narrowness, or the sharpness, of the resonance line of the interferometer, and consequently its ability to transmit radiant energy at its resonant wavelength, λ_o, and to attenuate radiant energy of nearby wavelengths. This is allied to the chromatic resolving power of the interferometer.

20.10.1.3 Resolving power of the F.P. interferometer. The narrowness of the resonance line in the frequency spectrum of any resonant device is proportional to the ability of the device to store energy with low loss of energy per cycle of oscillation. The dimensionless quantity "Q" of a resonant system is defined as:[55a]

$$Q = 2\pi \frac{\text{Energy stored in system}}{\text{Energy lost in one cycle}}, \qquad (57)$$

and is inversely proportional to the line width, $\Delta\sigma_{1/2}$. For example, the simple "LC" resonant circuit shown in Figure 20.101 stores energy in the electric field in the capacitor and in the magnetic field of the inductor. Each cycle a fraction of this energy is dissipated in the form of heat due to the finite resistance of the wire in the inductor and to losses in the dielectric of the capacitor. If this loss can be decreased, then the Q of the circuit will improve and its sharpness as a tuning element, say in a radio receiver, will improve. Similarly, the energy of a microwave cavity is usually extracted through a small hole in the wall of the cavity. During each cycle of oscillation, a small amount of the energy which is stored in the electromagnetic fields in the cavity leaks out of this hole and is also absorbed as Joule heat in the walls of the cavity. The Q of the cavity is improved by silver plating the cavity walls and thus reducing this loss. The case for the F.P. interferometer is completely analogous. Standing light waves are established in the gap between the two reflecting plates, and electromagnetic energy is stored in this gap. During each cycle of oscillation, which in the case of visible light is more than 10^{14} cycles per second, a small amount of this energy in the cavity is depleted by either being absorbed or transmitted through the coatings.

From the foregoing considerations, we would expect that the Q of a F.P. interferometer would increase as the reflectivity of the coatings on the plates is enhanced. Another method of improving the Q is to store more energy in the cavity, which is accomplished by simply making cavity larger - that is, by using a larger separation of the plates. A more quantitative analysis,[55b] such as the one in Section 5.16, leads to the relation

$$Q = \left(\frac{\lambda_o}{\Delta\lambda_{1/2}}\right)\left(\frac{\sigma_o}{\Delta\sigma_{1/2}}\right) = \left(\frac{\sqrt{R}}{1 - R}\right) m\pi . \qquad (58)$$

Thus an interferometer with $R = 0.95$ and a plate separation of 1 cm. has a Q over two million, which is larger by several orders of magnitude than any microwave device. The Q is a quite sensitive function of R, as R gets close to unity. The Q computed from Equation (58) can either be increased or decreased by the variation with wavelength of the phase shift on reflection of the two semi-transparent mirrors. A more exact formula is given in reference 56. It should be remarked that Q is used as a criterion of the narrowness of the pass band in preference to the chromatic resolving power, which is used in most books on physical optics. The reason is that there are many different criteria for defining the chromatic resolving power and it is not desirable that Equation (58) be confused with them.**

20.10.1.4 The phase shift upon reflection. A standing wave is created when a light wave is incident upon a reflecting surface. The positions of the nodes of this standing wave remain fixed in space. Suppose an incident light wave, whose electric vector is represented by

$$E = E_o\, e^{i(\omega t - 2\pi z/\lambda)} . \qquad (59)$$

* If the width $\Delta\lambda_{1/2}$ is translated into the corresponding width, $\Delta\sigma_{1/2}$, on a frequency (wave number) scale, they are related by: $\frac{\Delta\lambda_{1/2}}{\lambda_o} = \frac{\Delta\sigma_{1/2}}{\sigma_o}$, were $\lambda_o = \sigma_o^{-1}$

** For example, compare Eq. 58 in this text with Eq. 43 on page 334 of Born and Wolf[11].

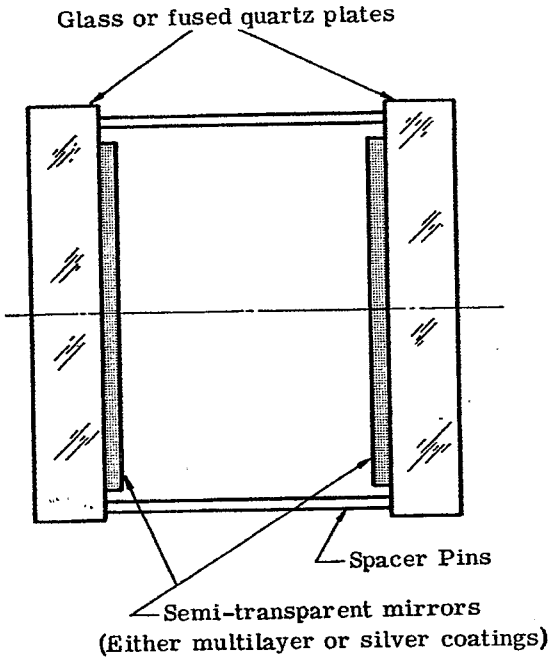

Figure 20.98- The essential parts of a Fabry-Perot interferometer.

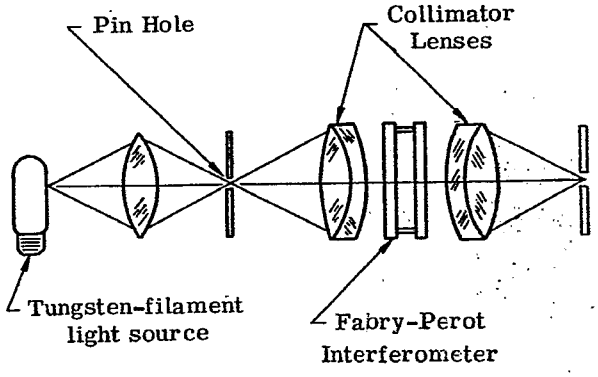

Figure 20.99- A method of illuminating the Fabry-Perot interferometer with collimated light so that it can be used as an optical filter.

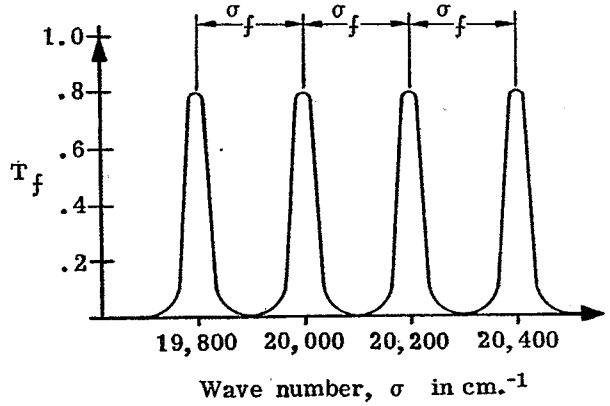

Figure 20.100 – The transmission as a function of wave number of a Fabry-Perot interferometer with t_g = 0.0025 cm .

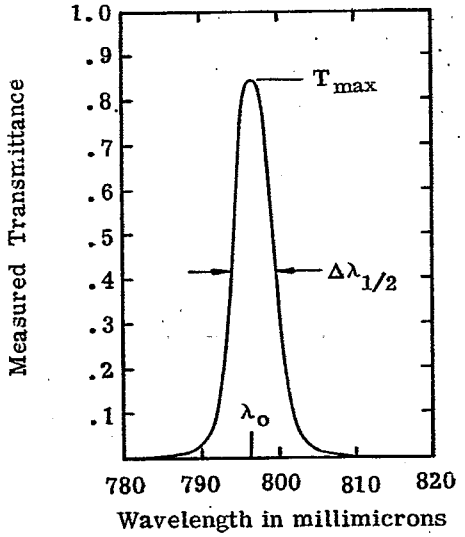

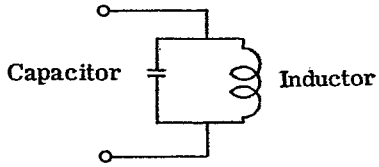

Figure 20.101- Measured spectral transmittance of Fabry-Perot type multilayer filter. Courtesy of Dr. C. Alley.
A parallel resonant circuit.

is reflected from a surface. If the reflected wave represented by:

$$E_r = R^{1/2} E_o e^{i(\omega t + \epsilon_1 + 2\pi z/\lambda)} , \qquad (60)$$

this defines the phase shift upon reflection, ϵ_1 . If the reflecting surface is a metal with infinite conductivity - that is, a perfect reflector, - then the standing wave has a node at the surface and the phase shift, ϵ_1, is 180°. At some instant of time, the amplitude of the light wave varies sinusoidally in space, as shown by the solid line in Figure 20.102; a half-cycle later it is represented by the dashed line. If ϵ is less than 180°, as would be the actual case for a silver mirror, then the node of the standing wave is to the right of the reflecting surface. If ϵ is greater than 180°, it is to the left, as shown in Figure 20.102. The phase shift upon reflection is exactly 180° for an air-glass interface, and does not vary with wavelength as long as the glass is optically non-absorbing. The ϵ for silver films changes slowly with wavelength, but this change is so small that it is usually neglected. The phase shift upon reflection for multilayer is much larger and, as is shown in 20.10.5, modifies the shape of the transmission band of a multilayer filter. It can also alter the wavelength at which the pass band occurs.[56]

20.10.1.5 Effect of ϵ on a resonant cavity. The effect of the phase shift upon reflection is to shrink or expand the walls of a resonant cavity. If the variable η in Equation (53) were defined as $\eta = 2\pi\sigma n_g t_g$, thus omitting the second term, this would tacitly assume that there is a node of the standing wave at each of the two reflecting surfaces. The addition term in Equation (53), $1/2 (\epsilon_1 + \epsilon_2)$ can be regarded as a correction term which accounts for the fact that the ϵ of each of the mirrors shifts the node of the standing wave. This shift in the node of the standing wave changes the resonant frequency of the cavity. If ϵ_1 and ϵ_2 change with wavelength, this alters the shape of the transmission band from the Lorentzian shape shown in Figure 20.101.

20.10.1.6 Shape of the transmission band. If the condition is fulfilled that ϵ_1 and ϵ_2 are constant with wavelength and that R_1 and R_2 are large enough so that F is much greater than one, then over the narrow wave number range near a pass band at σ_o , the sine function in Equation (49) can be replaced by its argument and T_f written as

$$T_f = (T_{max}) (1 + G \Delta^2)^{-1} \quad \text{where} \quad \Delta + \sigma_o = \sigma \qquad (59)$$

and constants such as F , 2π , t_g , etc. have been lumped together into G , which is essentially constant over the range of Δ, in which the approximation is valid . The point we wish to make is that this is a Lorentzian line shape (shown in Figure 20.101), and is similar to the shape power absorption curve of a series resonant "LC" circuit with a high Q[57] . A characteristic of the Lorentzian line shape is that a long tail which decreases slowly in amplitude extends to both the short and long-wave side. There are applications of F.P. type filters which require that the transmission on either the short-wave or long-wave side, decrease much more rapidly than is provided by a filter with a Lorentzian-shape transmission band. A few multilayers with a non-Lorentzian transmission band are shown in 20.10.7.

20.10.2 Fabry-Perot type multilayer filters. The Fabry-Perot interferometer described in the foregoing section is actually used as a band-pass filter in the laboratory. Notwithstanding the high Q which can be attained, it is not widely used because the optically polished plates are quite expensive and small mechanical vibrations or temperature changes cause the plates to warp out of parallel, thus degrading the Q of the instrument. These difficulties are partially avoided if the material in between the plates (i.e. the spacer) is a solid material. This is accomplished by depositing a mirror on a substrate by evaporation in a vacuum, then evaporating a spacer layer whose optical thickness satisfies Equation (55), and then evaporating another mirror. Another method is to use a thin piece of mica as the spacer material and to evaporate a mirror on both sides. This technique is discussed in 20.10.5.2.

20.10.2.1 Method of analysis. In the case of the Fabry-Perot interferometer, it is quite natural to analyze the performance in terms of Equation (49). This has the advantage that one does not need to know any of the details about the construction of the semitransparent mirrors on the two faces - it is only necessary to know the R, T, and ϵ of each mirror, and n_g , t_g . However, in the case where the spacer is evaporated as an integral part of the filter, such as the filters depicted in Figures 20.103 or 20.108, then there are many methods of analyzing its spectral transmission, as for example the admittance method[58] , the matrix method[59] or by considering it as a Fabry-Perot interferometer[60] . There is a large class of multilayer filters whose spectral transmission is most easily analyzed by treating them like a Fabry-Perot interferometer. This is accomplished by selecting one of the films in the stack - usually the center film if the stack has an odd number of layers and is symmetrical - and considering this film as a spacer layer with an optical thickness $n_g t_g$. The remaining films in the stack are divided into two groups - those between the spacer layer and the substrate form an effective interface "A" and the films between the spacer layer and the incident medium form the other effective interface.[60] The spacer layer is usually, but not

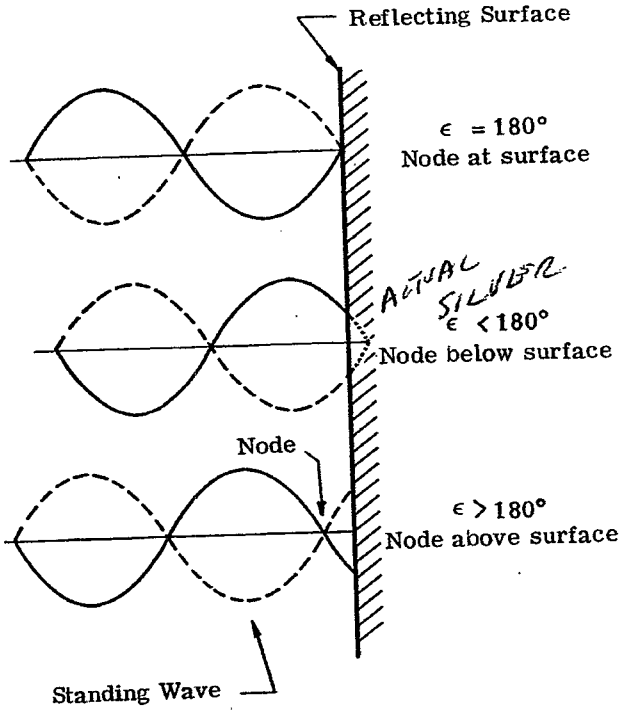

Figure 20.102- Showing the node of the standing wave as a function of the phase shift upon reflection, ϵ .

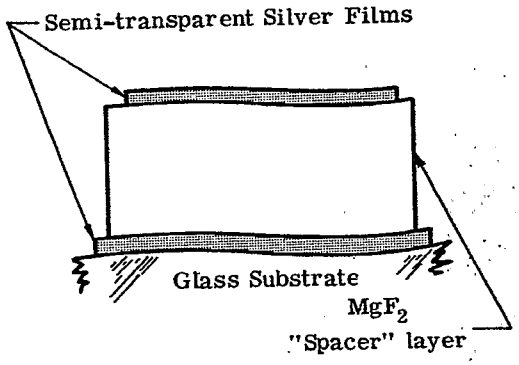

Figure 20.103- An enlarged view of a silver-dielectric-silver Fabry-Perot type filter, the lack of flatness of the substrate being exaggerated for purposes of illustration.

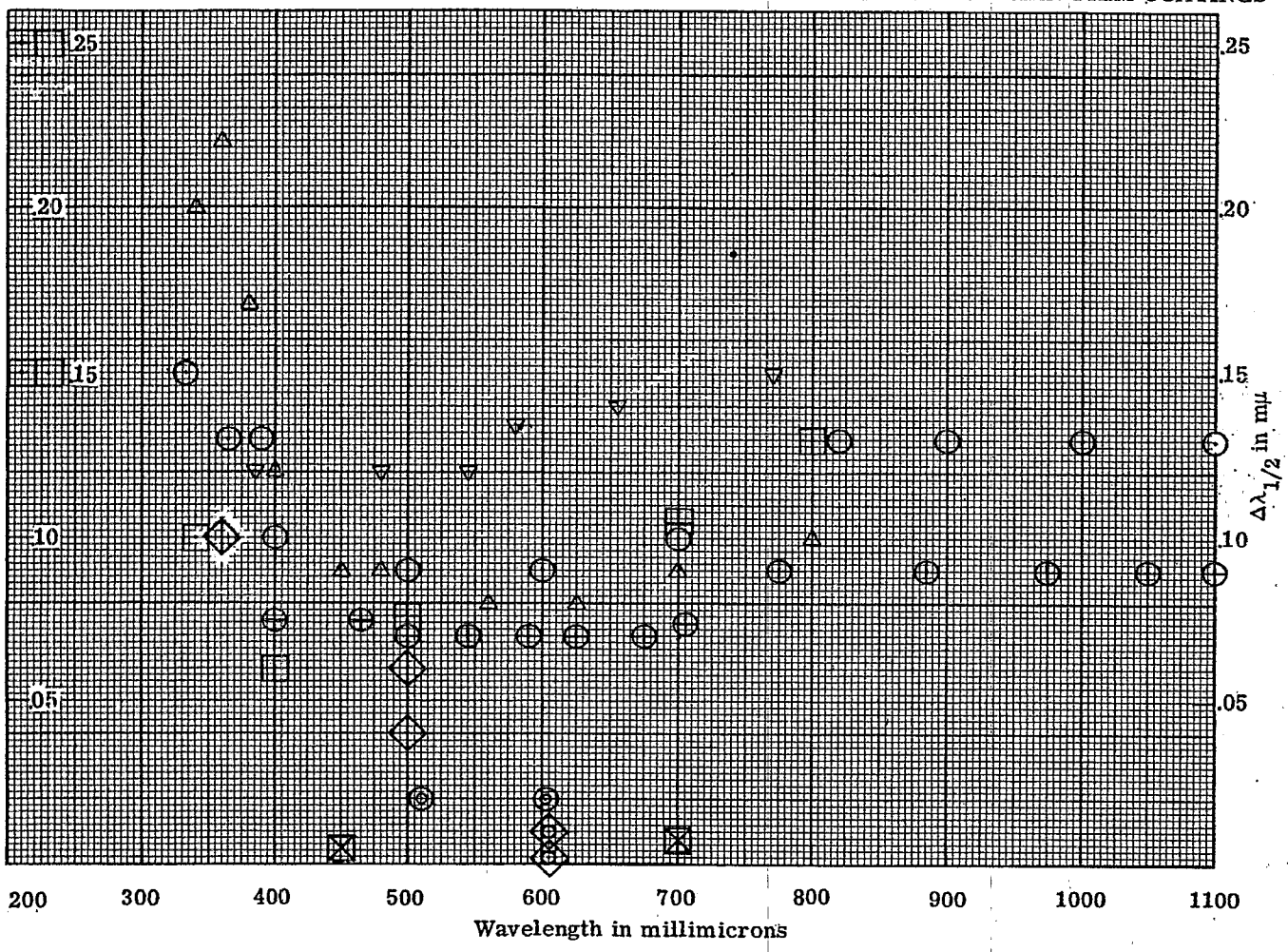

LEGEND: Filters contain metal unless specified otherwise.

- Baird-Atomic, Inc. Multilayer dielectric with Q = 1000 . $T_{max.}$ = 0.45 to 0.60 , blocking filters included.
- Baird-Atomic, Inc. Multilayer dieletric filter with rectangularly shaped pass band. $T_{max.} > 0.60$, blocking filters included.
- Baird-Atomic, Inc. Type "A"

$T_{max.}$			$\Delta\lambda 1/2$
0.15	→	0.20	25 mμ
0.10	→	0.15	15 mμ
0.05	→	0.10	10 mμ

- Bausch and Lomb, Inc. "Standard series" , second order interference, $T_{max.}$ = 0.30 to 0.35 .
- Carl Zeiss, Jena^{er}, "Single filters" , $T_{max.}$ = 0.25 in the u.v. and near i.r. . $T_{max.}$ = 0.35 in the visible.
- Carl Zeiss, Jena^{er}, "Double filter" (a composite filter) Type DSIF , $T_{max.}$ = 0.08 to 0.15 .
- Multilayer dielectric, $T_{max.}$ = 0.93 , without blocking filters. See reference 64 .
- Multilayer dielectric, consisting of from 21 layers ($T_{max.}$ = 0.55) to 29 layers ($T_{max.}$ = 0.15) . See reference 65 .
- Schott (Jena^{er} Glaswerke Schott & Gen., Mainz) These are "Line filters" of unspecified order of interference.
- Specially prepared F-P type filter consisting of nine dielectric films and two silver films . $T_{max.} \sim 0.40$. See reference 64 .
- Spectrolab, Inc. Published curves show $T_{max.} \sim 0.90$.

Figure 20.104- The total width at .5 $T_{max.}$, $\Delta\lambda 1/2$, and wavelength of the passband, λ_o , of some representative Fabry-Perot type filters composed of the metal-dielectric-metal type and all-dielectric type. See 20.10.2.2 for details.

always, an integral number of half-waves in optical thickness. References 60 and 61 show some exceptions. Thus by dividing a multilayer into a spacer layer and two effective interfaces, it can be analyzed as a Fabry-Perot interferometer and Equation (49) can be used to compute its transmission, provided R_1, T_1, ϵ_1, R_2, T_2, ϵ_2 for the interfaces are known.

The simplest type of multilayer whose performance can be analyzed as a F.P. interferometer is the silver-dielectric-silver interference filter (shown in Figure 20.103). When its discovery was announced, it was called an interference filter, since it was the first type of filter which operated on the basis of the interference of light, rather than absorption. When other types of multilayers came into use a decade later, it was recognized that all multilayers are in a sense "interference" filters, since their transmission characteristics depend upon the interference of light reflected from various layers within the multilayer. Thus in this section, the term "Fabry-Perot type filter" (F-P type) is used in preference to"interference filter".

20.10.2.2 Criteria for evaluating F-P type filters. Most F-P type filters are band pass filters and have a narrow transmission spike in the pass region and a high attenuation outside of that region. In order to compare the performance of different types of F-P filters, the following attributes are sometimes considered:

(1) The wavelength λ_o of the maximum transmission of the pass band.

(2) The maximum transmission of the pass band, T_{max}.

(3) The total width of the band at half intensity (i.e. at 1/2 T_{max}) $\Delta\lambda_{1/2}$. This is related to Q: $\Delta\lambda_{1/2} = \lambda_o/Q$.

(4) The Q of the filter, or alternatively, Q^{-1}.

(5) The extent of the attenuation region, and whether blocking filters need be added to extend this region.

(6) The shift of the transmission band as a function of the angle of incidence.

In comparing the literature of various manufacturers of multilayer F-P type filters, it is evident that even if all of these data are given, there is still no substitute for a spectral transmission curve. $\Delta\lambda_{1/2}$ is not necessarily a good criterion for comparing filters, because different types of filters have transmission bands of different shapes. For example, the pass band of the silver-dielectric-silver F-P type filter shown in Figure 20.105 has a Lorentzian line shape and shows the characteristic long tail of high transmission towards the blue, whereas the filter in Figure 20.118 has a pass band of a different shape and although its $\Delta\lambda_{1/2}$ is twice as large, the transmission in the blue decreases much faster. Sometimes the T_{max} given in the specifications of a manufacturer may or may not include the blocking filters which should be placed in series with the F-P type filter in order to eliminate unwanted transmission bands, as appear in the filters shown in Figures 20.105 and 20.115. Figure 20.114 shows how such a blocking filter is used to eliminate an unwanted transmission band at short wavelengths. The $\Delta\lambda_{1/2}$ at various λ_o of F-P type band-pass filters is shown in Figure 20.104. These data are compiled from the scientific literature and from the catalogues of manufacturers. In the latter case, they represent some of the filters produced by some manufacturers. This is definitely not a comprehensive list, but rather it is intended to give some idea of the range of the $\Delta\lambda_{1/2}$ and T_{max} which can be achieved at various wavelengths. Neither is this list intended to be encyclopedic, including all manufacturers. As was mentioned previously, the parameters T_{max} and $\Delta\lambda_{1/2}$ often do not adequately describe the performance of a filter, and hence it would be incorrect to conclude from Figure 20.104 that manufacturer "A's" filters are superior to "B's" filters. Evidently there is some variation in both the T_{max} and $\Delta\lambda_{1/2}$ between individual filters of a given type, because most manufacturers gave a range of values. Average values are used for the data shown in Figure 20.104

20.10.3 Band pass filters containing metal films.

20.10.3.1 The metal-dielectric-metal (M-D-M) Fabry-Perot type filter. The simplest filter of the F-P type is a three-layer filter consisting of a dielectric film, such as magnesium fluoride, sandwiched between two semitransparent metal films. In 1939 Geffcken [62,63] applied for a patent on the device in which both the metal films and the dielectric spacer layer film are evaporated. The beauty and simplicity of this method is that such a filter can be deposited on a substrate of common window glass, rather than an extremely precise optical flat, as is requisite for the F-P interferometer. The point is, that the surface of a piece of window glass deviates many wavelengths from being optically flat, but that the three or more layers in the multilayer coatings follow the contour of the substrate. The drawing in Figure 20.103 shows this effect; the lack of planeness in the substrate is greatly exaggerated. Actually, the lack of planeness in the substrate does broaden the transmission bands slightly, but this effect is certainly not noticeable with broad 10 mμ band widths typical of this type of filter.

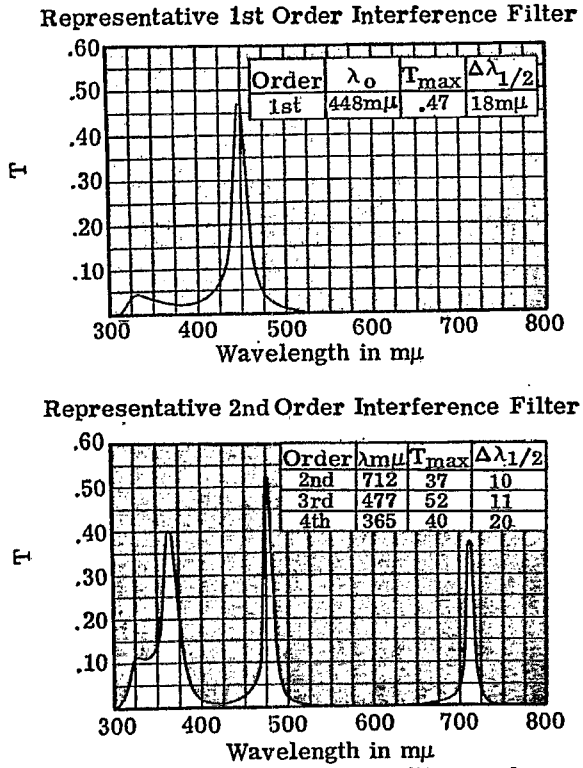

Figure 20.105- Measured transmittance of some metal-dielectric-metal Fabry-Perot type filters. Courtesy of Bausch and Lomb, Inc.

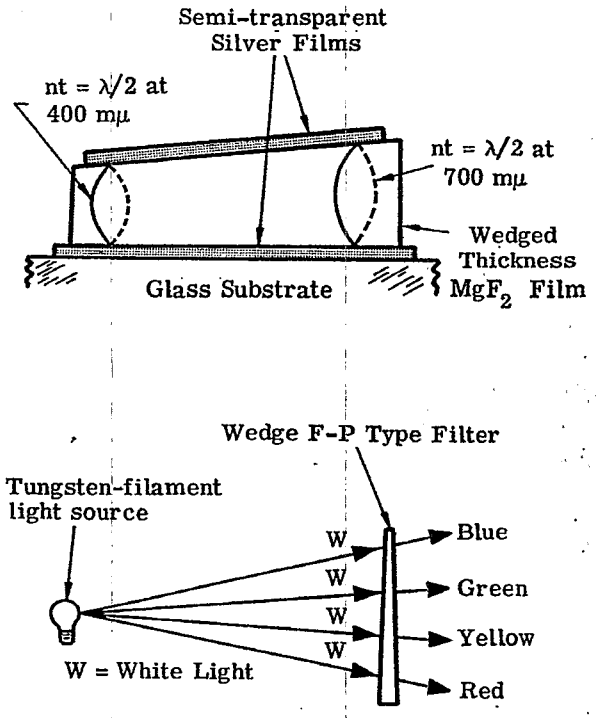

Figure 20.107- (Upper) A cross section of a wedge Fabry-Perot type filter. (Lower) Showing the use of this type of filter as a monochromator.

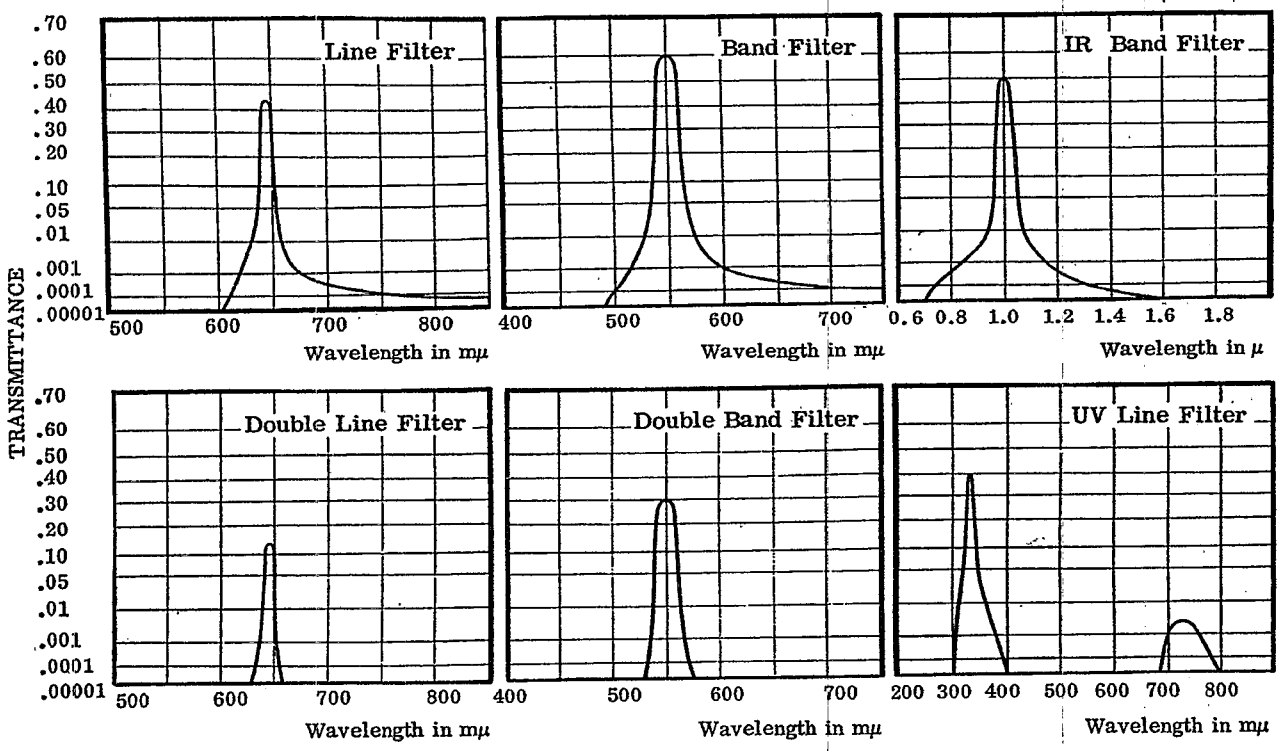

Figure 20.106- Measured transmittance (on a logarithmic scale) of silver-dielectric-silver Fabry-Perot type filters. Courtesy of Schott & Gen., Mainz, West Germany.

For wavelengths greater than 340 mμ , silver is the best metal film to use, having the highest reflectivity and lowest amount of absorption. Below 340 mμ the optical constants of silver change rapidly and the reflectivity drops to very low values. This is why silver-dielectric-silver F-P type filters have a transmission "leak" in this region, as is shown in Figure 20.105. At these shorter wavelengths aluminum is generally used as the metal film, although it absorbs a large fraction of the radiant energy and consequently these filters usually have a T_{max} of .10 to 20. Figure 20.105 shows the spectral transmittance of a silver-dielectric-silver F-P type filter with a first order transmission maximum at 450 mμ . The transmission "leak" in the ultraviolet is due to the loss in the reflectivity of the silver in this region. Also shown in Figure 20.105 is the transmittance of a filter which has a second order peak at 712 mμ , and third and fourth order peaks at shorter wavelengths. In Figure 20.106 is depicted the transmittance (on a logarithmic scale) of various types of M-D-M filters. The "double filter" consists of two identical filters cemented together to form a composite filter. Although the peak transmittance is low, (T_{max} is from 0.10 to 0.30), an extremely high attenuation in the reject region is attained - the optical density is greater than five. This high attenuation is achieved because the filters are absorbing and hence the considerations which apply to dielectric films (see 20.5.1.4) do not hold here.

20.10.3.2 The wedge M-D-M filter. Another interesting form of a M-D-M filter is the wedge Fabry-Perot type filter,[66] which is depicted in Figure 20.107. Two silver films are deposited on either side of a layer of magnesium fluoride, which is wedged shaped so that its thickness varies in a linear fashion along the length of the filter. At one end the optical thickness is a half-wave of violet light (400 mμ), so this portion passes the violet. At other positions along the filter the dielectric film is thicker and these portions pass the blue, green, yellow, and finally the red.* In actual practice, the filter is usually manufactured a second order filter, rather than first order, as shown, thus achieving a narrower band width. In this case, at the thick portion of the wedge the second order red and the third order blue overlap, and it is necessary to remove the blue by appropriate dye or glass filters. The $\Delta\lambda_{1/2}$ of this second order filter is 10 mμ , independent of wavelength. The slope of the wedge and the length of the filter are chosen so that a one millimeter slit gives this pass band. Thus by inserting a slit 1 mm wide in front of this wedge filter and illuminating it with white light, a rather inexpensive source of quasi-monochromatic light is obtained. This type of wedge can be deposited in an annular ring on a disk.[67] The wavelength scanning is accomplished by rotating the disk past a slit.

20.10.3.3 Other types of narrow pass-band filters which contain metal films. A higher peak transmission and narrower band width is attained with F-P type filters if several dielectric films are added to the stack in addition to the spacer layer.[64] Turner and Berning have devised some band-pass filters which contain a single silver film and many dielectric films.[68] M-D-M filters are also useful as reflection filters, particularly in the infrared spectral region.[64, 69]

20.10.4 All-dielectric Fabry-Perot type filters. The simplest form of this type of filter is shown in Figure 20.108. The silver films are replaced by semitransparent mirrors composed of dielectric materials, such as a quarter-wave stack. Thus the design of a filter consisting of seven layers would be:

glass H L H LL H L H air .

Here the H L H combination is a three-layer quarter-wave stack (H and L have a QWOT at λ_o) and LL represents a spacer layer of half-wave optical thickness at λ_o . The spectral transmission versus frequency of such a multilayer is shown in Figure 20.109. Although this and other multilayers which are used as illustrations can be used only in the infrared because they contain germanium as a high index material, the principles involved here apply to any spectral region.

20.10.4.1 T_{max} . The concept of an absentee layer (20.1.5.2.2) is useful in determining the transmission of this filter at the wavelength λ_o (i.e. g = 1.0) where the maximum of the pass band is located. At this wavelength the LL layer is absentee and hence it can be removed from the stack, leaving:

glass H L H H L H air.

This leaves two of the H layers next to each other, resulting in the layer HH which has an optical thickness of a half-wave. After removing this HH combination from the stack we are left with four layers:

glass H L L H air.

* In actual practice, the optical thickness of the dielectric spacer layer is slightly thinner than a half-wave, due to the phase shift upon reflection of the silver films. Also, the thickness of silver films varies along the wedge, due to the dispersion of the optical constants of the silver.

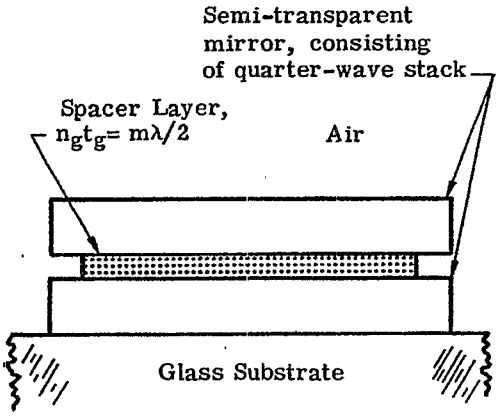

Figure 20.108- Design of a conventional all-dielectric Fabry-Perot type filter.

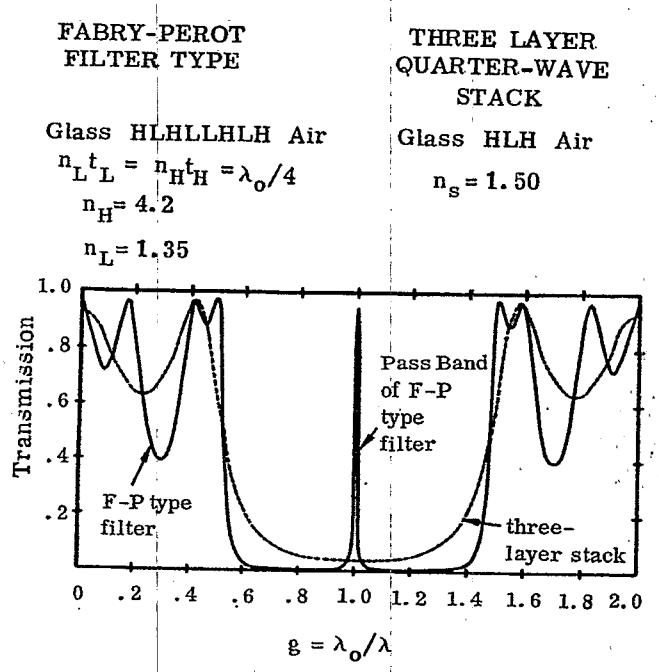

Figure 20.109- Computed spectral transmission of an all-dielectric Fabry-Perot type filter (solid curve) and a three-layer quarter-wave stack (dashed line).

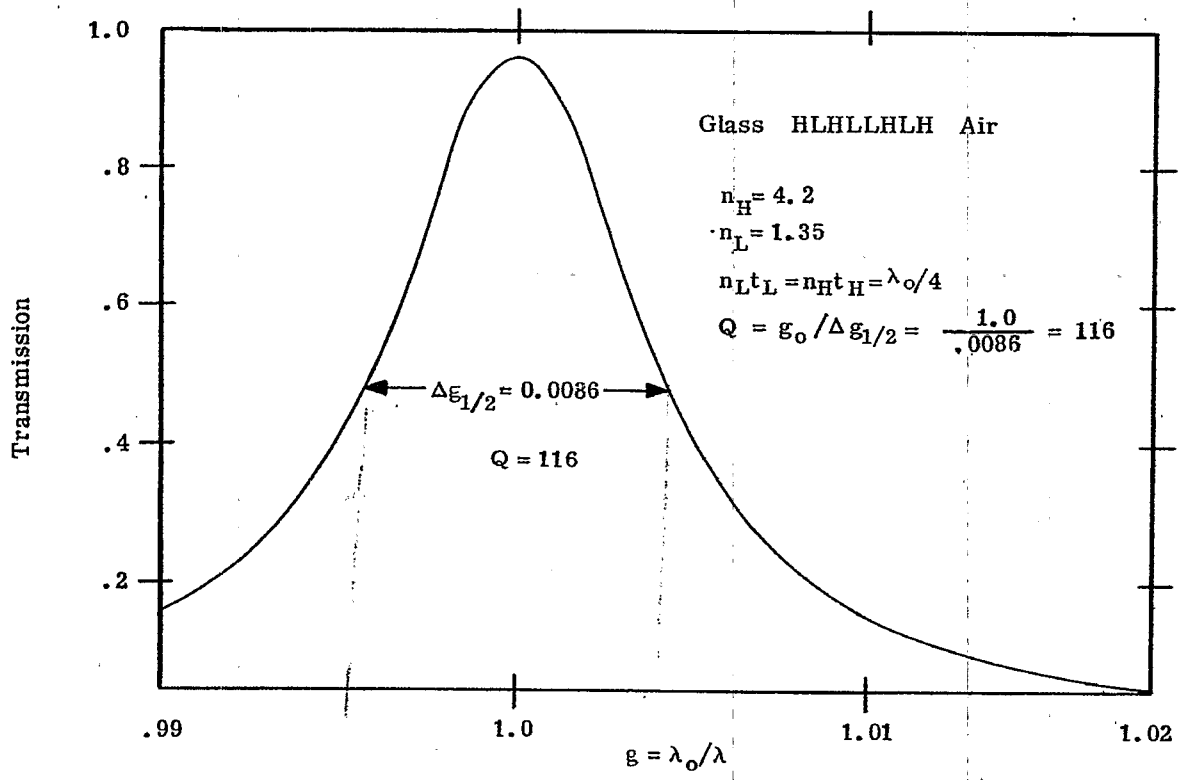

Figure 20.110- Computed transmission of the pass band of the Fabry-Perot type filter shown in Fig. 109.

The half-wave combination LL is absentee and can also be removed from the stack. Repeating this process, we see that at λ_o the transmission is the same as that of a single surface of uncoated glass of index 1.50, and thus from Equation (21), $T = 0.96$. This does not include the reflection loss at the second surface of the substrate.

20.10.4.2 It is instructive to compute the Q of this filter. First, it is necessary to compute the reflectivity, R_1 and R_2, of each of the effective interfaces. The first effective interface is:

glass H L H cryolite

and thus R_1 is computed from an incident medium of cryolite. R_2 is computed for a stack:

air H L H cryolite

where the substrate is air and cryolite ($n_o = 1.35$) is the incident medium. Utilizing Equations (40) and (43), we find that $R_1 = 0.953$ and $R_2 = 0.968$, whence $R = (R_1 R_2)^{1/2} = 0.961$. From Equation (58) a Q of 80 is computed. Figure 20.110 shows the computed spectral line shape of this filter, on a frequency scale. The Q, measured from this graph, is 116. The additional narrowing of the transmission band is attributed to the phase shift upon reflection of the three layers which constitute the effective interfaces of this F-P type filter. References 56 and 61 show how to include the effect of the phase shift in computing the Q of the system.

20.10.4.3 Effect of phase shift upon reflection. As an example of how the phase shift upon reflection can influence the shape of the transmission band of a F-P type filter, consider the following multilayers, which are designated as Design I and Design II :

I glass L H L HH L H L air

II glass HH L H L HH L H L HH air .

Design II is essentially Design I with an extra half-wave layer added to each end of the stack. At $g = 1.0$, the half-wave layers are absentee and the reflectivities of the effective interfaces of each of the two stacks is exactly the same. However, if we examine the transmission bands for these two stacks, shown in Figure 20.111, it is evident that the width $\Delta \lambda_{1/2}$ at $1/2\, T_{max}$ is somewhat less for Design I than for Design II. This can be attributed to the variation with wavelength phase shift upon reflection of the effective interfaces, which is shown in Figure 20.112. In each case the phase shift upon reflection is measured from inside of the germanium spacer layer. At $g = 1.0$ the phase shift is zero, which means that the node lies at the surface of the multilayer. At lower frequencies than $g = 1.0$ the node lies to the right of the surface. The shift of this node as the wavelength changes alters the shape of the transmission band.

20.10.4.4 The use of blocking filters. All-dielectric F-P type filters are usually used in conjunction with blocking filters. These blocking filters must in general have a much higher attenuation than the blocking filters which are used in conjunction with the M-D-M type filters. The reason is that in the former case, the unwanted transmission bands cover a wide spectral region, whereas the unwanted transmission bands of a M-D-M type are usually quite narrow. For example, suppose it is desired to use the transmission band at 477 mμ in the M-D-M type second order filter shown in Figure 20.105. In this case it is necessary to use an auxiliary blocking filter to eliminate the unwanted transmission bands below 425 mμ and the band at 712 mμ . There are many absorption type filters which could be used to attenuate below 425 mμ. The band at 712 mμ is comparatively narrow and hence the total amount of radiant flux which "leaks" through this band is not large. Consequently, the amount of attenuation required in the blocking filter is not as great as it would be if the pass band were wide. In the case of all-dielectric F-P type filters, the quarter-wave stacks which are used for the semitransparent mirrors do not reflect over a wide range of wavelengths. Thus a quite appreciable amount of radiant energy is liable to "leak" through the filter in the region outside of the high-reflectance zone of the mirrors. The narrower the pass band of the F-P type filter, the more effective should be the blocking filters to insure that the total amount of radiant flux transmitted in the spectral region of the pass band of the filter should be much greater than the flux which leaks through at other wavelengths. For example, the all-dielectric F-P type filters shown in Figures 20.115 and 20.116 have a substantial transmittance below 8.0 μ. The total transmitted radiant flux below 8.0 μ to 3.9 μ (where the PbTe films start to absorb) is considerably larger than the radiant flux transmitted through the pass band near 10 μ.

20.10.5 All-dielectric F-P type filters for the visible. All-dielectric F-P type filters are produced commercially for most of the visible spectral region with a wide range of Q . Filters with a Q from 10 to 1000 are available. Values of T_{max} from 0.45 to 0.60 are commonly attained, which includes the appropriate blocking filters. The spectral transmission of an all-dielectric F-P type filter which has its pass

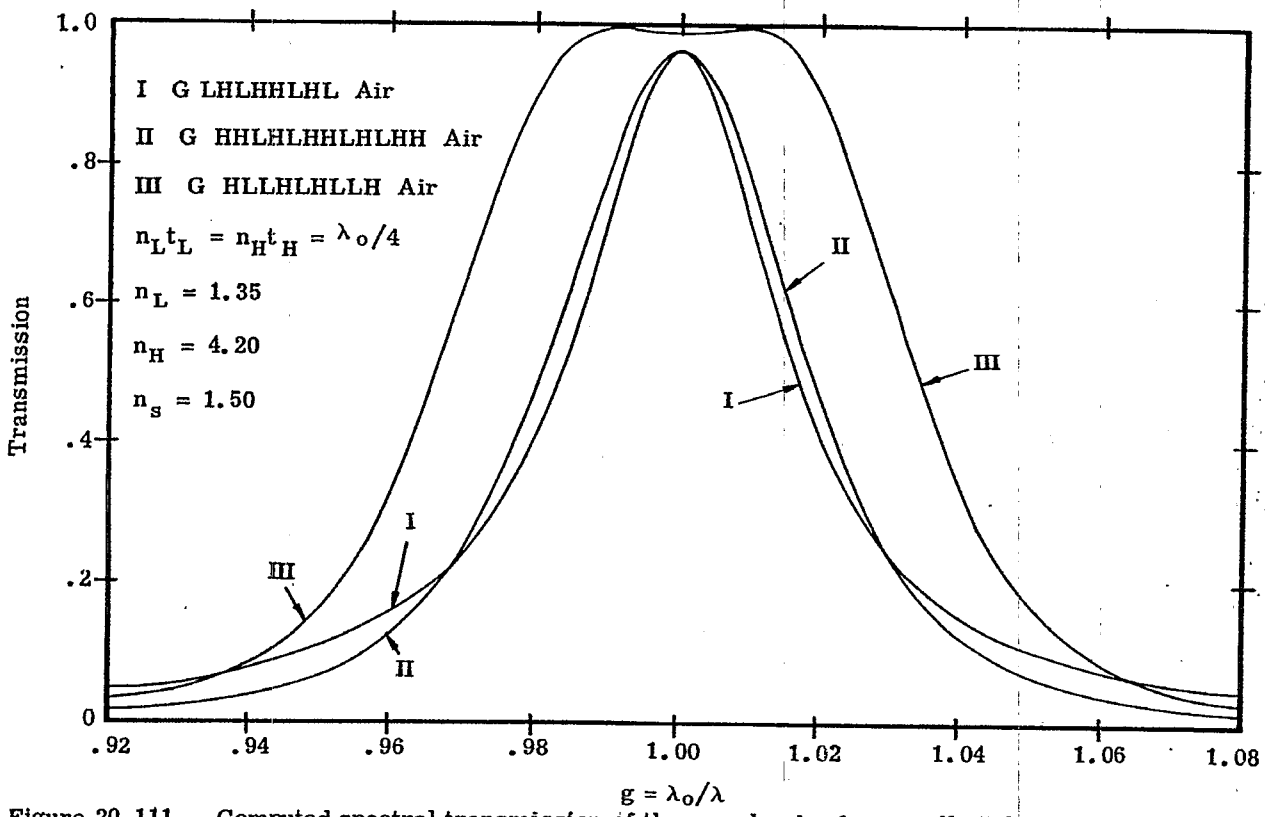

Figure 20.111- Computed spectral transmission of the pass bands of some all-dielectric Fabry-Perot type filters. Filter III has non-Lorentzian shaped pass band.

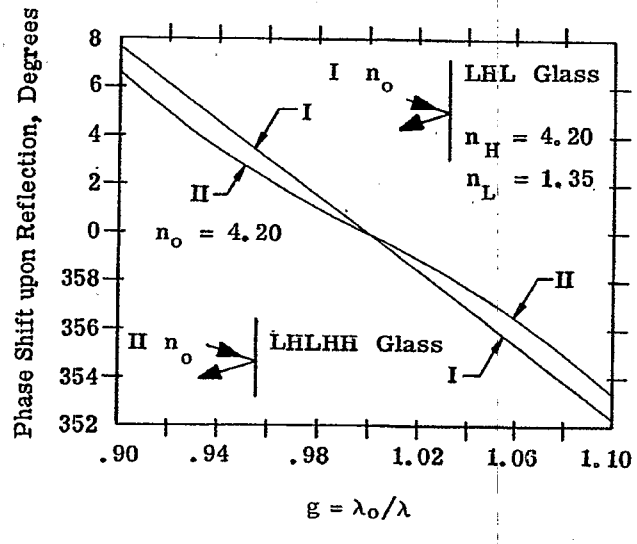

Figure 20.112- The phase shift upon reflection, ϵ , of the "effective interface" of the filters I and II in Fig. 111.

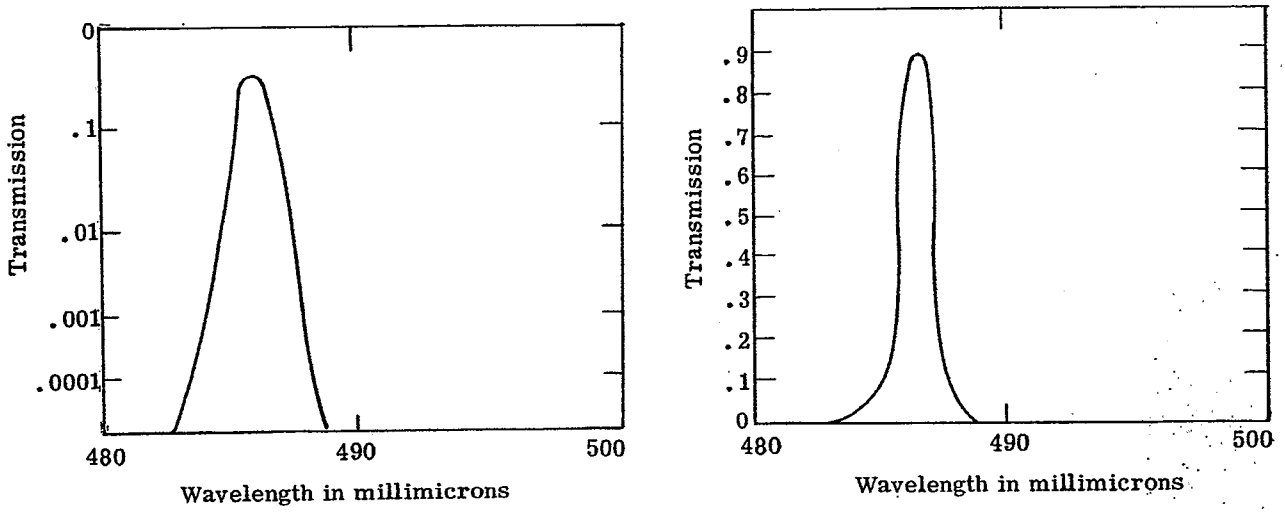

Figure 20.113- Measured transmittance of an all-dielectric Fabry-Perot type filter on a linear and logarithmic scale. Courtesy of Spectrolab, a Division of Textron Electronics, Inc.

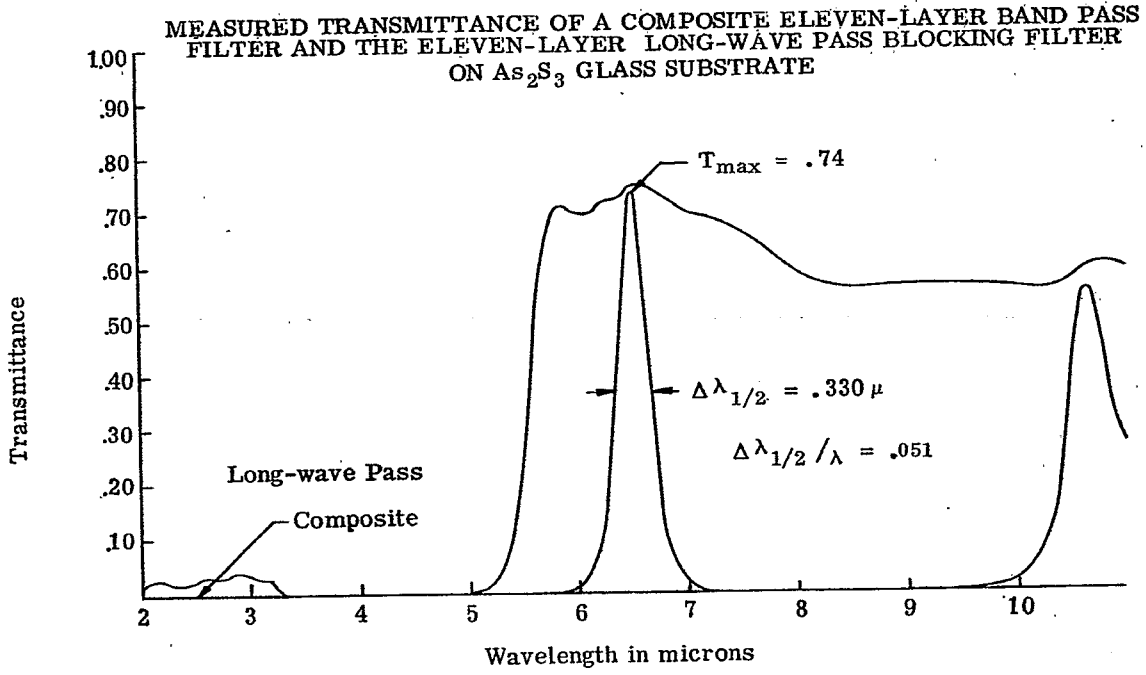

Figure 20.114- Measured spectral transmittance of a Fabry-Perot type filter and auxillary blocking filter composed of ZnS and PbTe .

band in the blue, is shown in Figure 11-. Although the peak transmission would be lowered slightly if a blocking filter were added in tandem, the T_{max} is still quite high. Also, the attenuation is quite high; an optical density of 4.0 is achieved at $3\,\Delta\lambda_{1/2}$ from the wavelength of maximum transmission.

20.10.5.1 Extremely narrow bandwidth filters. From theoretical considerations alone, one might conclude from Equation (58) that it is possible to construct all-dielectric multilayer F-P filters which have Q's of 10,000 and hence a band width of 0.05 mμ at 500 mμ in the visible. Such filters would be quite useful to astronomers, who have been using the expensive Lyot type polarization filters to isolate the H^{α} line. These filters would also find many applications in spectrochemical analysis; in some instances they could replace costly spectrometers which contain diffraction gratings. One method of attaining such large values of Q would be to increase the number of layers in the quarter-wave stacks which constitute the effective interfaces, and thus obtain higher reflectivities. The same practical difficulties which were described in 20.8.2.3 are encountered. The small amount of absorption and scattering in each film degrades the reflectivity and consequently sets a lower limit on the bandwidth of F-P type filters. Thus it is not too difficult to manufacture all-dielectric F-P type filters for the visible spectral region with a $\Delta\lambda_{1/2}$ of from 1.0 mμ to 1.5 mμ and a T_{max} of greater than 0.50 (this does not include blocking filters). A Russian publication [65] reports that filters with a $\Delta\lambda_{1/2}$ of 0.13 mμ and a T_{max} of 0.15 have been produced.

20.10.5.2 Filters which use a mica spacer. Another method of increasing the Q of a filter is to increase the order of interference m. The mechanical stress in the films (Section 20.2.3.2.4) makes it impractical to use thick layers of evaporated material to manufacture a spacer layer with a high order of interference. By using a thin sheet of mica as a spacer in a F-P type filter,[70,71] it is possible to attain values of m in the range from 70 to 700. Both sides of the mica spacer, which is usually from 0.005 to 0.0005 inches in thickness are coated with a semitransparent multilayer mirror, such as a quarter-wave stack. Using this technique, a filter which isolates one of the lines of the yellow sodium doublet has been produced.[71] A filter with a pass band at 570mμ, a $\Delta\lambda_{1/2}$ of 0.1 mμ and a T_{max} of 0.25 is reported.[71] The difficulty of using filters with a high order of interference is mentioned in 20.10.1.2, namely the problem of blocking out adjacent transmission bands which, in the case of the filter cited in the foregoing sentence, occur at intervals of 1.1 mμ on either side of the main pass band. This can be accomplished by inserting additional mica F-P type filters in tandem, but this reduces the T_{max}.

20.10.5.3 F-P filters at non-normal incidence. If a F-P type filter of the type shown in Figure 20.108 or 20.103 is inserted in a collimated beam of light at non-normal incidence, the following effects are observed as ϕ increases:

(1) The transmission pass band broadens and shifts to shorter wavelengths (i.e. a blue shift). This is because $n_g t_g$ in Equation (55) is replaced by an effective thickness (see 20.1.6.2) which is less than its original value. Hence a smaller λ_o satisfies this equation.

(2) The transmission band is partially linearly polarized. If the incidence angle ϕ is increased to large enough angles, two distinct bands are seen, each at a different wavelength. The light in one band is linearly polarized in the "s" plane, and the other in the "p" plane.

This angle shift of the maximum of the pass band can often be used to good advantage. For example, suppose it is desired to isolate the mercury green line at 546μ, and a F-P type filter which is available has a pass band at 550mμ. The spectral position of the pass band can be easily shifted so that it passes the Hg green line by tilting the filter less than ten degrees. Of course, the performance of the filter has been degraded by this tipping because the pass band has been broadened, but the loss is not serious if the pass band is wide to begin with. It is also evident that if a F-P type filter is placed in a beam of convergent light, then the angle shift broadens the transmission band asymmetically towards shorter wave-lengths. Thus a filter which is placed in a convergent beam should have its λ_o at normal incidence at a slightly longer wave-length. For example, Lissberger and Wilcock,[72a],[72b] calculate that a filter which is to have its optimum performance at 5000 mμ is placed in an f 2.0 beam, then at normal incidence its T_{max} should be located at $\lambda_o = 502$ mμ. It is also evident that filters which have extremely narrow band widths should be used at normal incidence, in a well collimated beam to prevent the loss of the narrow bandwidth by the angle shift broadening. The spectral transmittance curve in Figure 20.115 shows the angle shift of an all-dielectric F-P type filter for the infrared.

20.10.6 All-dielectric F-P type filters for the infrared. All-dielectric F-P filters are available for the infrared spectral region with a Q as large as 200. Figures 20.114, 20.115, and 20.116 show the spectral transmittance of some all-dielectric F-P type filters which are used in the infrared. These curves are intended to present a sample of what can be accomplished. The filter shown in Figure 20.114 is intended to have a

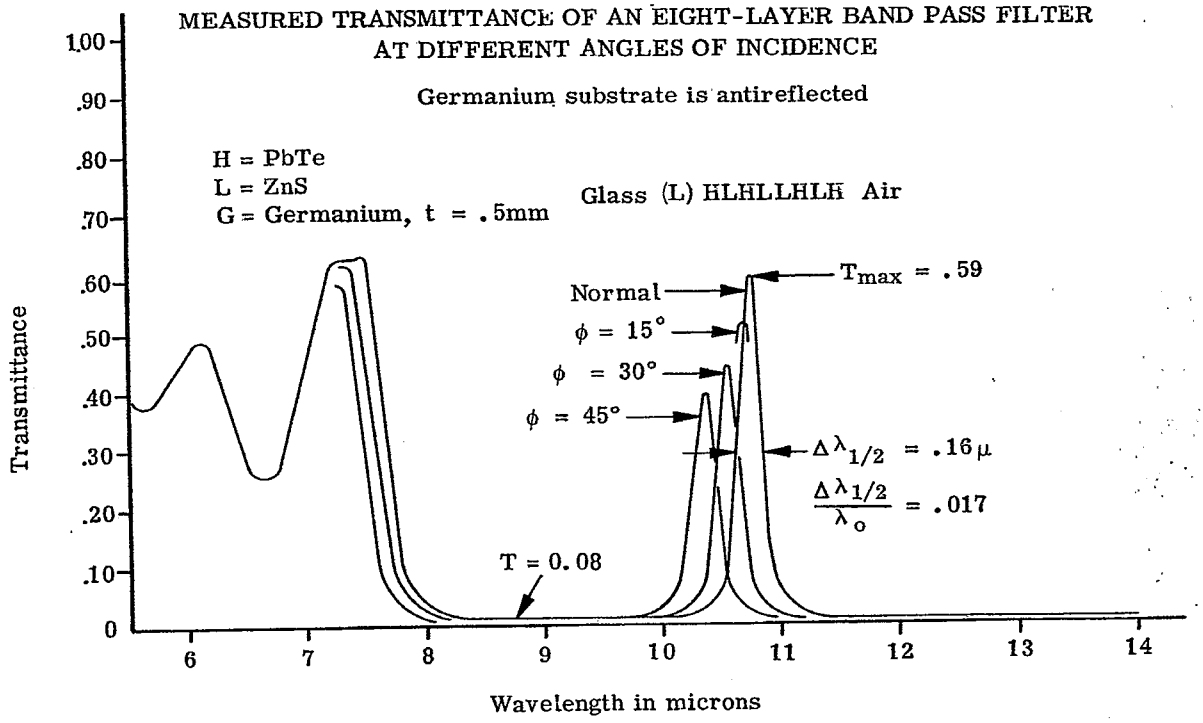

Figure 20.115- Measured spectral transmittance of a Fabry-Perot type filter at various values of ϕ. The decrease in T at $\phi = 45°$ is due to vignetting in the spectrophotometer. Courtesy of Bausch and Lomb, Inc.

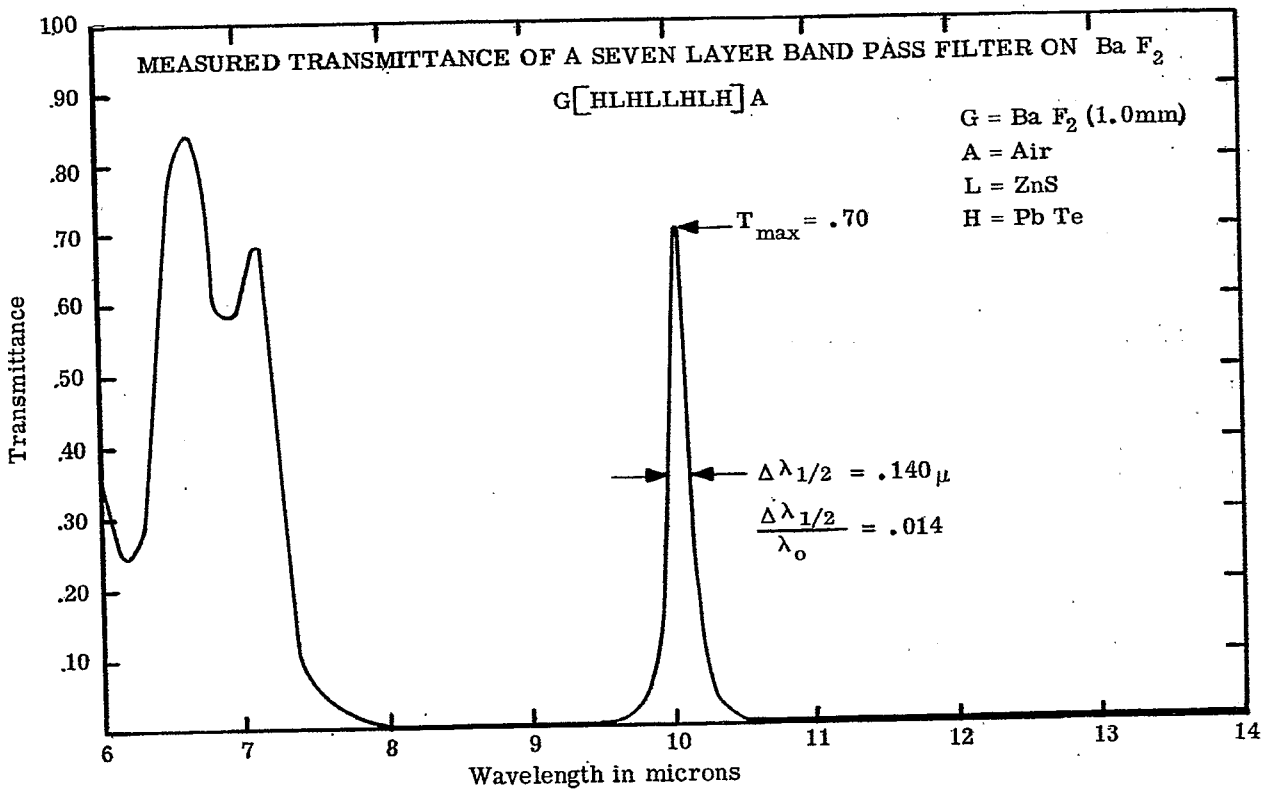

Figure 20.116- Measured spectral transmittance of a Fabry-Perot type filter on a BaF_2 substrate. Courtesy of Bausch and Lomb, Inc.

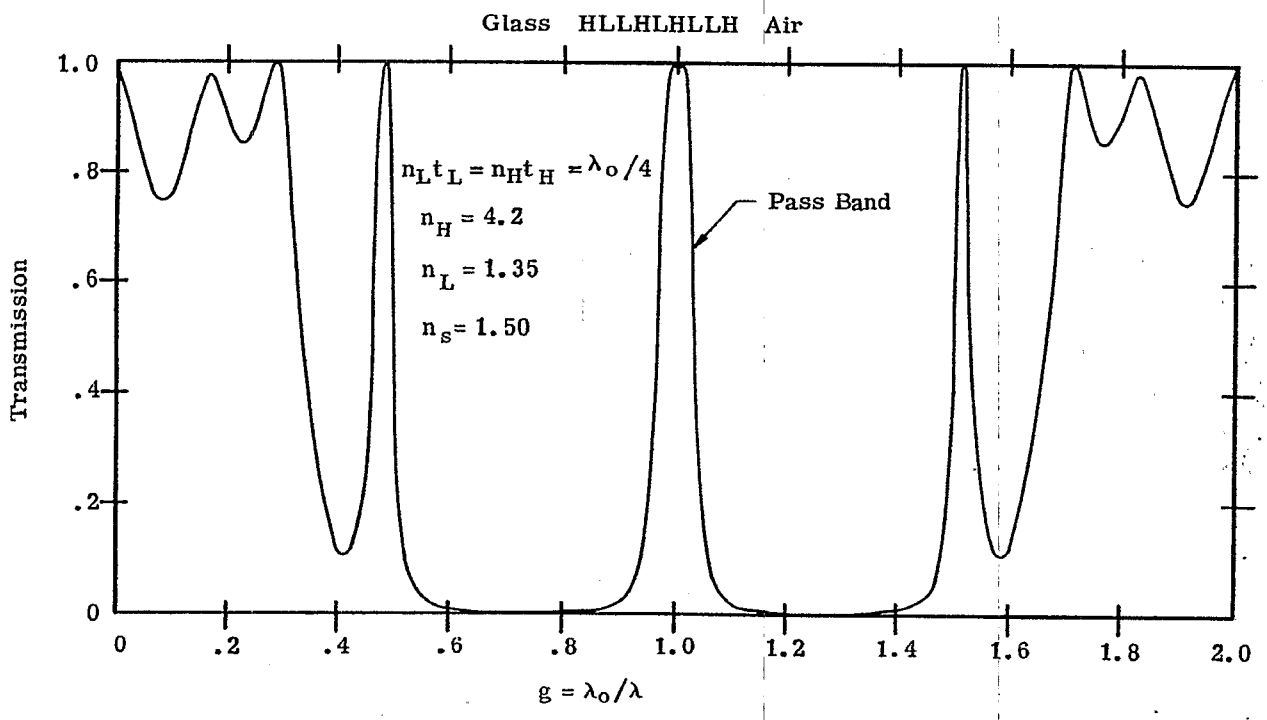

Figure 20.117- Computed spectral transmission of a Fabry-Perot type filter which has a non-Lorentian shaped pass band.

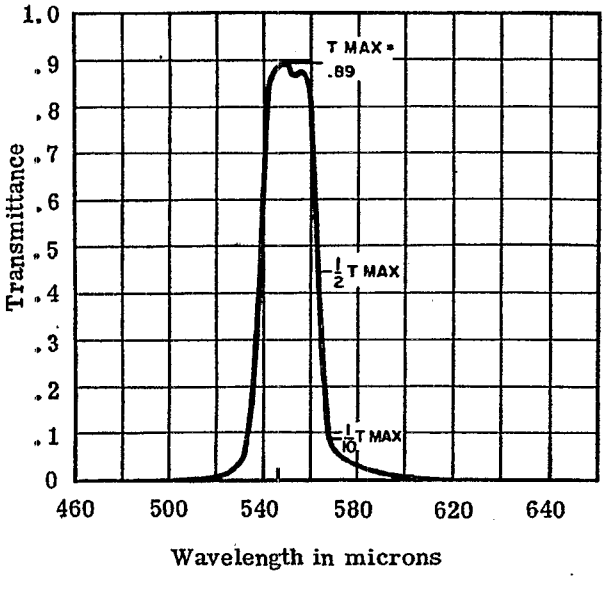

Figure 20.113 – Measured spectral transmittance of a narrow band-pass filter which has a nearly rectangular shaped pass band. Courtesy of Baird-Atomic, Inc.

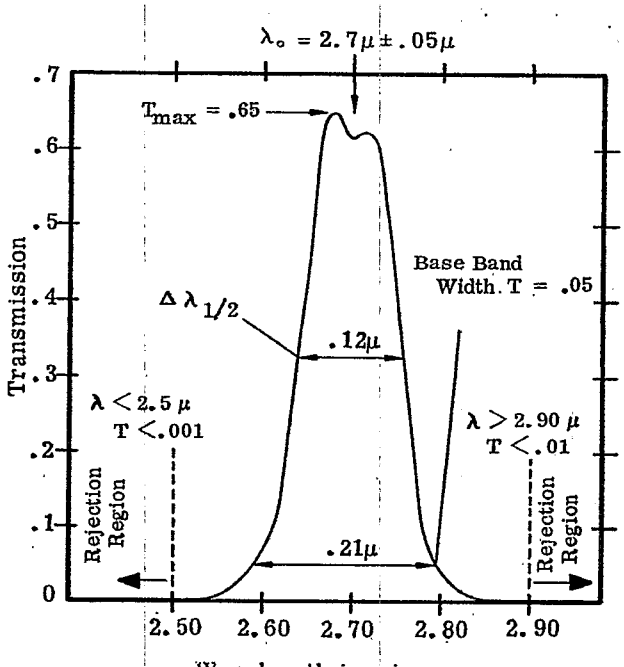

Figure 20.119- Measured spectral transmittance of a narrow band-pass filter which has a nearly rectangular shaped pass band. Courtesy of Eastman Kodak Company.

broad pass band; the Q is about 20. A long-wave pass blocking filter is inserted in tandem to attenuate the unwanted transmission "leak" below 3.3 μ. The region of high transmission above 10 μ is outside of the high-reflectance zone of the dielectric mirrors in the effective interfaces. The F-P type multilayer shown in Figure 20.115 is deposited on a substrate of germanium. The "L" layers which are in parenthesis, sic. (L) , are antireflection coatings for the germanium substrate. At λ_o , which is close to 10.8 μ at normal incidence, the same analysis which was applied in 20.10.5 is used here to remove absentee layers from the stack, thus leaving (L) germanium (L) , a germanium slab with an "L" antireflection coating on either side. Although the refractive index of this L layer (see 20.3.3) is not the optimum value, it still improves considerably transmission at λ_o . If these (L) coatings were not added, then T_{max} would be less than 0.47, instead of the value of 0.59 which is shown. The angle shift of the pass band to shorter wavelengths is also shown in Figure 20.115. The decrease in the T_{max} at non-normal incidence can be attributed to vignetting in the spectrophotometer which measured the transmittance. Figure 20.116 shows essentially the same type of coating, but on a substrate of barium fluoride. The substrate is a low-index material, and hence it is unnecessary to add the (L) coatings to antireflect the substrate, as is necessary for the multilayer shown in Figure 20.115. Comparing Figures 20.115 and 20.116, the effects of using a different substrate are manifested in the greater T_{max} for the multilayer on the CaF_2 substrate, a slightly narrower width of the pass band, and the higher transmission in the short-wave region below eight microns. Of course the latter effect is undesirable in many applications; the "leak" in the transmission in the short-wave region of the multilayers shown in Figures 20.115 and 20.116 could be removed by the addition of suitable blocking filters, as is done in Figure 20.114. Lead telluride is used as a high-index film material in this spectral region because it is transparent and has a large refractive index - and hence a filter with quite respectable Q is obtained with a small number of layers. Zinc sulfide is used as the low index material because it does not have a large mechanical stress (see 20.2.4.2.4) and also because it is transparent in this long-wave region. Silicon monoxide is not used in this spectral region because it has a strong absorption band starting at 8 μ .[72c] Greenler[16] has fabricated Fabry-Perot type filters with pass bands in the 10 μ region by using tellurium as a high-index material and sodium chloride as a low-index material. Using the same materials it is possible to manufacture filters with a pass band at wavelengths as long as 20μ .

20.10.7 F-P type filters with a pass band of non-Lorentzian shape. The F-P type filters which are described in 20.10.4 and 20.10.5 have a transmission pass band which is essentially Lorentzian in shape. The main drawback of this type of line shape is mentioned in 20.10.1.6, namely that unless the pass band is narrow, the filter has a long transmission tail which decreases in amplitude quite slowly. For example, suppose it is desired to use a multilayer filter to isolate the emission line at 491.6 mμ of a mercury discharge lamp. The lamp does not emit lines of any strength for at least 40 mμ on both the short-wave and long-wave side of 491.6 mμ. Therefore, it is not important that the filter have a narrow transmission band, in fact, the $\Delta\lambda_{1/2}$ could easily be as large as 20 mμ , provided the discharge tube does emit an appreciable amount of continuum radiation. However, it is quite important that the emission lines at 435.8 mμ in the blue and at 546.1 mμ in the green be attenuated very effectively, because these lines are at least a thousand times more intense than the 491.6 line. Thus, if the 491.6 mμ which passes through the filter is to be merely ten times more intense than the light from the blue and green lines, then the transmission of the filter is at 496 mμ and 546 mμ must be at least 10^{-4} of T_{max} . A M-D-M type filter would not furnish this much attenuation. A double filter of this type would furnish this much attenuation, but at the expense of a very low T_{max} . An all-dielectric F-P multilayer would furnish this degree of attenuation, provided that a large number of layers were used in the filter. However, this would mean that the transmission band would be quite narrow, whereas a narrow transmission band is not requisite. Such a filter with a narrow band would be expensive for two reasons: First, it contains a large number of layers, and is expensive to manufacture. Second, because the transmission band is narrow, the thickness of the layers must be controlled to quite close tolerances, so that the peak transmission of the filter occurs at exactly the desired wavelength of 491.6 mμ. The latter difficulty is avoided if a multilayer has a pass band which is essentially rectangular in shape, as is shown in Figures 20.117 to 20.121. Space does not permit us to elaborate some of the methods which are used to achieve transmission bands of this shape. One filter of this type is called a double half-wave system; the theory of such filters is discussed by Smith.[60] The spectral transmission of such a filter is shown in Figure 20.117. When analyzed as a F-P type filter, each of the effective interfaces is the film combination H LL H and contains a half-wave film; hence the name, double half-wave. The spacer layer is a quarter-wave optical thickness, rather than a half-wave layer. Figure 20.111 shows the transmission in the pass region so that it can be compared with the Lorentzian-shaped transmission bands of a conventional all-dielectric filter shown in the same Figure. Figure 20.118 shows the transmittance of a multilayer of this type with its pass band in the visible spectral region, while Figures 20.119, 20.120, and 20.121 depict infrared filters which pass at 2.70 μ , 4.50 μ , and 10.8 μ , respectively. Additional blocking filters have been added to the filters whose transmission curves are shown in Figures 20.119 and 20.120.

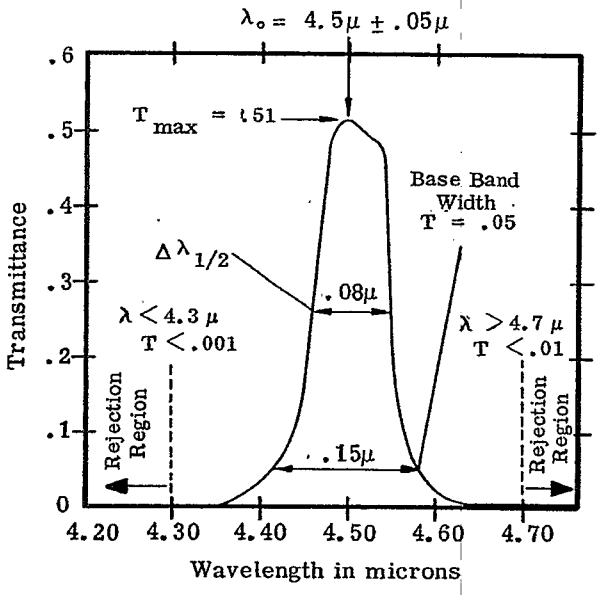

Figure 20.120- Measured spectral transmittance of a narrow band-pass filter which has a nearly rectangular shaped pass band. Courtesy of Eastman Kodak Company.

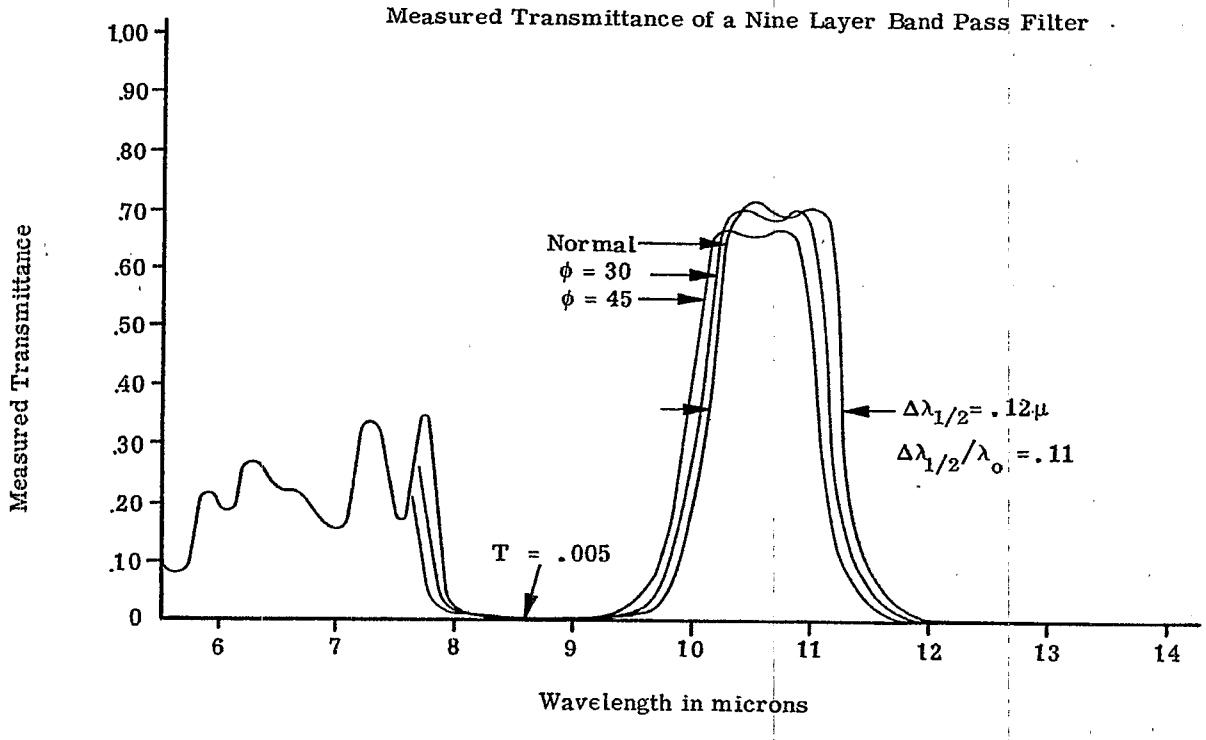

Figure 20.121- Measured spectral transmittance of a narrow band-pass filter which has a nearly rectangular shaped pass band. Courtesy of Bausch and Lomb, Inc.

20.11 REFERENCES FOR FURTHER STUDY

Publications on thin film optics can usually be placed in either of two categories:

(1) Thin film science: This is a study of the fundamental properties of thin films, with an emphasis on knowledge for the sake of knowledge, rather than on knowledge for the sake of ultimately producing some gadget. This includes a study of the physical structure and optical properties of thin films, the thermodynamics and chemistry of their formation, the properties of the films as related to the physics of solids, and so on.

(2) Thin film technology. Section 20 has been devoted to one aspect of this topic, namely how our knowledge of thin films can be utilized to provide useful optical components, such as filters, beam splitters, and other devices. Included in this broad classification are methods and techniques of preparing films, controlling their thickness, methods of multilayer filter design, and so on. The optical applications of thin film technology began to expand rapidly after 1946. A conference on thin film optics was held in 1950 and the papers which were presented at this conference [73] are a good summary of the state of the art up to that time. In 1955 Heavens [1] published a book which not only covers many aspects of thin film science, but he also devotes the later part of this book to some applications of thin films. Therein is presented some of the topics which have not been covered in Section 20, such as multilayer polarizers, frustrated total reflection filters, and so on. Another publication of Heavens [21] surveys more recent developments. Both Weinstein (Welford) [5] and Abeles [12] both present terst and correct mathematical treatments of the theory of the reflectivity of multilayers. Vasicek's book [74] contains some useful information, but very often it is hidden in endless pages of redundant and repetitive derivations of recursion formulae. The practical aspects of depositing thin film coatings are lucidly presented in a Navy Department pamphlet. [75] Holland's book [18] is more recent and presents a vast amount of valuable lore on how to evaporate thin films in a vacuum.

REFERENCES

1. Heavens, O. Optical Properties of Thin Solid Films (Butterworth Scientific Publications, 1955) p. 238
2. ibid, p. 221
3. Strong, John. Concepts of Optics (Freeman, 1958) p. 251
4. Heavens, O. op cit p. 66
5. Weinstein, W. (W. Welford) Vacuum 4, 3 (1954)
6. Terman, F. E. Radio Engineering (McGraw Hill, 1947) 3rd. ed. p. 75
7. Drumheller, Carl "Silicon Monoxide Evaporation Techniques" - A monograph available from the Kemet Company, Cleveland, Ohio. (1960)
8. Drumheller, Carl "Properties and Application of Silicon Monoxide" - A monograph available from the Kemet Company, Cleveland, Ohio. (1960)
9. Weinstein, W. op cit p. 5
10. Heavens, O. op cit Chapter 4
11. Born, M and Wolf, E. - Principles of Optics (Pergamon, 1959) p. 54
12. Abelés, F. Ann. de physique, 5, 103 (1950)
13. Welford, op cit p. 5
14. Pohlack, Hubert "Zum Problem der Reflexionsminderung optisher Gläser bei nichtsenkrechtem Lichteinfall" Jenaer Jahrbuch (VEB Optik Carl Zeiss Jena, 1952)
15. Hass, G. and Tousey, R. J. Opt. Soc. Am. 49, 593 (1959)
16. Greenler, R. G. J. Opt. Soc. Am. 47, 130 (1957)
17. Hass, George and Turner, A. F. "Preparation of Thin Films" - in Volume 6 of Methods of Experimental Physics, L. Marton, Editor in Chief. (Academic Press, 1959)
18. Holland, L. - Vacuum Deposition of Thin Films (Chapman and Hall, 1956)
19. Ballard, S., McCarthy, K. A. and Wolfe, W. L. State-of-the-Art Report: Optical Materials for Infrared Instrumentation. (Report No. 2389-11-S: I.R.I.A, Univ. of Michigan, 1959)
20. Turner, A. F. et al - Thick Thin Films - Quarterly Technical report #4 under contract with U.S. Army Engineer Research and Development Laboratories, Fort Belvoir, Va. (1951)
21. Turner, A. F. and Truby, F. K. U. S. Patent 2,858, 240 (Issued October 1958)

22a Heavens, O. Reports on Progress in Physics, 23,60 (1960)

22b Hass, G., Ramsey, J. B. and Thun, R. J. Opt. Soc. Am. 49, 116 (1959)

23. Huldt, Lennart and Staflin, T. Optica Acta 6, 27 (1959)
24. Hass, G. Vacuum 2, 331 (1952)
25. Pohlack, Hubert. loc cit p. 106
26. Baumeister, P. Optica Acta 8, 105 (1961)

REFERENCES (continued)

27. Hass, George and Turner, A. F. "Coatings for Infrared Optics" in Ergebnisse der Hochvakuumtechnik und der Physik dünner Schichten (Wissenschaftliche Verlagsgesellschaft Stuttgart, 1957)

28. Cox, J. T., Hass, G. and Jacobus, G. F., J. Opt. Soc. Am. 51, 714 (1961)

29. Cox, J. T., Hass, G., and Rowntree, R. F. Vacuum 4, 445 (1954)

30. Turner, A. F., Berning, P. et. al. Infrared Transmission Filters, Quarterly Technical Report #6, under contract DA44-009-eng-1113 with the U. S. Army Engineer Research and Development Laboratories, Fort Belvoir, Va. (1953)

31. Hass, G. and Cox, J. T. Published in Vol. 52 of J. Opt. Soc. Am. (1962)

32. Turner, A. F., Epstein, I., et. al. Optical Properties of Multilayer Films and Interference Filters in the 10 Micron Region. Quarterly Technical report #5 under contract with the U. S. Army Engineer Research and Development Laboratories, Fort Belvoir, Va. (1951)

33. Brillouin, Leon. Wave Propagation in Periodic Structures. (McGraw-Hill, 1946 or Dover, 1953)

34. Seitz, Frederick, The Modern Theory of Solids Chapter 9 (McGraw-Hill, 1940)

35. Epstein, I. J. Opt. Soc. Am. 42, 806 (1952)

36. Baumeister, P. J. Opt. Soc. Am. 48, 955 (1958)

37. Dimmick, G. L. and Widdop, W. E. J. Soc. Motion Picture Engrs. 58, 36 (1952)

38. Carlson, F. E., Howard, G. T., Turner, A. F. and Schroeder, H. H. J. Soc. Motion Picture Engrs. 65, 136 (1956)

39a Turner, A. F. & Schroeder, H. H. J. Soc. Motion Picture Engrs. 69, 351 (1960)

39b Koch, George U. S. Patents 2,552, 184 and 2,552, 185

40. Epstein, L. I. J. Opt. Soc. Am. 45, 360 (1955)

41. Thelen, A. "The Use of Vacuum Deposited Coatings to Improve the Conversion Efficiency of Silicon Solar Cells in Space." Progress in Astronautics and Rocketry Academic Press, (1961) p. 373

42. Sennett, R. S. and Scott, G. D. J. Opt. Soc. Am. 40, 203 (1950)

43. Holland, L. Vacuum 3, 159 (1953)

44. Turner, A. F. and Schroeder, H. H. J. Soc. Motion Picture Engrs. 61, 628 (1953)

45. American Institute of Physics Handbook (McGraw-Hill, 1957) p. 6-108

46. Jenkins, F. A. J. phys. radium 19, 301 (1958)

47. Kuhn, H. and Wilson, B. A. Proc. Phys. Soc. (London) B 63, 754 (1950)

48. Stone, J. M. J. Opt. Soc. Am. 43, 927 (1953)

49. Baumeister, P. W. and Stone, J. M. J. Opt. Soc. Am. 46, 228 (1956)

50. Ring, J. and Wilcock, W. L. Nature 171, 648 (1953)

51. Giacomo, P. J. phys. radium 19, 307 (1958)

52. Giacomo, P. Rev. Opt. 35, 317 (1956)
35, 442 (1956)

REFERENCES (continued)

53. Jenkins, F. A. and White, H. E. Fundamentals of Optics (McGraw-Hill, 1957) Third Ed. p. 273

54. Born, M. and Wolf, E. op cit p. 322

55a. Terman, F. E. op cit p. 39

55b. Fox, A.G. and Li, T. Bell System Tech. J. 40, 453 (1961)

56. Baumeister, P. W. and Jenkins, F. A. J. Opt. Soc. Am. 47, 57 (1957)

57. Terman, F. E. op cit p 42

58. Stone, J. M. Ph. D. Thesis, University of California, Berkeley, 1953 (unpublished)

59. Mielenz, K. D. J. Opt. Soc. Am. 50, 1014 (1960)

60. Smith, S. D. J. Opt. Soc. Am. 48, 43 (1958)

61. Baumeister, P. W., Jenkins, F. A. and Jeppesen, M. A. J. Opt. Soc. Am. 49, 1188 (1959)

62. Geffcken, W. agnew. Chem., A, 60 1 (1948)

63. Geffcken, W. Deutsches Reich Pat. #716,153 (Dec. 1939)

64. Turner, A. F. J. phys. radium 11, 444 (1950)

65. Korolev, F. A., Klement'eva, A. Yu., and Meshcheryakova, T. F. Optics and Spectroscopy (translation of Optika i Spectroskopia) 6, 341 (1960)

66. Turner, A. F. and Ullrich, O. A. J. Opt. Soc. Am. 38, 662 (A) (1948)

67. Mann, A. E. and Rock, F. C. J. Opt. Soc. Am. 38, 280 (A) (1958)

68. Berning, P. H. and Turner, A. F. J. Opt. Soc. Am. 47, 230 (1957)

69. Hadley, L. N. and Dennison, D. M. J. Opt. Soc. Am. 38, 483 (1948)

70. Ring, J., Beer, R., and Hewison, V., J. phys. radium 19, 321 (1958)

71. Dobrowolski, J. J. Opt. Soc. Am. 49, 794 (1959)

72a Lissberger, P. H. J. Opt. Soc. Am. 49, 121 (1959)

72b Lissberger, P. H. and Wilcock, W. L. J. Opt. Soc. Am. 49, 126 (1959)

72c Hass, G. and Salzburg, C. D. J. Opt. Soc. Am. 44, 181 (1954)

73. J. phys. radium 11, 305-480 (July 1950)

74. Vasicek, A. Optics of Thin Films (North-Holland, 1960)

75. Naval Ordnance Pamphlet (OP) 1952, Optics Filming, U.S. Gov. Printing Office, (1945)